c1

A PKP STUDY OF THE EARTH'S CORE USING THE WARRAMUNGA SEISMIC ARRAY

by

AIMÉE ELIZABETH SURRENDRA BERTRAND

B. Sc. University of the West Indies, 1970

A THESIS SUBMITTED IN PARTIAL FULFILMENT OF
THE REQUIREMENTS FOR THE DEGREE OF

MASTER OF SCIENCE

in the Department

of

GEOPHYSICS

We accept this thesis as conforming to the

required standard

THE UNIVERSITY OF BRITISH COLUMBIA

August, 1972

In presenting this thesis in partial fulfilment of the requirements for an advanced degree at the University of British Columbia, I agree that the Library shall make it freely available for reference and study. I further agree that permission for extensive copying of this thesis for scholarly purposes may be granted by the Head of my Department or by his representatives. It is understood that copying or publication of this thesis for financial gain shall not be allowed without my written permission.

Department of Geophysics

The University of British Columbia
Vancouver 8, Canada

Date 12th August 1972

ABSTRACT

PKP core phases recorded at the U.K.A.E.A. - type seismic array, WRA, in Northern Territory, Australia over the distance range 113° to 176° are used to determine a velocity-depth model for the earth's core. Paper recordings played out at high speed (40 mm/sec) from analog magnetic tape with amplitude gain control and narrow bandpass filters provided the data available for analysis. Such data enabled precision measurement of relative times between seismic traces.

Four distinct traveltime branches were observed. Two of these are the well-known PKP_{AB} and PKP_{DF} branches which are transmitted through the outer and inner cores, respectively. The two additional branches are forerunners to the DF branch at distances less than 143°. In recent years, the existence of one of these branches designated PKP_{GH}, has been accepted to account for observed precursors. However, the existence of a distinct second branch, designated PKP_{IJ}, has been a subject for debate. Since the precursor branches provide information about the "transition region" between the fluid outer core and the solid inner core, the identification in this study of two distinct sets of forerunners is of some importance.

Traveltime and traveltime gradient ($dT/d\Delta$) measurements of each phase observed on the seismograms were made. The $dT/d\Delta$ values were measured by a least-squares technique. These measurements were strongly perturbed by structure beneath the array and it was necessary to correct for the effect by an empirical approach. The corrected $dT/d\Delta$ values were smoothed by the method of summary values and, for comparison, by a polynomial regression technique. The smoothed $dT/d\Delta$ values for all four

branches were inverted by the Herglotz-Weichert method in order to obtain a velocity-depth model for the earth's core. The final velocity model, UBC1, determined in this manner was the one which gave the best fit to all observations in this study.

Near a depth of 4000 km., UBC1 required a slight reduction in the Jeffreys-Bullen (1940) velocities in order to obtain traveltimes that agreed with the observations for the outer core. The model exhibits three velocity discontinuities at depths of 4393 km, 4810 km, and 5120 km. The magnitude of the velocity increases at the discontinuities are 0.10, 0.24 and 0.92 km/sec, respectively. These discontinuities define two shells surrounding the inner core. In the outermost shell, 417 km thick, the velocity gradient is near zero in magnitude. In the second shell, 300 km thick, the velocity gradient is slightly negative.

ACKNOWLEDGEMENTS

I greatly appreciate the advice and encouragement given to me by my supervisor Dr. R. M. Clowes.

Special thanks should be given to Dr. J.R. Cleary, Mr. H.G. Doyle and the Department of Geophysics and Geochemistry, Australian National University for their hospitality to Dr. Clowes while he obtained the data used in this study. The help of Dr. C. Wright in providing many of the computer programs used in this study is deeply appreciated.

Financial assistance for this project was provided by a University of the West Indies Postgraduate Scholarship, a National Research Council Bursary, and National Research Council operating and computing grants numbered A-7707 and C-1257, respectively of Dr. R. M. Clowes.

TABLE OF CONTENTS

		Page
1.	INTRODUCTION	1
1.1	The Project	1
1.2	Previous Work on Core Structure	2
1.2.1	Discovery of Central and Inner Core	2
1.2.2	Velocity Solutions for Earth's Core	4
1.3	Seismic Velocities and Physical Properties of the Core	14
1.3.1	Central Desity of the Core	14
1.3.2.	Solidity of the Inner Core	15
1.4	The Warramunga Seismic Array	17
1.5	Use of an Array in Determining Structure	19
2.	MEASUREMENT AND ANALYSIS	21
2.1	Determination of $dT/d\Delta$ and Azimuth From a Seismic Array	21
2.1.1	Some Possible Methods	21
2.1.2	Details of the Least Squares Method	23
2.2	Measurement Techniques	26
2.2.1	Data Available for the Study	26
2.2.2	Measurement of $dT/d\Delta$ and Azimuth	29
2.2.3	Sources of Systematic Error in $dT/d\Delta$ and Azimuth Measurements	34
2.3	Smoothing of Corrected $dT/d\Delta$ Values	52
2.3.1	Smoothing of $dT/d\Delta$ by the Method of Summary Values	52
2.3.2	Smoothing of $dT/d\Delta$ by UBC TRIP	63
2.4	Inversion of Smoothed $dT/d\Delta$ Data Using the Herglotz-Wiechert Integral	66
2.4.1	Description of the Herglotz-Wiechert Technique	66

TABLE OF CONTENTS
(cont'd)

		Page
2.4.2	Application of the Herglotz-Wiechert Method to $dT/d\Delta$ Values for the Earth's Core	70
3.	DISCUSSION	73
3.1	General Observations	73
3.2	Specific Observations	76
3.2.1	Identification of Phases	76
3.2.2.	Turning Points and End Points for the Travel-time Branches	77
3.2.3	Amplitude Observations	80
3.2.4	A Record Section for the Core Phases	82
3.3	Discussion of the Analyzed Data	83
3.3.1	Corrected $dT/d\Delta$ Measurements	83
3.3.2	Traveltime Measurements	87
3.4	Velocity Model UBC1	93
4.	CONCLUSION	100
	BIBLIOGRAPHY	103
	APPENDICES	
	APPENDIX I. Seismic Ray Theory	107
	APPENDIX II. List of Earthquakes Used in Study	116
	APPENDIX III. Ellipticity and Focal Depth Corrections to Measured Traveltimes	120
	APPENDIX IV. Method of Summary Values	123
	APPENDIX Va UBC TRIP - Triangular Regression Package	126
	Vb List of $dT/d\Delta$ Smoothed by UBC TRIP	129

LIST OF FIGURES

FIGURES		Page
1.1	Velocity models of Gutenberg and Richter	3
1.2	Bolt's 1964 T_2 velocity model	7
1.3	Adams and Randall 1964 velocity model	9
1.4	Buchbinder's 1971 velocity model	12
1.5	Warramunga Array, Australia	16
2.1	Diagram to illustrate a least squares technique of determining $dT/d\Delta$ and azimuth	22
2.2	Example of data used in the study	27
2.3	Matching waveform technique used to determine relative arrival times at each seismometer	30
2.4	Measured traveltimes	33
2.5	Reduced traveltimes	34
2.6	Refraction of a planar seismic beam incident on a dipping interface between a half-space and the overlying layer.	41
2.7	Measured $dT/d\Delta$	49
2.8	$dT/d\Delta$ corrected for local structure beneath the array	50
2.9	$dT/d\Delta$ smoothed by the method of summary values	62
2.10	Comparison of $dT/d\Delta$ smoothed by polynomial regression and method of summary values	65
3.1	Traveltime - distance plot of seismograms	81
3.2	Fit of smoothed $dT/d\Delta$ curves to corrected data	84
3.3	Fit of smoothed traveltime curves to data	85
3.4	Fit of smoothed reduced traveltime curves to data	86
3.5	Traveltime residuals (O - C)	89
3.6	Traveltime differences	90

LIST OF FIGURES
(cont'd)

		Page
3.7	The velocity model UBC1 for the earth's core	92
A-1	Seismic ray theory	108
A-2	Seismic ray theory for discontinuous increase in velocity at a boundary.	112
A-3	Seismic ray theory for discontinous decrease in velocity at a boundary.	114

LIST OF TABLES

TABLE		Page
1.1	Coordinates of the individual seismometers of the Warramunga array	18
2.1(a)	Summary points for the DF branch	56
(b)	Summary points for the GH branch	57
(c)	Summary points for the IJ branch	58
(d)	Summary points for the AB branch	59
2.2	List of $dT/d\Delta$ smoothed by method of summary values	60
2.3	Equations for $dT/d\Delta$ smoothed by polynomial regression	64
3.1	Equations for traveltimes smoothed by polynomial regression	88
3.2(a)	Position of traveltime cusps in velocity model UBC1	96
(b)	Velocity-depth relationship for velocity model UBC1	96
3.3	Traveltimes for model UBC1	97

CHAPTER I
INTRODUCTION

1.1 The Project

The core of the earth is less accessible than most of our planetary neighbors and its properties are almost as difficult to determine. Physical characteristics of the earth's core can only be inferred from measurements made near the surface. Seismological investigations have proved most successful in this regard. The analysis of seismic body waves which have penetrated the earth's core (e.g. PKP, SKS and other phases) is one such method which has provided detailed information concerning the physical properties of the core.

The present study uses PKP phases recorded at the Warramunga seismic array in Northern Territory Australia as a means of deriving a velocity-depth model for the earth's core. Emphasis is placed on the controversial 'transition region' - that region, a few hundred kilometres thick, which separates the 'fluid' outer core from the 'solid' inner core. The PKP phases which travel through the earth's inner core are often designated PKIKP. The precursors or forerunners to the PKIKP phases provide information on the nature of the transition region. These precursors are normally too small to be readily identified on individual seismograms, except for large earthquakes. The significance of the array study is that these precursors, in addition to the major PKIKP phases, can be identified, not just by their traveltimes, but even more definitively by their apparent velocities or traveltime gradients ($dT/d\Delta$).

The remainder of this chapter is devoted to a brief discussion of the work done in the past regarding the structure of the earth's core. The relationship of seismic velocities with the physical properties of the core are briefly described. The Warramunga seismic array is described in some detail, and mention is made of the use of an array in determining

structure. Chapter 2 is devoted to details of the measurement and analysis techniques used, and the results obtained. Chapter 3 concerns a discussion of the results. A brief digression on the basic seismic ray theory involved in this study is presented in Appendix I.

1.2 Previous work on core structure

1.2.1 Discovery of the Central and Inner Core

At the turn of this century, observational seismologists noted that up to distances of about 100°, both P and S waves were recorded with more or less uniform amplitudes; beyond 100°, the amplitudes decayed rapidly with complete extinction of short period waves at distances greater than 105°. Short period P waves appeared consistently and strongly again at distances greater than about 143°, but at these distances, were delayed some two minutes compared with the extension of the traveltime curve for distances less than 105°. The corresponding short period S waves did not reappear. The explanation suggested (Gutenberg, 1914) was that at a depth of about 2900 km, there was a sharp discontinuity at which the velocity of P waves fell by approximately 40%. This discontinuity marked the boundary between solid material (mantle) and liquid material (since S waves were not transmitted throught it). Thus, the existence of a liquid core of the earth was postulated.

It was not long before more sensitive seismographs showed that the P wave traveltime curve, which extended from 143° to 180°, was associated near its beginning with small amplitude P-wave onsets, extending as far back as 110°. The immediate explanation of these observations was that the waves were motion which was diffracted at a cusp in the traveltime curve near 143°. A competing hypothesis, suggesting the existence of an inner core in which the P velocity was greater than in the outer core, was advanced in 1936 by the Danish seismologist I. Lehmann. This hypothesis

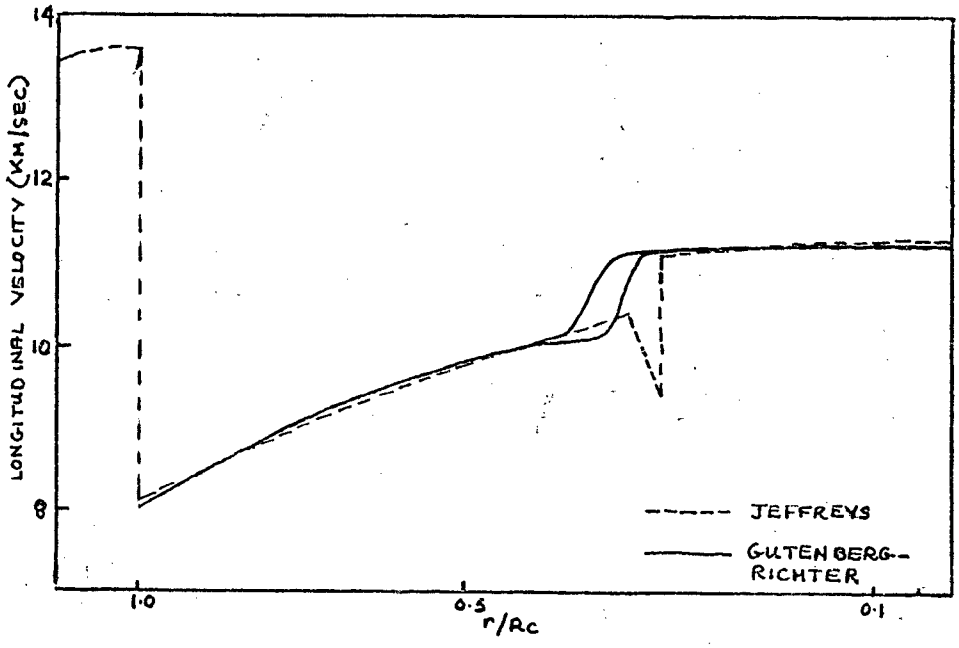

I.Ia. Velocity models of Jeffreys and Gutenberg-Richter

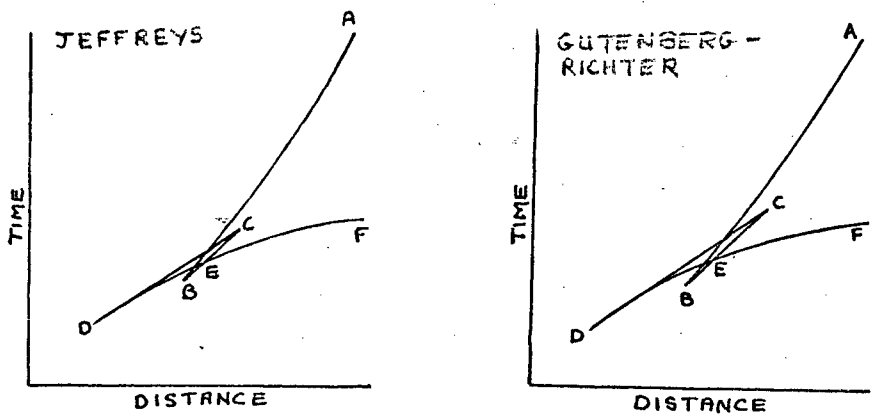

I.Ib. Traveltime Curves

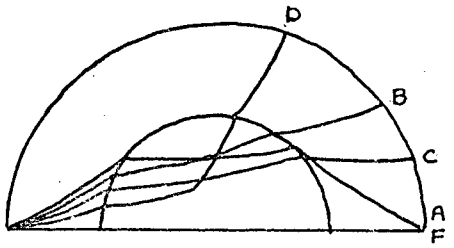

I.Ic. Ray paths through core corresponding to traveltime curves

Figure I.I Velocity Models of Jeffreys and Gutenberg-Richter.

proved consistent with observations of the traveltime curves at all distances. It was accepted instead of the diffraction hypothesis, after Jeffreys (1939) showed by an extension of Airy's theory of diffraction near a caustic, that for waves with periods of approximately 1 sec., diffraction could not occur more than 3° from the cusp at 143°.

With the discovery of the inner core, all the main boundaries within the earth had apparently been located, and the bulk of P and S wave observations could be explained by the geometry of a tripartite earth consisting of a mantle, inner and outer core. The next step was to obtain velocity-depth solutions consistent with observations for a tripartite earth, and in particular for the core of the earth.

1.2.2 Velocity Solutions for Earth's Core

Gutenberg and Richter (1937) favored a velocity distribution in which the velocity of P waves increased with depth down to the mantle-core boundary at about 2900 km, where it dropped sharply from 13.7 km/sec. to approximately 8 km/sec. The velocity then increased slowly to 10.2km/sec at a depth of 4850 km, thereupon increasing rapidly and continuously to 11.4 km/sec. over a depth of 300 km, and finally decreasing slowly to 11.3 km/sec. at the earth's center. They therefore postulated a transition region 300 km thick to exist between the inner and outer core, with the inner core boundary at a depth of 5150 km. Jeffreys (1939) model differed from that of Gutenberg and Richter in that it showed a velocity decrease from a depth of 4980 km to 5120 km, followed by a sharp increase of 1.8 km/sec. at the boundary of the inner core. The velocity decrease in the zone surrounding the inner core was needed to explain his observed traveltimes. The two models are shown in Figure 1.1a, and the form of the corresponding traveltime curve is shown in Figure 1.1b. Note the difference in the lengths of the branch BC. The ray which leaves the focus at the shallowest angle necessary to enter the core corresponds to the point A on the curve, and successively steeper rays trace the traveltime curve ABCDEF. Rays corresponding to the branches AB and BC

penetrate only the outer core, the cusp at B being a direct consequence of the discontinuous decrease in velocity at the mantle-core boundary and the subsequent P velocity variation in the outer core, and is associated with a caustic (i.e. large amplitudes). The branch CD of the traveltime curve represents rays which undergo total internal reflection at the boundary of the inner core. Rays that represent the branch DF penetrate the inner core; the point F thus corresponds to a ray travelling diametrically through the earth. The paths of these rays are illustrated in Figure 1.1c, in which the points of emergence of rays that correspond to the points in Figure 1.1b are shown by the same letters.

The hypothesis of a single velocity jump in the transition region between the inner and outer cores proved inadequate, however, with the discovery (Gutenberg, 1957, 1958) of short period precursors to the DF branch in the approximate distance range $125^{\circ} < \Delta < 143^{\circ}$. These precursors arrived at the stations up to 15 seconds earlier than the DF arrivals. Gutenberg (1957) suggested, on the basis of experiments on viscosity by Kuhn and Vielhauer (1953), that the PKP wave pulse may become dispersed into a frequency - dependent wave train in a transition zone between a liquid outer core and a more viscuous inner core. However, his suggestion became unacceptable when no gradual increase in wave periods could be observed in the time interval from the beginning of the short period precursors to the arrival of the DF phases. Another possible mechanism for the early PKP onsets was discussed by Knopoff and MacDonald (1958), in a study of the effects of a postulated magnetic field in the inner core. They predicted that a toroidal field of about 5×10^{6} oersted was required to split PKIKP pulses into two components differing in transmission time by 12 secs. at $\Delta = 140^{\circ}$, and that the pulse separation would be independent of frequency. They observed however, that a field of that strength was unlikely, since the seismological evidence for the equality of the traveltimes of the axial and equatorial PKIKP waves, with

allowance for ellipticity, placed an upper limit of order 5×10^5 oersted on the magnitude of the magnetic field, provided the field was toroidal.

Bolt (1959, 1962, 1964) suggested that the precursors to the PKIKP waves (DF branch) could be caused by an additional discontinuous increase in velocity at a shallower level than the previously accepted boundary of the inner core. The replacement of a single velocity discontinuity by two adjacent jumps has the following consequences for the traveltime curve: let the jumps occur at radii R_1 and R_2 inside the core of radius R_c = 3,473 km where $R_2 < R_1 < R_c$. As shown in Figure 1.2a, the family of rays through the mantle and outer core which are defined by decreasing valves of ray parameter $p = dT/d\Delta$, first generate the locus ABC as previously described. At C, a ray becomes tangential to the spherical surface of radius R, and for steeper angles of incidence (smaller p) the rays are totally internally reflected to generate the receding branch CG. The velocity contrast or magnitude of the velocity jump at R_1 determines the critical angle for total internal reflection, and hence determines the point at which refraction beneath R_1 commences - i.e. it determines the position of the point G. The rays refracted normally in the shell of the core between radii R_1 and R_2 $(R_1 > R_2)$ generate the advancing branch GH. At H, a ray once again becomes tangential to the spherical surface of radius R_2, and the totally reflected rays generate the receding branch HD. As before, the magnitude of the velocity jump at R determines the position of the cusp at D, where refraction beneath R_2 begins. The rays refracted beneath R_2 (that is, through the inner core) generate the advancing branch DF which has monotonically decreasing gradient p.

The main point of the double-jump hypothesis is immediately apparent - it produces an additional section of the PKP curve - CGH - to which the observed precursors to PKIKP (DF branch) may be referred (cf. Figure 1.1 for one velocity jump). By extension of the preceding arguments to a triple velocity jump hypothesis, it can be seen that the

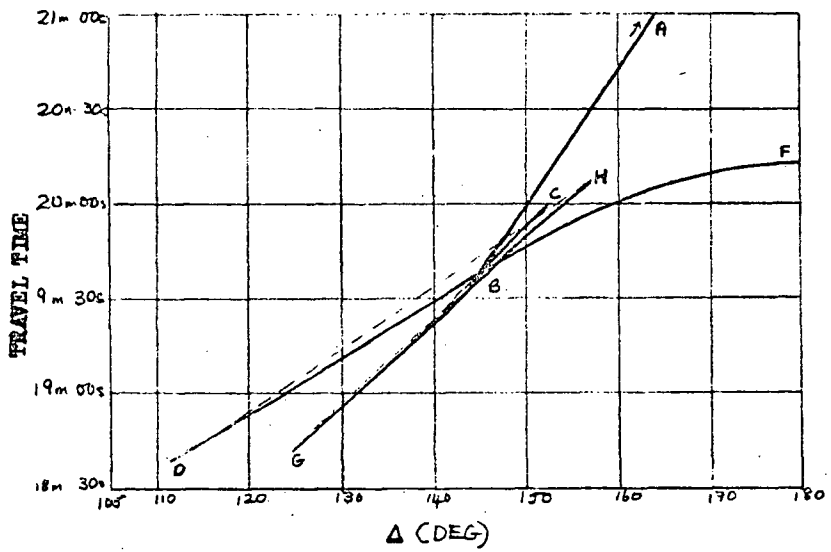

I.2a. Bolt's Traveltime Curves

Solution T2 :

R^*, V^*, -1806 km (0.52R) 10.03 km/sec

R_F, V_F, -1667 km (0.48R) 10.31 km/sec

R_G, V_G, -1216 km (0.35R) 11.23 km/sec

Cusp	T	Δ (Deg)	dT/dΔ (Sec/Deg)
C	19m 56.2s	151.2	2.90
G	18m 41.9s	124.7	2.82
H	20m 06.3s	156.5	2.05
D	18m 37.5s	111.0	1.89

I.2b. Bolt's Solution T2.

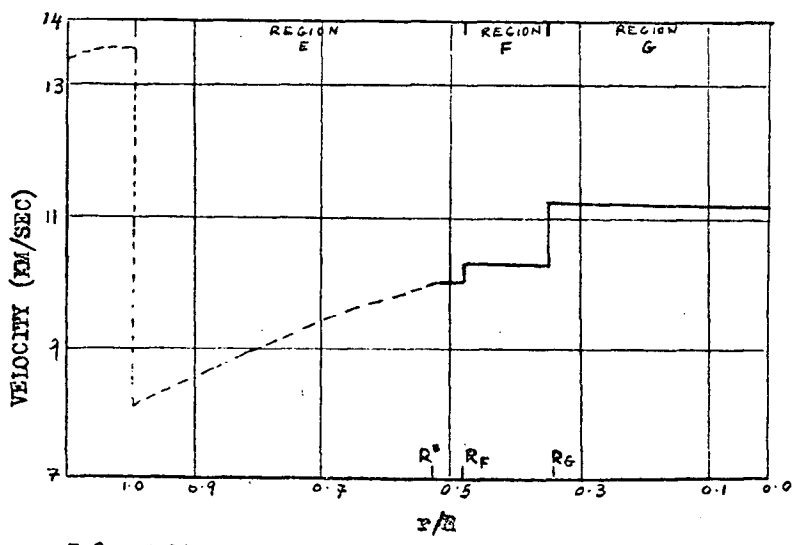

I.2c. Bolt's Velocity Model

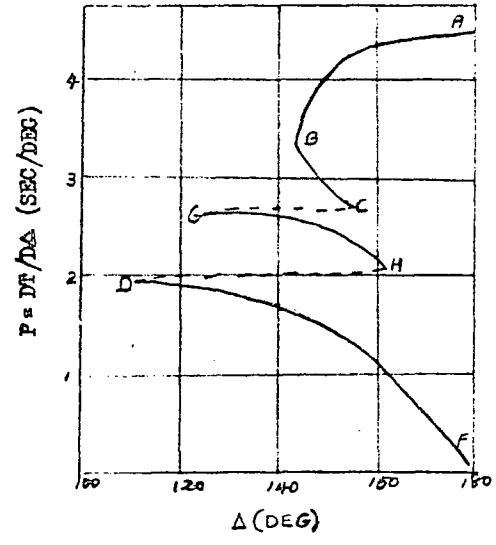

I.2d. Bolt's dt/dΔ Model

Figure I.2. Bolt's 1964 T2 Model.

results would be the addition of two branches of precursors to the DF branch.

For any hypothesis to be useful, it must be shown to lead to complete traveltime curves which do not violate accepted constraints such as those provided by ray theory. For example, ray theory demands that the receding branches CG and HD generated by totally reflected rays must be concave upwards, while the advancing branches generated by refracted rays must be concave downwards. The branches CG and GH must extend practically straight from C and G respectively, with the main curvature near G and H. Since the velocity increases discontinuously at R_1 and R_2, it is expected that the only cusp to be associated with large amplitudes would be the one at B. These constraints are discussed more fully in Appendix I. Empirical constraints are provided by observed traveltimes for the individual branches.

Using the velocity tables of Jeffreys (1939) as his starting point, Bolt found that he could retain the caustic at B, and at the same time eliminate the negative velocity gradient of Jeffreys' solution only by a reduction of Jeffreys' velocity just beneath the region producing the caustic. His final procedure was to take the velocity as constant at 10.03 km/sec. from this region to the first discontinuity (i.e. from 0.52 R_c to 0.48 R_c or depths of 4,564 km to 4,602 km), assume the velocities in the shell bounded by R_1 and R_2 and in the inner core to be constant, and to calculate solutions for R_1 and R_2 by building up times for the three superimposed shells. Three solutions, T_1, T_2 and T_3 were determined, of which his preferred solution, T_2, is illustrated in Figure 1.2b. The corresponding velocity model is shown in Figure 1.2c and the resulting $dT/d\Delta$ vs Δ curve in 1.2d. Bolt concluded that "there is in the core a discrete shell with thickness of order 420 kms, and with a mean P velocity near 10.31 km/sec. This shell surrounds the inner core having mean radius 1,220 kms and mean P velocity 11.22 km/sec. The material in the intermediate shell is not likely to have marked rigidity.

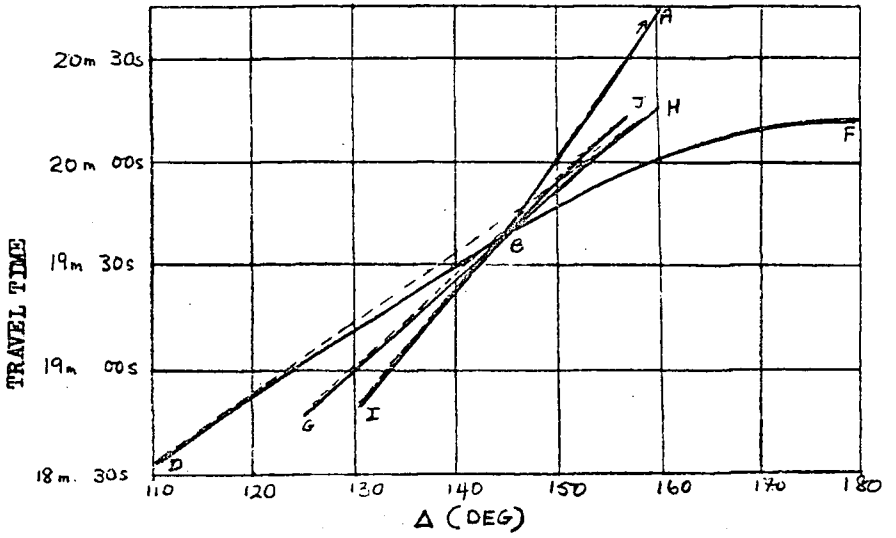

I.3b. A-R Traveltime Curves.

R_I, V_I , -1978 km (0.57R_e)
9.87 -10.00 km/sec

R_G, V_G , -1579 km (0.455R_e)
9.98 -10.41 km/sec

R_D, V_D , -1249 km (0.362R_e)
10.15 -11.16 km/sec

Cusp	T	Δ (DEG)	dT/dΔ (SEC/DEG)
B	18m 37.2s	144.1	3.501
I	18m 48.1s	130.0	3.455
J	20m 13.2s	156.4	2.764
G	18m 46.9s	125.0	2.650
H	20m 17.4s	160.5	2.161
D	18m 33.2s	110.0	1.956

I.3a. A-R Velocity Solution

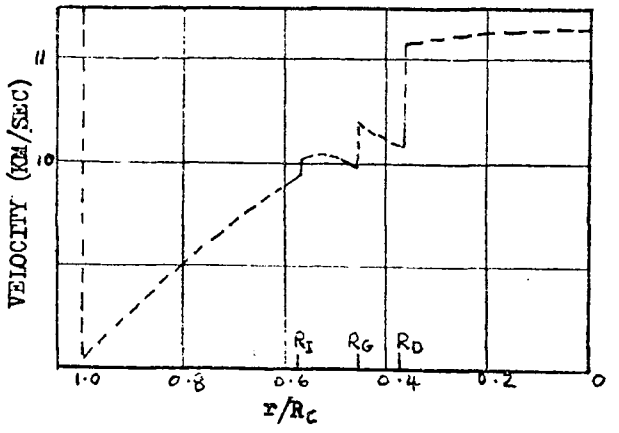

I.3c. A-R Velocity Model.

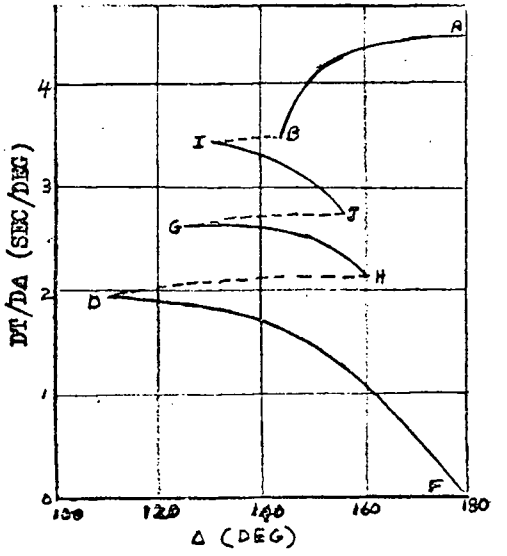

I.3d. A-R dt/dΔ Model.

Figure I.3. Adams and Randall 1964 Velocity Model

The inner core is likely to be solid." Julian, et al (1972) have since reported that they may have observed the phase PKJKP on seismograms recorded at the LASA array in Montana. The PKJKP phase is one which travels through the inner core as an S wave and elsewhere as a P wave. A liquid inner core would prevent the conversion from P to S.

Adams and Randall's (1963) analysis of seismograms written from certain New Zealand earthquakes in the range $148^{\circ} < \Delta < 156^{\circ}$ confirmed the existence of the latter part of the GH branch introduced by Bolt, and observations published by Nguyen-Hai (1961) are now known to belong to this branch. In 1964, Adams and Randall used traveltime data from 24 earthquakes and one series of nuclear explosions, together with observations published by other workers, to determine yet an additional branch to the traveltime curve derived by Bolt. This additional branch, IJ in their notation, was introduced to explain the earliest precursors observed, and necessitated the introduction of an additional velocity discontinuity at a radius $r = 0.57\ R_c$ (depth of 4,390 km) where R_c is the radius of the earth's core. This discontinuity is above the level of $r = 0.54\ R_c$, which is the depth to which rays would have to penetrate the core before a caustic would be formed at B, as in Bolt's model and consequently their model does not exhibit this feature. The second discontinuity was placed at a depth of 5,112 km. Their results were obtained by differentiating the traveltime data to obtain a $P - \Delta$ relationship. The Herglotz-Wiechert inversion technique, to be described later, was then used to obtain a velocity-depth model for the core. The details of their final model are shown in Figure 1.3a with the corresponding traveltime curve, velocity model, and $P-\Delta$ curves in Figures 1.3b, 1.3c, and 1.3d respectively. Thus Adams and Randall (1964) suggested the existence of two shells, each between 300 and 400 km thick, surrounding the inner core, with a small negative velocity gradient in each shell required to explain the observed traveltimes. Hannon and Kovach (1966) velocity filtered data from several events in the range 130° to 160°. The data were recorded at the extended

Tonto Forest Array in Arizona. The velocity filtering technique, in the form of time delaying and summation across the large array, in conjunction with conventional amplitude and traveltime analysis, yielded evidence of two short period precursors, IJ and GH, to the DF arrival at distances less than 140°. At least one of these precursors became an intermediate arrival to DF and AB at distances greater than 145°. Their results supported the model of Adams and Randall (1964).

From an analysis of traveltime and amplitude distance data of the World Wide Standardized Seismograph Network (WWSSN), Ergin(1967) found evidence for the existence of the GH and IJ branches of Bolt and Adams and Randall, and attributed the branches to two discontinuous increases in velocity at depths of 4,500 km and 4,685 km respectively. Delays in PKIKP traveltime observed at 153° and 162° were interpreted as the result of two low-velocity layers within the inner core. Ergin obtained two AB branches instead of one, as in previous models, the second branch being 3-6 seconds later than the first, and interpreted as the result of a decrease in velocity at a depth of 4,015 km. To obtain AB traveltime near 180° and beyond, he found that lower velocity was needed at the base of the mantle, and that this reduction in velocity resulted in the propagation of direct P up to 130° and beyond. Based on amplitude variations, the beginning of the PKIKP branch (that is, the point D in the previous models) was put at around $\Delta = 125^\circ$, and waves observed along the DF branch at distances shorter than 125°, down to 106° were interpreted as ordinary reflections from the core boundary, which were not quite extinguished at the critical angle.

Bolt (1968) found no evidence for the delays at 153° and 162° reported by Egin (1967). A group of small DF arrivals about 1 second earlier than expected in the range $156^\circ < \Delta < 160^\circ$ seemed to indicate either that the curvature in that range had been overestimated, or the presence of a slight discontinuity in the inner core near a depth of 5,520 km.

Gogna (1968) analysed traveltimes of about 3000 observations from 35 earth-

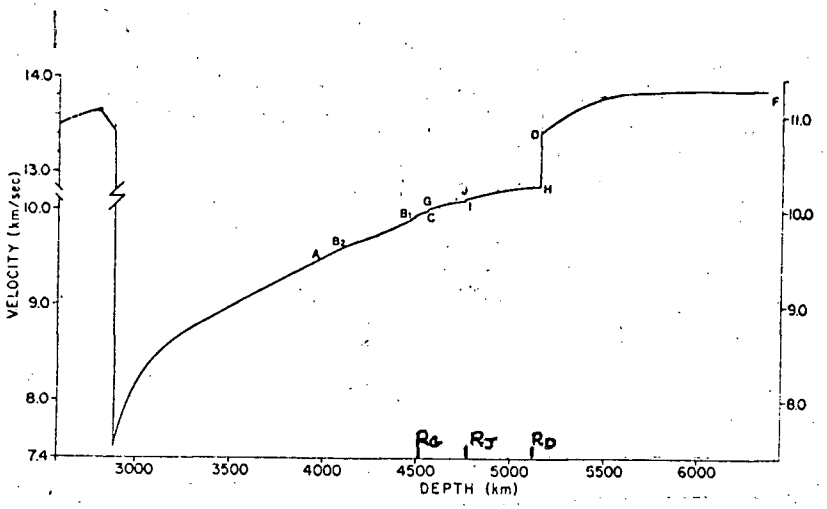

I.4b. Buchbinder's Velocity Model.

R_G, V_G, -1821 km (0.524R_c)
9.99 -10.00 km/sec

R_J, V_J, -1521 km (0.437R_c)
10.15-10.17 km/sec

R_D, V_D, -1226 km (0.353R_c)
10.26-10.83 km/sec

Cusp	Δ (Deg)	DT/DΔ (Sec/Deg)
G	140.0	3.18
J	142.0	2.61
H	156.0	2.08
D	120.0	1.91

I.4a. Buchbinder's Velocity Solution

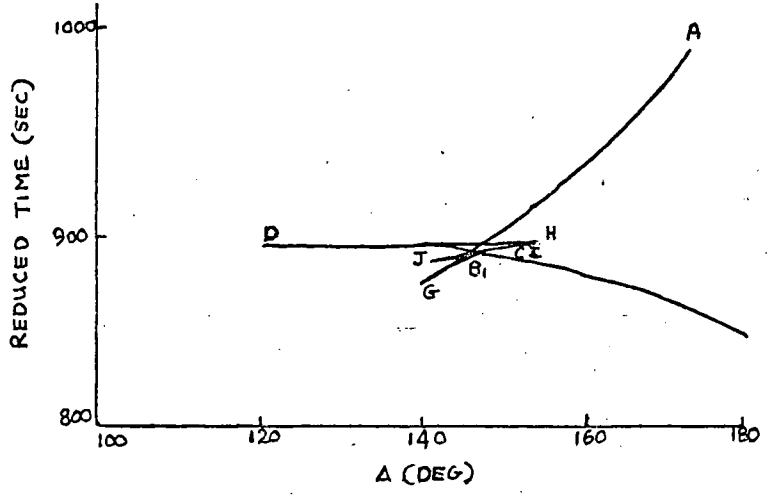

I.4c. Buchbinder's Reduced Times.

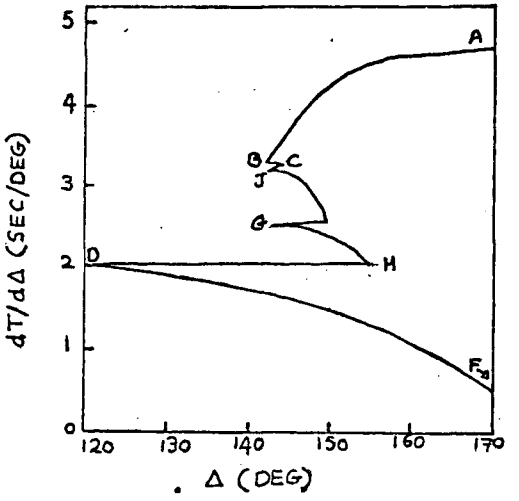

I.4d. Buchbinder's dt/dΔ Model.

Figure I.4. Buchbinder's 1971 Velocity Model.

quakes and confirmed, once more, the existence of the GH branch of precursors as postulated by Bolt. On his model, GH extended from 130° to 153°, but the possibility of it extending beyond 153° was not ruled out. In contrast, he obtained no evidence in support of the additional IJ branch as suggested by Adams and Randall.

Buchbinder (1971) examined traveltimes and amplitudes of PKP and higher multiple K phases from a worldwide distribution of short period seismograms. In his resulting velocity model, the velocity at the bottom of the mantle is 13.44 km/sec. resulting in a negative velocity gradient, the velocity decreasing from 13.6 km/sec. at a depth of 2,700 km to 13.44 km/sec. at the core-mantle boundary, placed at a depth of 2,892 km. The caustic B is placed at $\Delta = 143^{\circ}$. The observed traveltimes and amplitudes of PKP were interpreted to give the turning points D and G near 120° and 140° respectively rather than at 110° and 125° as in previous models. Together with the traveltimes and amplitudes of the higher multiple K phases these resulted in a velocity discontinuity of 0.01 km/sec. at a depth of 4,550 km to account for the earliest forerunners of PKP, and a second discontinuity of 0.02 km/sec at a depth of 4,850 km to account for the later forerunners. Since he could not resolve the forerunner data into branches, he was not able to define the discontinuity precisely, but instead produced the two branches of forerunners to illustrate the possible range of traveltimes and amplitudes. The top of the inner core boundary was placed at a depth of 5,145 km $\pm$ 10 km, and represented a discontinuity of 0.576 km/sec. These results are listed in Figure 1.4a. Figures 1.4b, c and d show Buchbinders velocity model, the reduced traveltimes, and the $P - \Delta$ curves correspo nding to his model. The branches CGG' and IJJ' of Buchbinder's model correspond to the IJ and GH branches, respectively, of the model of Adams and Randall (1964). A significant difference is that on Buchbinder's model, the sections GG' and JJ' of the respective branches

represent phases partially reflected off the corresponding boundaries, whilst they represent the transmitted phases on the Adams and Randall model.

1.3 Seismic Velocities and Physical Properties of the Core.

1.3.1 Central Density of the Core

The velocities of P and S body waves, α and β respectively, are given by the equations (Bullen, 1963).

$$\rho\alpha^2 = k + 4/3\mu, \quad \rho\beta^2 = \mu$$

where k is the bulk modulus or incompressibility of the medium ρ is the density, and μ is the corresponding rigidity. From these equations, we can obtain the quantity

$$\phi = k/\rho = \alpha^2 - 4/3\beta^2$$

The variation of density ρ with depth for a non-homogenous region is given by (Bullen, 1963).

$$d\rho/dz = \theta g\rho/\phi$$

where g is the gravitational force per unit mass and

$$\theta = dk/dp - g^{-1}\, d\phi/dz \qquad (1)$$

Here the quantity p denotes hydrostatic pressure. For a chemically homogenous medium, θ is unity. For values greater than unity, θ gives a measure of the addition of heavy material in excess of purely hydrostatic compression of a homogenous medium.

The Jeffreys' model for the core, with its large negative velocity gradient in the transistion region yields a value of $d\phi/dz \simeq -15 \times 10^3$ cm/sec Assuming gravity at a depth of 5000 km to be approximately 600 cm/sec^2, equation (1) becomes

$$\theta = dk/dp + 25$$

Reasonable values for dk/dp in the core, based on the theory of solid state, range from 3 to 5 units. Consequently, with a velocity decrease in the transistion region, as in the Jeffrey's model, θ becomes approximately 30 units. This value for θ is not only greater than at any other region

in the earth, but implies the admixture of a considerable proportion of material which is denser than inthe outer core. This entails, in turn, a large density increase at the inner core boundary, and a central denisty of about $20 g/cm^3$. On the other hand, Bolt's (1964) T_2 model has zero velocity gradient in the transition region, and Θ is then of the order of 5 units, implying a central density of about 15 gm/cm^3. This lower value of central density is more compatible with results of recent laboratory experiments using transient shock wave techniques to infer the elastic properties of iron at 4 megabars These results indicate a maximum terrestrial central density of the order of $13 g/cm^3$.

The effect of positive velocity gradients in the transition region, such as those in Buchbinder's (1971) model would be to reduce the index θ even further, and to bring the central density even lower than in the Bolt case. The effect of combined positive and negative velocity gradients, as in the Adams and Randall (1964) model, would, providing the negative gradient is reasonably small, result in a central density for the core slightly higher than that predicted in the Bolt case.

It is apparent, then, that core velocity models do provide empirical restraints on acceptable density profiles with the core, and vice versa.

1.3.2 Solidity of the Inner Core

That the outer core is in a fluid state has been established by the failure to observe transmitted S waves in the appropriate distance range. The velocity of S waves is a direct function of the rigidity of the medium, which, for a liquid, has the value zero.

At the boundaries of the transition region in the Bolt (1964) model, the velocity of P waves, α, increases by 3% and 9%, corresponding to 6% and 18% increases in α^2. If the transition region were in a liquid state, the velocity of P waves through it would be given by (since $\mu = 0$)

$$k = \rho\alpha^2$$

The jump in α^2 of 6% at the first boundary requires a corresponding increase

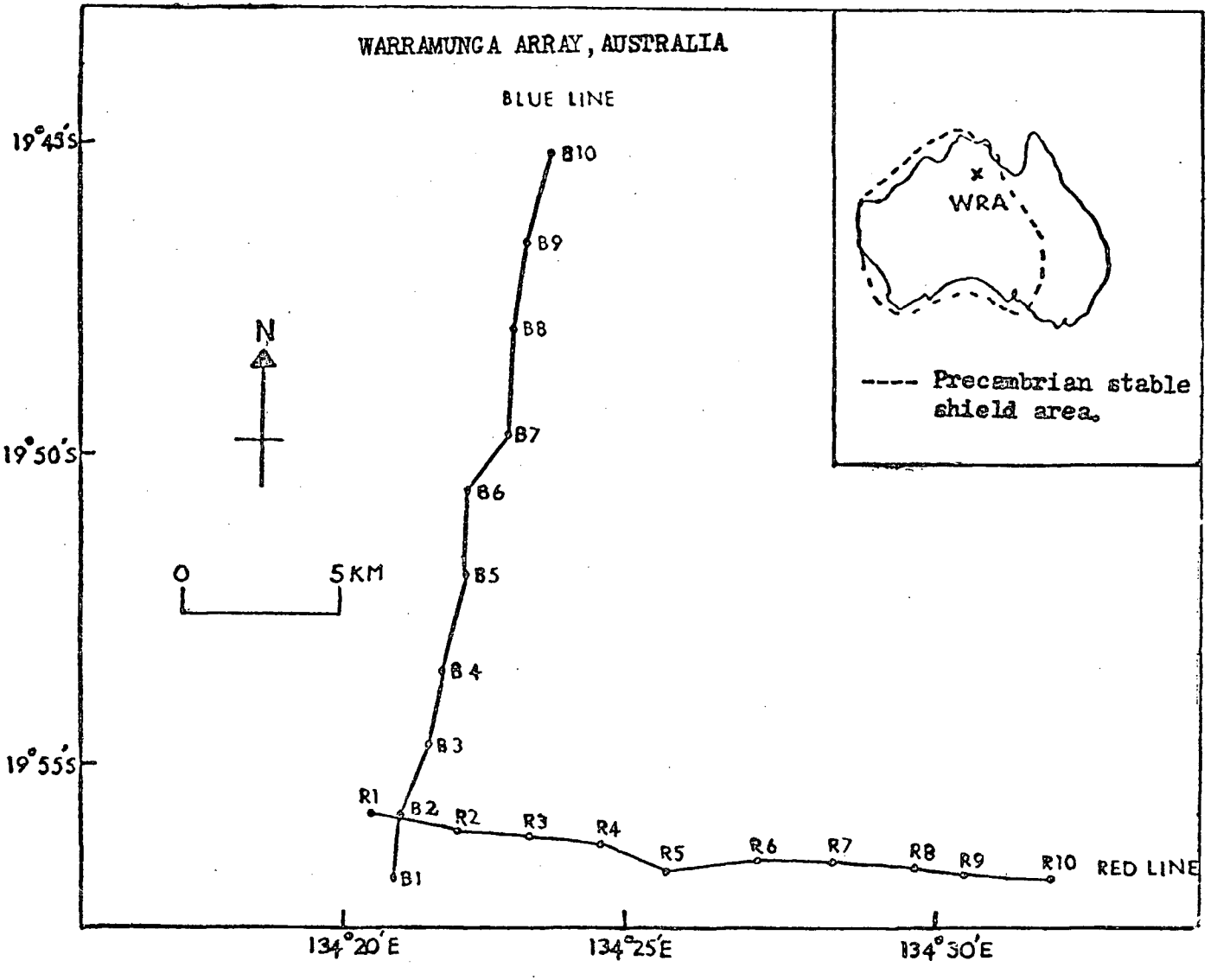

Figure I.5. The Warramunga seismic array. The inset shows the location of the array in the stable shield area.

in k of about 6%, since the density ρ is not likely to increase by any large amount. Bullen (1963) has indicated that an increase in k of this magnitude is unlikely, and consequently the equation has to be modified to include the rigidity term μ i.e.

$$k + 4/3\,\mu = \rho\alpha^2$$

With this modification, some of the increase in α^2 at the boundary can be taken up by the rigidity term, resulting in a smaller increase in k at the boundary. This implies that the material in the transition zone has significant rigidity, and is therefore not completely liquid as in the outer core. Similarly, the larger jump in α^2 of 18% at the boundary of the inner core requires an even larger increase in rigidity in the inner core, indicating the inner core to be completely solid. Bullen (1963, p.243) advances further arguments in favor of a solid inner core. That the inner core is solid has been confirmed recently by observation of the PKJKP phase by Julian *et al* (1972)

1.4 The Warramunga Seismic Array

The Warramunga seismic array (WRA) situated near Tennant Creek in Northern Territory, Australia is one of four seismic arrays of the United Kingdom Atomic Energy Authority (U.K.A.E.A.) type which were deployed as a means of detecting and identifying underground nuclear explosiions. The other three arrays are located in Canada (YKA), Southern India (GBA) and in Brazil. Another British designed array (EKA), smaller than any of the others, is located in Scotland.

WRA began operation in 1965. It is situated on granite outcrops in the stable Precambrian shield area, approximately 500 km from the nearest point of the Australian coast (see inset, Figure 1.5). It is a medium aperture array consisting of twenty short-period vertical component Willmore Mk II seismometers with a natural period of one second and a damping factor of 0.6. The seismometers are arranged in two lines approx-

Table 1.1 Coordinates of the Individual Seismometers of the Warramunga Seismic Array

Seismometer	Latitude E	Longitude S	Cartesian Coordinates X, km	Y, km	Elevation, feet
B1	134.34776	19,96097	-0.310	-1.476	1294.85
B2	134.35250	19.94417	0.183	0.373	1284.27
B3	134.35681	19.92453	0.638	2.558	1265.89
B4	134.36050	19.90497	1.025	4.724	1252.65
B5	134.36954	19.87971	1.762	7.519	1218.72
B6	134.36852	19.85645	1.863	10.095	1200.07
B7	134.38080	19.84227	3.150	11.662	1268.09
B8	134.38213	19.81541	3.291	14.635	1176.96
B9	134.38530	19.79286	3.623	17.132	1184.94
B10	134.39418	19.76862	4.554	19.816	1188.50
R1	134.34085	19.94411	-1.033	0.391	1281.07
R2	134.36555	19.94890	1.552	-0.140	1265.19
R3	134.38831	19.95000	3.934	-0.264	1236.49
R4	134.40802	19.95181	5.998	-0.465	1228.55
R5*	134.42764	19.95949	8.052	-1.314	1217.83
R6	134.45578	19.95525	10.998	-0.846	1155.42
R7	134.47742	19.95667	13.263	-1.004	1167.15
R8	134.50191	19.95726	15.826	-1.074	1212.53
R9	134.51631	19.95912	17.334	-1.281	1190.68
R10	134.54195	19.96109	20.016	-1.502	1161.54

* moved to new site 18 September, 1968.

R2 and R6 have subsequently been moved to new sites.

The geographic coordinates of the origin of the cartesian coordinate system are 19.94777°S, 134.35081°E.

imately at right angles to each other (see Figure 1.5), each line being 22.5 km long and consisting of ten seismometers equally spaced. The geographic coordinates of the individual seismometers and the Cartesian coordinates relative to the point of intersection of the two arms of the array are listed in Table 1.1.

The seismometers are operated at a displacement magnification of about 250,000. The signals from each seismometer are telemetered to a central recording station where they are recorded simultaneously with a digital time code on 24-track FM magnetic tape. The precision timing and FM telemetry system are described in detail by Truscott (1964), and Keen et al. (1965). All data are forwarded to the U.K.A.E.A. center in England.

A duplicate recorder is operated by the Australian National University. As a means of improving its efficiency, a small array consisting of two lines, each of length 2.5 kilometres and containing five vertical component seismometers, was installed in 1967, parallel to the main arms of the array. This small array or 'cluster' discriminates against random noise by direct summation, and triggers the tape recording system only when the conelator output exceeds a specified trigger level. The mode of operation is similar to that of the 24 element cluster in use at YKA and is described in Whiteway (1965).

1.5 Use of an Array in Determining Structure

Before the development of seismic arrays, the traveltimes of P and S waves provided the most reliable means for investigating the structure of the earth's interior. Differentiation of the smoothed traveltime-distance ($T-\Delta$) curves yielded the first derivative, $dT/d\Delta$, as a function of distance, Δ. This derivative was then used in the Herglotz-Wiechert integral (to be described later) in order to determine a velocity-depth profile for the region under consideration. Extensive use of this method has yielded velocity-depth profiles that are in reasonable agreement except in the upper 1000 kms of

of the mantle and the anomalous transition region of the core. However, an array can be used to measure $dT/d\Delta$ directly, and is capable of supplying more fine-structure detail than the conventional traveltime method. Also, the signal enhancing ability of an array makes possible the detection and identification of phases too small to be detected on a single seismogram. These properties of an array are utilized fully in this study.

Past use of seismic arrays in the investigation of the structure of the earth's interior has been confined almost exclusively to studies of the earth's mantle. Such studies were pioneered by Niazi and Anderson (1965) who investigated the upper mantle structure beneath western North America by measurement of P-wave traveltime gradients at the Tonto Forest Array (TFSO) in central Arizona. The first studies of this nature at WRA were made by Cleary et al (1968) who concluded, among other things, that the $dT/d\Delta$ measurements were strongly perturbed by variations in structure underneath the array. Wright (1968) using $dT/d\Delta$ measurements at WRA from 30 earthquakes in the Marianas Islands and surrounding regions found evidence for a low velocity layer at a depth close to 800 km in the mantle. His complete work on the lower mantle using WRA data is contained in his doctoral thesis (Wright, 1970).

As the present study is of similar type to that made by Wright, many of the techniques of measurement and analysis devised and used by him have been adopted for use in this study. These will be fully described in Chapter 2.

CHAPTER 2

MEASUREMENT AND ANALYSIS

2.1 Determination of $dT/d\Delta$ and azimuth from a seismic array.

2.1.1 Some Possible Methods

In order to obtain a velocity distribution for the earth's core, knowledge is required of the variation of the traveltime gradient, $dT/d\Delta$, with depth in the core. This is obtained by determining $dT/d\Delta$ for those seismic waves which are known to pass through the earth's core, arriving at the surface at distances in the range 110° to 180° for PKP. Both $dT/d\Delta$ and the azimuth of arrival at a seismic array can be estimated from the arrival times at the individual seismometers in at least three ways:

(1) A Correlation Method:

The appropriate time delays corresponding to tuning to a particular azimuth and $dT/d\Delta$ for each of the two lines are inserted for each seismometer of the array, and a summed output determined for each line. The normalised output amplitudes of the summed lines are cross-correlated assuming a sinusoidal signal and the correlator output, determined as a function of azimuth and $dT/d\Delta$, gives maximum value at the signal azimuth and velocity, (Birtill and Whiteway, 1965). This method was explored in some detail by Wright (1970) who concluded that it gave insufficiently high precision to be of any use in his work on mantle P-wave velocities. Even higher precision is required when dealing with the earth's core, since the $dT/d\Delta$ values for the core are at most half as large as the $dT/d\Delta$ values for the mantle. A new correlation technique which may give more reliable azimuth and $dT/d\Delta$ measurements has been described by Muirhead (1968).

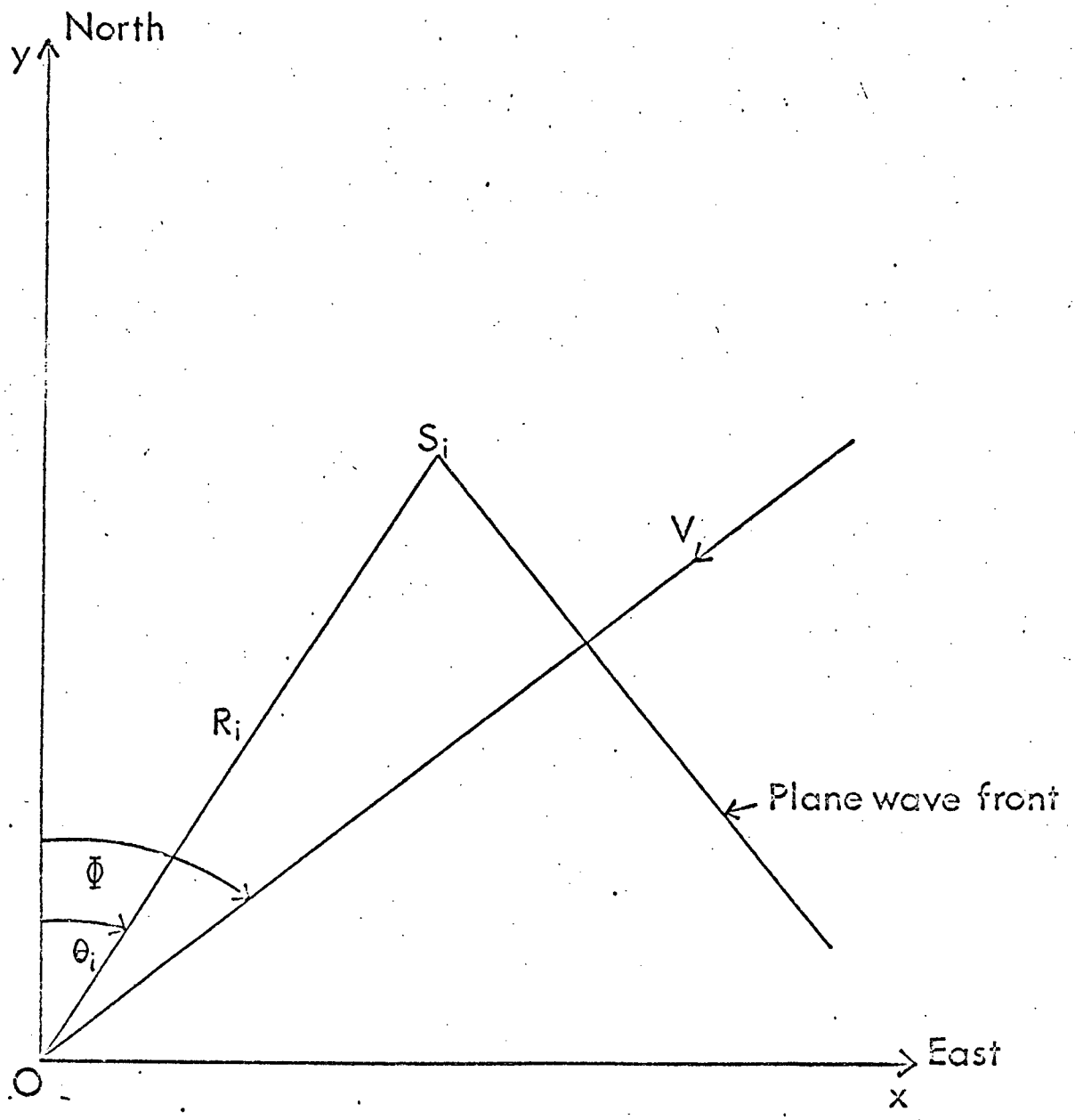

Figure 2.1 Diagram to illustrate a least-squares method of estimating $dT/d\Delta$ and azimuth.

(2) A Fourier Transform Technique:

$d\Delta/dT$ and azimuth values are determined at a number of different frequencies by measurement of differences in phase angle of Fourier spectral densities across a fixed array (Shima et al, 1964). Again, however, this method does not appear to be precise enough for use in deep earth investigations.

(3) A Least-Squares Technique:

The best straight line is fitted to the set of arrival times at the individual seismometers by the method of least squares. The individual arrival times are functions of the azimuth of arrival, the arrival time at the origin of the array and the traveltime gradient or apparent velocity. Consequently their least-squares fit results in the best possible estimate of all three parameters, for the particular event being analysed. Since this method was used in obtaining the $dT/d\Delta$ measurements in this study, it will now be described in more detail.

2.1.2 Details of the Least Squares Method

The least squares method has been described by Kelly (1964) and Otsuka (1966). Let the origin O in Figure 2.1 be the point of intersection of the two arms of WRA, and take a cartesian coordinate system with the y and x axes pointing north and east respectively, in the direction of the two arms of the array. For a medium aperture array such as WRA, and at the distances in question, the wave front can be assumed to be plane provided the structure of the crust and upper mantle in the vicinity of the array is reasonably simple. Consider a seismometer at S_i, distance R_i from O_1 and let $\angle S_i O_y$ by θ_i. Suppose a P wave arrival crosses the array from azimuth $\emptyset$ with apparent

surface velocity V, and let the arrival time at S_i be T_i subject to an error e_i. Let the arrival time at the origin of the array be To. It can be seen from Figure 2.1 that

$$T_o = T_i + R_i \cos(\phi - \theta_i)/v + e_i$$

$$\therefore e_i = T_o - T_i - v^{-1}(R_i \cos\phi \cos\theta_i + R_i \sin\phi \sin\theta_i)$$

$$= T_o - T_i - v^{-1}(y_i \cos\phi + x_i \sin\phi)$$

where $y_i = R_i \cos\theta_i$ and $x_i = R_i \sin\theta_i$. Furthermore, if we let $P = \sin\phi/v$ and $Q = \cos\phi/v$, then

$$e_i = T_o - T_i - (y_i Q + x_i P)$$

and if N is the number of seismometers in the array,

$$\sum_{i=1}^{N} e_i^2 = \sum_{i=1}^{N} (T_o - T_i - (x_i P + y_i Q))^2$$

$$= f(P, Q, T_o)$$

To obtain best estimates of the three unknowns P, Q, and To, and hence best estimates of azimuth Ø, apparent velocity V, and traveltime To at the origin of the array, the least squares condition that the sum of the errors, or f(P, Q, To), be a mimimum is used. Thus

$$\partial f/\partial P = \partial f/\partial Q = \partial f/\partial T_o = 0$$

This gives rise to the three normal equations:

$$\sum_{i=1}^{N} x_i (T_o - T_i - (x_i P + y_i Q)) = 0$$

$$\sum_{i=1}^{N} y_i (T_o - T_i - (x_i P + y_i Q)) = 0$$

$$\sum_{i=1}^{N} (T_o - T_i - (x_i P + y_i Q)) = 0$$

or, if we let $\sum_{i=1}^{N} x_i y_i = [xy]$, $\sum_{i=1}^{N} x_i^2 = [xx]$ etc, the equations can be written:

$$[xx]P + [xy]Q + [xT] - [x]T_o = 0$$

$$[xy]P + [yy]Q + [yT] - [y]T_o = 0$$

$$[y]P + [x]Q + [T] - NT_o = 0$$

The values of x_i and y_i, the cartesian coordinates of the individual seismometers, are known and the values of T_i are determined by measurement of the arrival times at each of the seismometers. Consequently the three normal equations can be solved to give the best estimates of P, Q, and To. From these, we obtain:

$V=(P^2 + Q^2)^{-\frac{1}{2}}$ $\equiv$ apparent velocity of P wave

$dT/d\Delta = r_o/V$ at the deepest point of the ray (r_o is the mean radius of the earth)

and $\phi = \mathrm{Tan}^{-1}\ (P/Q) \equiv$ azimuth of arrival at the array.

A knowledge of To, the arrival time at the origin of the array, and the N.O.A.A. (National Oceanic and Atmospheric Administration of the U.S.) origin time of the event enables the traveltime to be determined.

Knowledge of the errors in the calculated quantities, particularly in the $dT/d\Delta$ values, are essential if statistical significance tests are to be applied in the smoothing of the data at a later stage. On the assumption that the errors e_i in the measured onset times are independent Gaussion variables, each with mean zero and variance Kelly (1964) showed that the root-mean-square errors in V_1, $dT/d\Delta$ and ϕ are given by:-

$$(\delta V/V)_{r.m.s.} = (\delta(dT/d\Delta)/\ dT/d\Delta)_{r.m.s} = \sigma V/(ND)^{\frac{1}{2}} (\mathrm{Var}\, x\, \mathrm{Cos}^2\phi - 2\,\mathrm{Cov}(x,y)\,\mathrm{Sin}\,\phi\,\mathrm{Cos}\,\phi + \mathrm{Var}\, y\ \mathrm{Sin}^2\phi)^{\frac{1}{2}}$$

$$(\delta\phi)_{r.m.s.} = \sigma V/(ND)^{\frac{1}{2}} (\mathrm{Var}\, x\ \mathrm{Sin}^2\phi + 2\,\mathrm{Cov}(x,y)\,\mathrm{Sin}\,\phi\,\mathrm{Cos}\,\phi + \mathrm{Var}\, y\ \mathrm{Cos}^2\phi)^{\frac{1}{2}}$$

(in radians)

where $D = \mathrm{Var}\, x\ \mathrm{Var}\, y - (\mathrm{Cov}(x,y))^2$

$$\mathrm{Var}\, x = 1/N \sum_{i=1}^{N} (x_i - \bar{x})^2$$

$$\mathrm{Var}\, y = 1/N \sum_{i=1}^{N} (y_i - \bar{y})^2$$

$$\mathrm{Cov}(x,y) = 1/N \sum_{i=1}^{N} (x_i - \bar{x})(y_i - \bar{y})$$

$$\bar{x} = 1/N \sum_{i=1}^{N} x_i$$

$$\bar{y} = 1/N \sum_{i=1}^{N} y_i$$

The estimation of the quantity σ, poses a slight problem. Corbishley (1970) approached the problem by estimating a random reading error for a number of events occurring in a small region of the earth. Wright (1970) preferred to calculate a value of σ for each set of relative onset times on the grounds that the error in each onset depends on four main factors: (1) The waveform of the event, since low frequency events give less clearly defined peaks and zeros. (2) The signal-to-noise ratio since random bursts of noise cause spurious changes in waveform from one seismometer to the next. (3) The instrumental constants of the seismometers which vary slightly from seismometer to seismometer and (4) rapid variation in local structure, an azimuth-and-distance-dependent feature. Each value of residual ϵi is calculated after P, Q and To have been determined.

Assuming that the residuals have zero mean and variance σ^2 characteristic of that particular set of arrival times, then

$$\sigma^2 = \sum_{i=1}^{N} \epsilon_i^2 / N-3$$

The value of σ thus determined contains not only random reading errors, but also systematic errors due to possible differences in instrumental constants of the individual seismometers and rapid variations in local structure.

2.2 Measurement Techniques

2.2.1. Data Available for the study

As mentioned previously, data acquired by the Australian National University for WRA are recorded on 24 Channel FM analog magnetic tape. At the time the data used in this study were acquired,

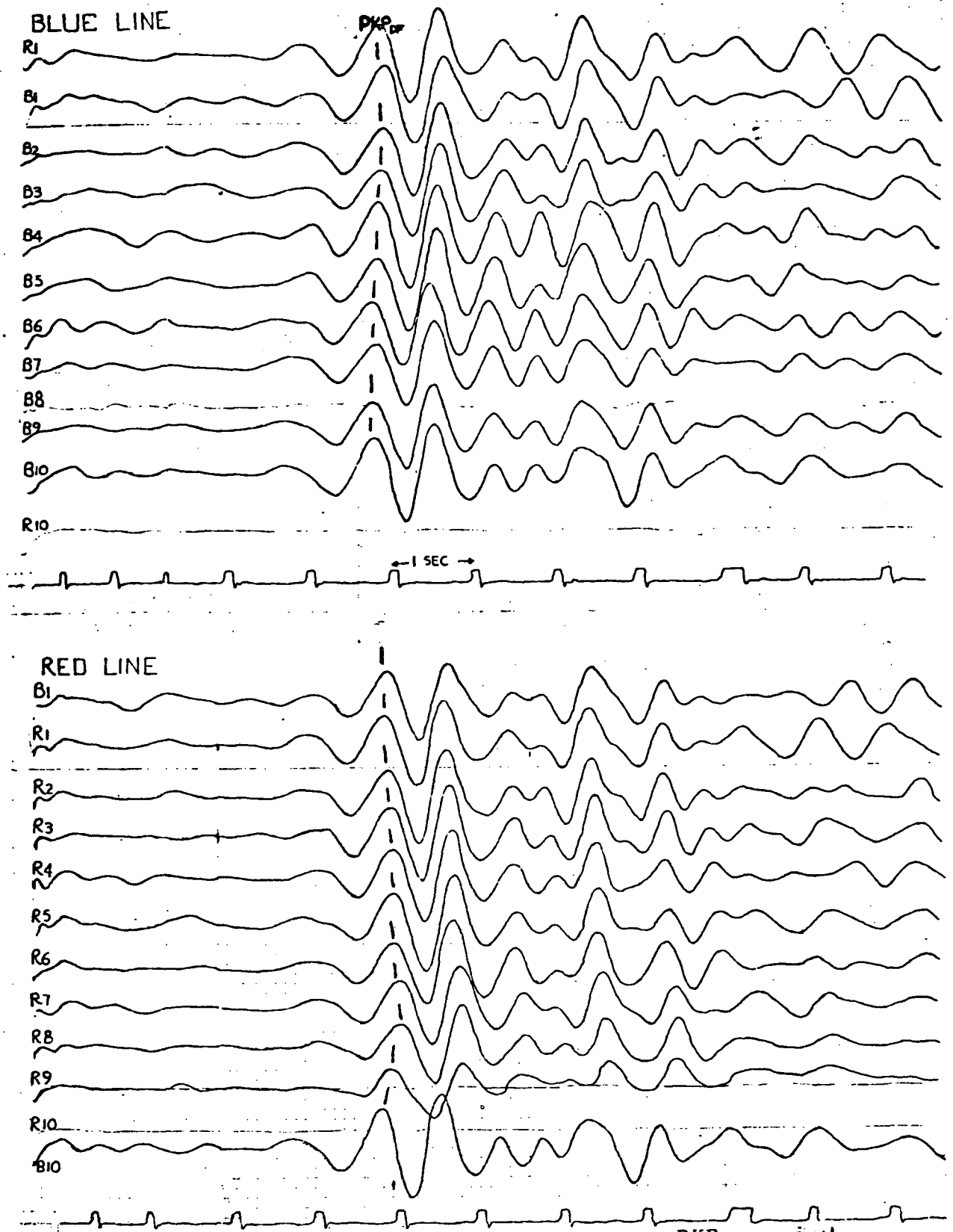

Figure 2.2 Example of data showing strong PKP_{DF} arrival.

a system of digital conversion and analysis had not been instituted. Consequently, the usual procedure was to play back the data onto chart paper.

Firstly, the seismic signals on tape were filtered using narrow bandpass filters (0.4 to 2.0Hz) having identical characteristics. A 16-channel chart recorder was the only one available at the time, and the twenty seismic traces were therefore played out in a two-step procedure. The signals from one line of the array, together with the signals from the end seismometers of the other line and a timing signal were reproduced in one pass. The line positions were reversed and the procedure repeated. It was often noted that the amplitude of the seismic traces varied considerably over the time range of interest. This necessitated duplication of certain parts of the records at higher or lower gain settings in order to obtain amplitudes best suited for analysis. The playback speed (40 mm/sec) used in obtaining the paper records enabled high resolution timing to be achieved. An example of the paper seismograms is shown in Figure 2.2. Note the clear waveforms which enabled precision measurement of the relative distances between peaks or troughs of a given cycle across the array.

Seismograms from the 115 earthquakes used in this study were reproduced in the above manner. They represented data over the distance range of 113° to 176° although this range is not uniformly covered due to the location of active seismic zones with respect to WRA. The majority of events occurred over the distances of 130° to 150°. Among other things, this uneven spread of the data later resulted in some difficulty in smoothing the measured $dT/d\Delta$ values. The sparseness of data in the ranges 120° to 130° and 150° to 160° led to difficulty in determining precisely the end points of the

precursor branches of the traveltime curve, a point which will be discussed later. A list of the earthquakes used in this study is given in Appendix II.

2.2.2 Measurement of $dT/d\Delta$ and Azimuth

If precision in measurement of $dT/d\Delta$ comparable to precision obtained from an array such as LASA is to be obtained on a medium aperture array such as WRA, onset times must be measured with a standard deviation of between 0.01 and 0.03 seconds. The measurement of P onset times with such accuracy is extremely difficult, if not impossible. Measurement, instead, of relative P times obtained by matching P waves recorded at each seismometer can yield accuracy of the required degree. Since the method was first described by Evernden (1953), the technique of measuring relative onset times by matching waveforms has been commonly used in the calculation of phase velocities of surface waves across tripartite arrays. Matching surface waves with periods of 20 seconds or larger to an accuracy of 0.2 seconds is comparable to matching P waves with periods of about 1 second to an accuracy of 0.01 sec. With the chart speed of 40mm/sec used for the paper records, waveforms could be matched to an accuracy of $\pm$ 0.5 mm, which corresponds to an average timing error of 0.012 sec. Thus the precision in timing measurement was satisfactory.

The technique used in matching the waveforms is as follows: (1) The paper speeds on the two lines of the array, the Red and Blue lines, were determined by averaging at least five sets of measurements of the distance between 5-sec. intervals in the region of measurement of $dT/d\Delta$, for each line. The two values thus obtained were further averaged to give an overall value for the particular event. It was

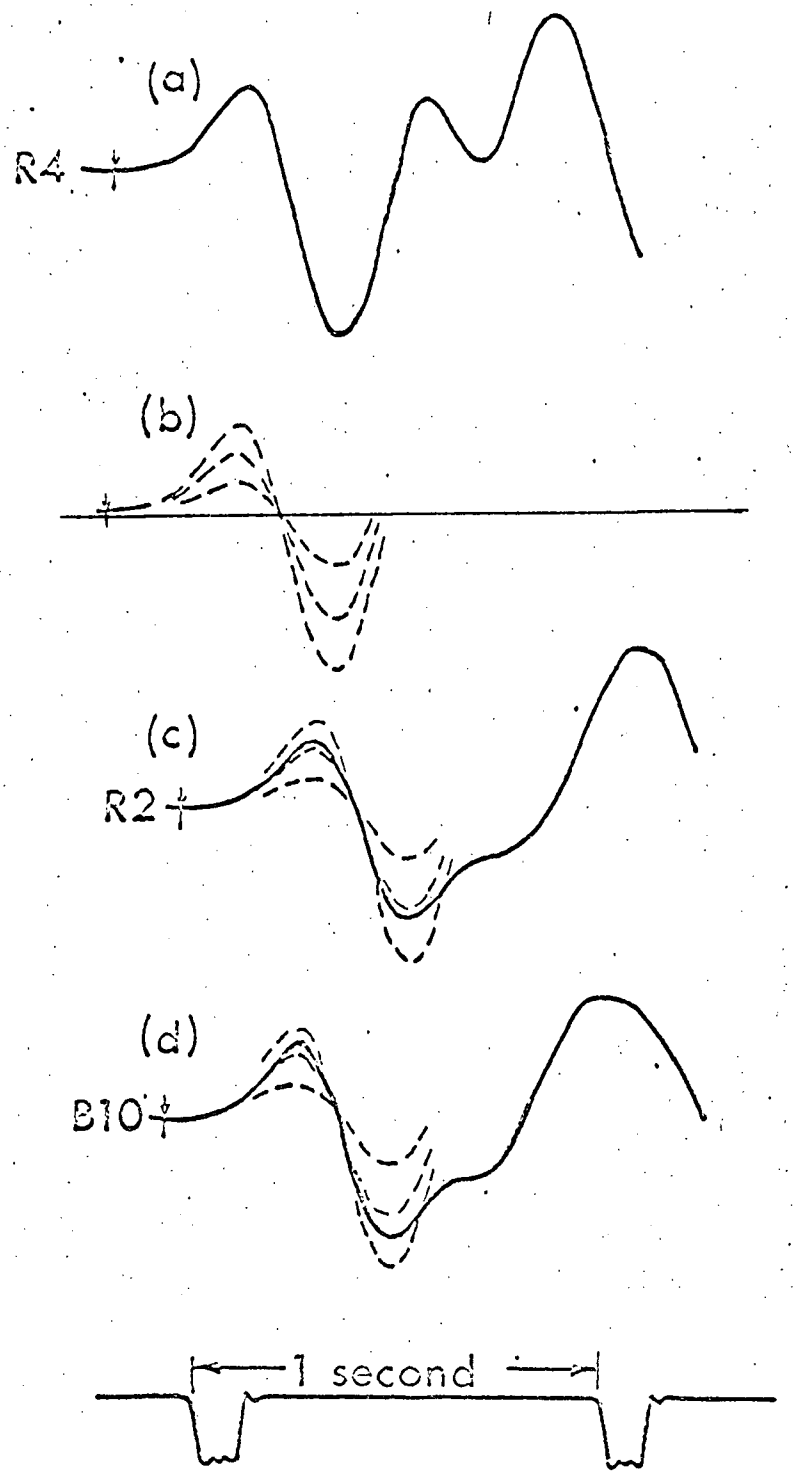

Figure 2.3. Matching technique for determining relative arrival times at each seismometer. From the record at pit R4(a), a family of curves with different amplitudes is constructed (b), and matched with the records at the other pits (c), (d).

found in practice that this overall speed was within 0.10 mm/sec of the speed of either line, thus eliminating the necessity of a correction term. (2) Parallax corrections in millimetres were determined for each trace by observing the distance deviations in the onset of square wave pulses applied simultaneously to all traces at the start of the record. The corrections were never more than 1 mm with the vast majority centering around 0.5 mm. (3) A trace was selected from both lines of the array, which appeared to be the least contaminated by noise or other interferences (Figure 2.3a). One cycle of the phase whose $dT/d\Delta$ value was to be measured, was traced onto transparent paper. The vertical line corresponding to a chosen reference time mark was drawn on the transparent paper, as was the horizontal line indicating the zero-signal level of the trace. In order to compensate for variations in amplitude between traces for a particular event, the selected curve was used to construct, on the same transparent paper, a series of curves of different amplitudes, as shown in Figure 2.3b. (4) Using this transparent paper as an overlay, the curves on it were matched with each seismometer output for that event, and the position of the first zero of each seismometer output was determined relative to the reference time mark. In addition the relative times of the first peak and first trough of the appropriate cycle for each trace were measured. Thus three sets of relative onset times were determined for the particular phase of the particular event. In some cases, only one or two sets of relative times could be determined, depending on the clarity of the waveform.

The reason for determining more than one set of onset times, and hence $dT/d\Delta$ and azimuth, for a particular phase is to compensate to some extent for the changes in waveform fromone seismometer to another. These changes may be due to rapid variations in local structure beneath the array or even to multiple arrivals caused by structure at the deepest point of the ray. Random noise effects could also play an important part in causing changes of waveform for the precursors to the PKIKP phases, which were often far smaller than PKIKP in the early parts of the appropriate distance ranges. Each set of arrival times, and consequently each $dT/d\Delta$ and azimuth determination for a particular phase, was regarded as independent.

By means of a computer program (Wright, 1970) the arrival times were used to calculate a least square value of $dT/d\Delta$, azimuth $\emptyset$ and arrival time To at the origin of the array. Residuals of the measured times relative to their least squares fit, were determined. If a seismometer residual was found to exceed 0.02 seconds, the corresponding onset time was discarded and the entire procedure repeated using the remaining times. In poorer fits from lower quality data, a rejection value of a 0.04 seconds was used. This rejection procedure ensured that the standard deviations of the onset times were kept less than 0.03 seconds, and consequently ensured the high precision of this method of determining $dT/d\Delta$ and azimuth. The root-mean-square errors in the least squares $dT/d\Delta$ and azimuth determination were also calculated by the program to facilitate future weighting of the data.

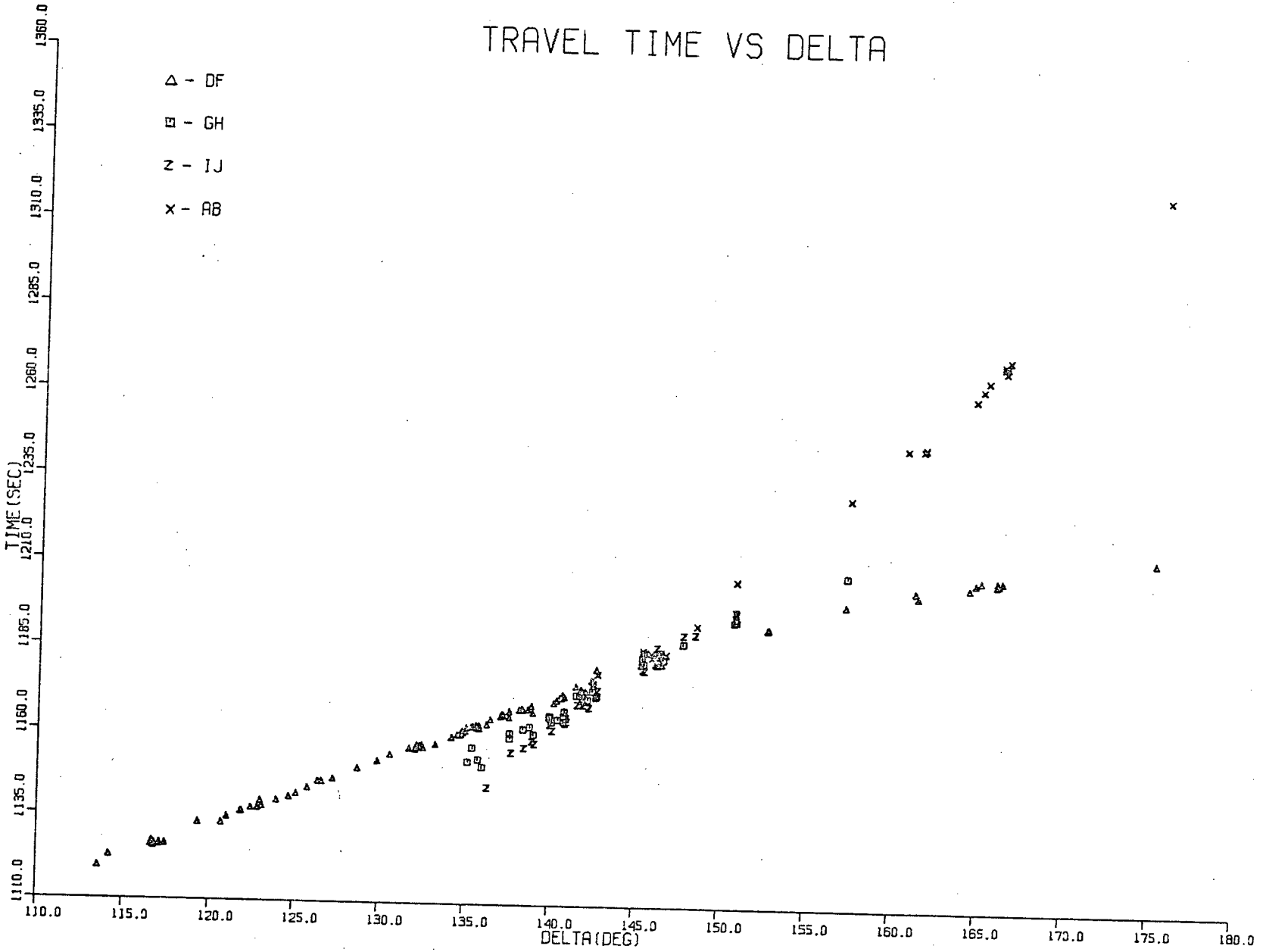

Figure 2.4. Measured Traveltimes

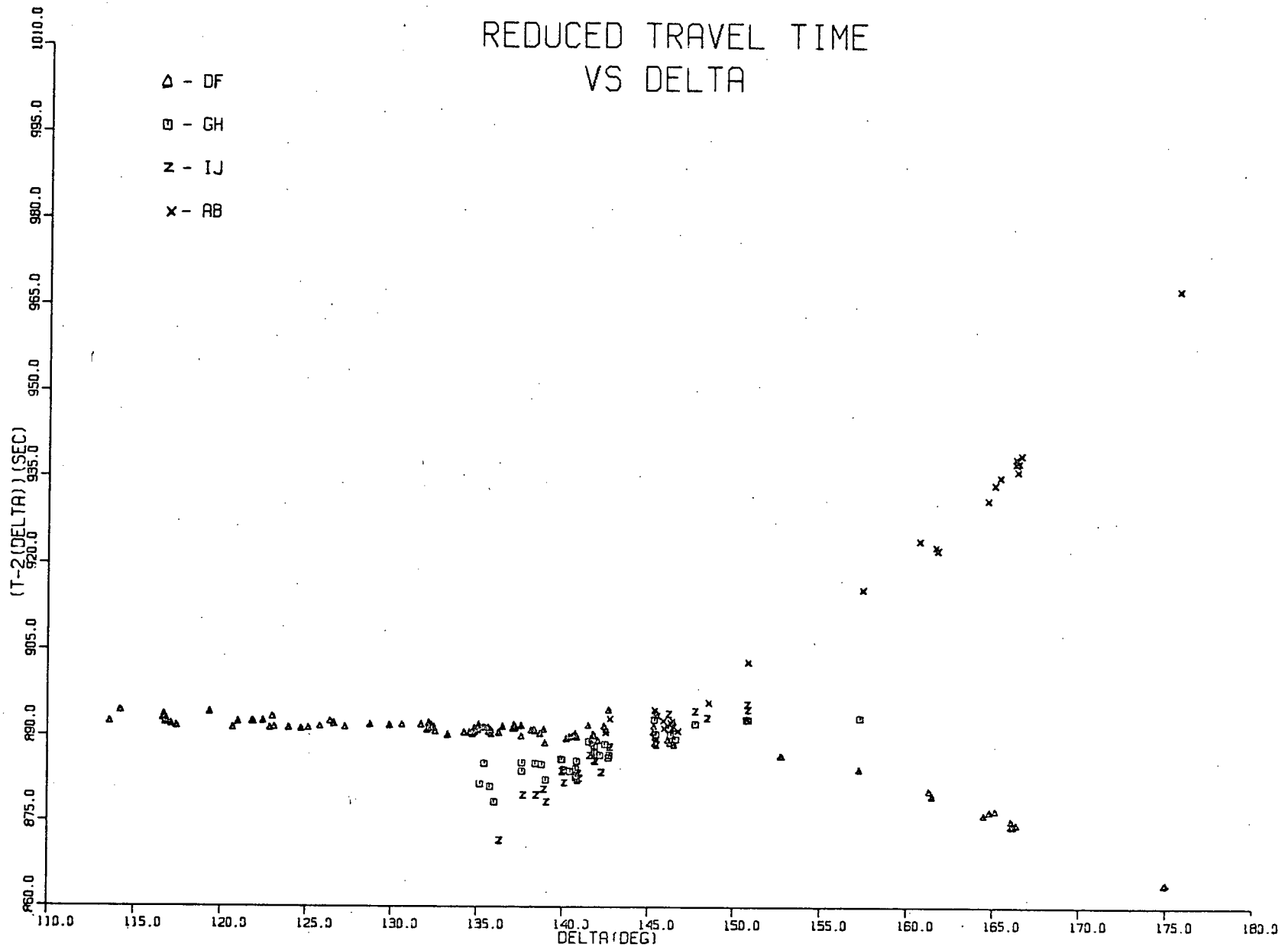

Figure 2.5. Reduced Traveltimes.

This matching waveform technique and subsequent calculations were carried out for any coherent signal observed on the seismograms within the time range of interest. It was often necessary, in the early parts of the appropriate distances ranges, to resort to the high amplitude data in order to measure the precursors to PKIKP.

If a particular phase was identified as belonging to one of the time travel branches on the basis of its $dT/d\Delta$ value and a rough estimate of its travel time, the actual travel-time was determined by measuring the onset time of a clear wave and subtracting from it the origin time as given by N.O.A.A. It was often difficult to pick the onset of the phase on the seismogram accurately, because of the background noise and in some cases where all phases arrived closely together, because of interference from preceding phases, for example in the range 140°- 145°. This resulted in quite a large scatter of travel-times and, as will be seen later, in the residuals with respect to the smoothed travel-times. To ensure uniformity, ellipticity and, focal depth corrections as described in Appendix III were applied to the travel-times.

The 115 events analysed in the above manner yielded a total of 574 $dT/d\Delta$ and 188 traveltime measurements for all PKP phases. Figures 2.4 and 2.5 show the traveltime and reduced traveltime measurements. These will be discussed further in Chapter 3. The $dT/d\Delta$ measurements are shown in Figure 2.7. The large scatter exhibited by the $dT/d\Delta$ values is mainly a consequence of systematic errors in their measurement. These errors now will be discussed in more detail.

2.2.3. Sources of Systematic Error in $dT/d\Delta$ and Azimuth Measurements

Systematic errors in $dT/d\Delta$ and azimuth measurements can be attributed to four main sources: (1) The effect of differences in seismometer constants (2) Differences in elevation of the individual seismometers (3) Ellipticity of the earth and (4) The effect of structure beneath the array.

(1) The effect of differences in the seismometer constants. Muirhead (1968) investigated the problem of phase shifts due to small differences is seismometer constants in a medium aperture array, and showed that for an instrument with a natural frequency of 0.9 Hz recording a sinusoidal motion of a period of 1 sec., the first zero of cross-over point of the recorded wave would be 0.04 sec. later than if the instrument had a natural frequency of 1.1Hz. He also showed that the effect of differences in the damping constants of the seismometers was of the second order and could be safely neglected. The seismometer calibration scheme in operation for U.K.A.E.A. arrays is described by Keen et al (1965). The natural frequencies of the instruments at WRA show small differences from one seismometer to another, with a maximum difference of about 0.18 Hz between R6 and B9. In addition, the frequencies vary slightly from day to day, again with a maximum variation of about 0.20 Hz from 0.9 to 1.1 Hz. In principle, it is possible to remove such errors. Wright (1970) investigated this problem fully, and obtained corrections to $dT/d\Delta$ with a maximum valve of about 0.05 sec/deg . He concluded that "the effect of differences in the natural periods of the seismometers on the onset times is, in almost all instances, too small to produce appreciable scatter of systematic errors in the values of $dT/d\Delta$ and azimuth". He investigated

parameters of the order of 8 - 10 sec/deg in magnitude, and consequently a correction of 0·05 sec/deg to these values is almost negligible. In the case of the earth's core, however, where the PKIKP branch has a value of $dT/d\Delta$ ranging from about 2.0 sec/deg to 0.0 sec/deg at 180°, a correction of that magnitude is more significant. Nevertheless, in the face of corrections for local structure (to be described later) which amounted in some instances to as much as 0.9 sec/deg, the correction for differences in seismometer constants seemed insignificant, and was consequently ignored in this study.

(2) Differences in Elevation of Individual Seismometers. The difference in elevation of the highest and lowest seismometers of the array is less than 0.05 km. At the large distances involved, the systematic difference in arrival time due to this difference in elevation is less than 0.01 sec. assuming a P wave velocity of 6km/sec at the earth's surface, and can consequently be ignored.

(3) Ellipticity of the Earth. The ellipticity correction to traveltimes is given by the following equation (see Appendix III).

$$\delta T = f(\Delta)(h_0 + h_1)$$

It is also possible to correct the $dT/d\Delta$ values for ellipticity by calculating δT for a number of imaginary epicentres at regular intervals of distance and azimuth, and differentiating the resulting tables to obtain $\delta(dT/d\Delta)$ - the ellipticity correction for the $dT/d\Delta$ measurements. Wright (1970) carried out this procedure and obtained maximum corrections of about 0.024 sec/deg . On the basis of larger corrections to be determined such as those involved in correcting for structure under the array and in restraining the smoothed $dT/d\Delta$ values to an acceptable travel time curve , he prefferred to ignore the ellipticity corrections to $dT/d\Delta$. The

same procedure is adopted in this study for similar reasons.

(4) Effect of Structure Underneath the Array. By far the most serious source of systematic errors in $dT/d\Delta$ and azimuth values determined at WRA, is that due to the structure of the crust and upper mantle in the vicinity of the array. One stringent requirement of an ideal arraysite is that the geology should be reasonably homogenous and uncomplicated by major elastic discontinuities. Initially, it was expected that the WRA situated in the middle of the Australian stable shield fulfilled these requirements. However, when the array records of the nuclear explosion Longshot were analysed towards the end of 1966, they yielded a value of $dT/d\Delta$ which was about 11% higher than the value expected on the basis of the Jeffrey-Bullen tables. Studies by Cleary and Hales (1966) and Carder et al (1966) strongly suggested that at the distance in question, the J-B tables, and hence the expected $dT/d\Delta$ value was in error by less than 1%. This provided the first hint of an anomalous structure under the array, and the large discrepancy between the measured and expected $dT/d\Delta$ values was attributed to this structure. From the results of the seismic experiment WRAMP, Underwood (1967) inferred the presence of a near-surface dipping structure underneath the array. Unfortunately, he used too little data to enable a really detailed model of the region beneath the array to be determined. As more $dT/d\Delta$ and azimuth measurements accumulated, it became evident that the structure beneath the array could not be approximated by a single plane dipping interface, and in fact, appeared to diverge considerably from that simple approximation.

Owing to the fact that details of the structure underneath

the array are not yet available, and that the structure appears to be one of great complexity, an empirical method of correcting the $dT/d\Delta$ and azimuth measurements for structure must be used. Wright (1970) devised such a method of correction based entirely on Niazi's (1966) theory on the effect of a dipping layer measurements of $dT/d\Delta$ and azimuth. The method involves selecting a realistic model of the crust and adjusting the dip angle and dip direction, keeping the P wave velocities constant, until the apparent velocity and azimuth calculated by Niazi's theory agreed with the measured values of $dT/d\Delta$ and azimuth. The weakness of this method lies in the fact that any number of models fit the data, and any structure with a specific velocity contrast could be replaced by an equivalent structure with a different velocity contrast and dip angle. If, however, certain limits based on observational evidence are placed on parameters such as the dip angle of the structure, and expected apparent velocity, the method is capable of yielding fairly accurate results. Niazi (1966) has shown how data from earthquakes at almost equal distances and at opposite azimuths from the array can be used to separate the effects of a structure consisting of a single plane dipping interface from errors in a given $dT/d\Delta$ curve. Cleary, Wright and Muirhead (1968) used this technique to work out a simple model of the crust beneath the array, and determined the dipping interface to have a dip angle around 6° - 7°, dip direction of around 230°, and a velocity ratio of 0.7. The corresponding parameters deduced by Underwood (1967) were a dip angle of 5°, dip direction of 200° and velocity ratio of about 0.9. Wright (1970), using the same method as in 1968, estimated a dipping interface with dip angle of about 6.5° to 7°, and dip direction 215° - 235°, with a velocity contrast of 0.7 to give the best corrections for $dT/d\Delta$ and azimuth. Consequently,

the predominant evidence indicates that the dip angle of the inclined plane assumed to be responsible for the large $dT/d\Delta$ and azimuth anomalies is about 6° or 7°, with a velocity contrast of approximately 0.7. The dip direction is somewhat more flexible, but seems to be near 220°.

It should be noted that the above structures used to correct the $dT/d\Delta$ and azimuth measurements are all single dipping plane structures, whereas, it appears that the structure underneath the array is far more complicated and may consist of a number of different dipping planes. However, an important fact, noted by Wright (1970) is that the effect of several plane dipping interfaces on $dT/d\Delta$ and azimuth measurements is indistinguishable from that of a single interface, and consequently, the assumption that the structure underneath the array could be approximated by a single plane dipping interface is justified. The effect of a single plane dipping interface is to introduce approximately sinusoidal variations in azimuth and $dT/d\Delta$ as a function of azimuth that are 90° out of phase. The $dT/d\Delta$ anomaly is least in the dip direction and the azimuth anomaly changes from negative to positive.

A close look at the $dT/d\Delta$ and azimuth measurements made in this study reveal not only startling discrepancies between expected and observed values but also great fluctuations in the amount of the discrepancy (Figure 2.7). Quite often it was possible to correlate the magnitude of the anomaly with azimuth. Although the azimuth range was not uniformly covered, the residuals of the measured $dT/d\Delta$ values with respect to the expected values exhibit a quasi-sinusoidal variation. The azimuth residuals also indicate some degree of sinusoidal variation but changed more rapidly than do the $dT/d\Delta$ residuals and are not coincident with them. On this

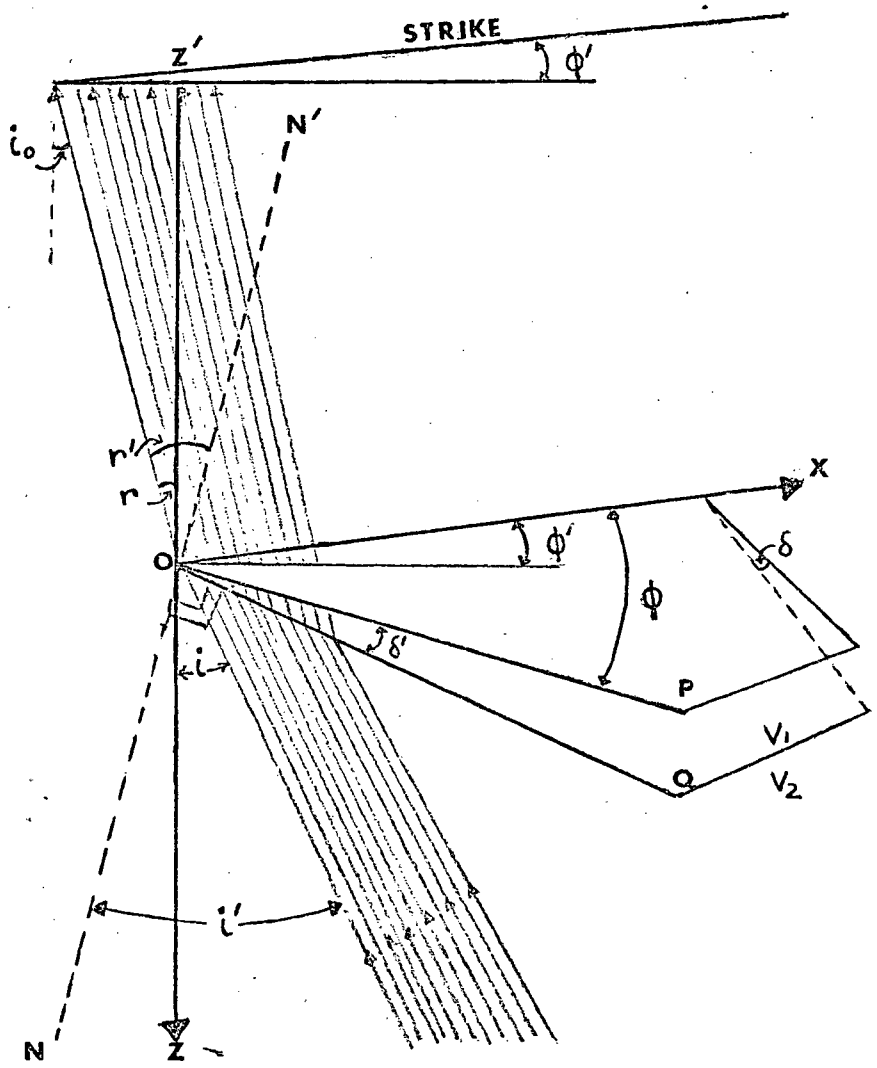

Figure 2.6 Refraction of a planar seismic beam incident on a dipping interface between a half-space and the overlying layer.

basis, the assumption of a single plane dipping interface underneath the array as used in the empirical method of correction, seems to be a justifiable one.

For purposes of analysis a computer program written by C. Wright was used to work out the effect on $dT/d\Delta$ and azimuth, of any combination of dipping interfaces for a seismic event whose azimuth and distance are accurately known. The program is based entirely on Niazi's theory, which will be briefly outlined below.

The geometry of a thin planar beam of seismic waves incident on a dipping interface from beneath is shown in Figure 2.6. The intersection of the dipping interface with an imaginary horizontal plane (i.e. the direction of strike) is taken as the x axis. OP and OQ are the intersections of the vertical plane containing the incident beam with the imaginary horizontal plane and the dipping interface, respectively. The dip angle is denoted by symbol δ , and the angle between the seismic beam and vertical axis OZ, i.e. the true angle of incidence, is denoted by i. The angle ϕ between OP and the x-axis is the true azimuth from which the beam has been incident on the interface. i_o is the angle of incidence at the free surface. The refraction of the rays takes place according to Snell's law with i' and not i being the angle of incidence, where i' is the angle subtended between the ray and the normal to the interface ON. Consequently, the angle of refraction will be r' , which is different from $r = i_o$. In the process of refraction, in general, the rays do not remain in the vertical plane, but appear to be arriving at the surface from a new azimuth, the apparent azimuth ϕ', the corresponding apparent dip being δ' . Niazi (1966) has shown that the direction

cosines of the beam reaching the surfaces are given by

$$l = (-m\beta + n\gamma)/\alpha$$

$$m = (\cos r' - n\cos\delta)/\sin\delta$$

$$n = \cos r'\cos\delta \pm \alpha\sin\delta\sin r'$$

where α, β, γ are the direction cosines of the line perpendicular to the apparent plane of incidence, i.e. to both the incident rays and ON, and $\alpha^2 + \beta^2 + \gamma^2 = 1$. If v_1 and V_2 are the wave velocities in the upper and lower medium respectively, then

$$\sin r' = v_1 \sin i'/v_2 = v_1(1 - (\sin i \sin\phi \sin\delta + \cos i\cos\delta)^2)^{\frac{1}{2}}/v_2$$

since $\cos i' = \sin i \sin\phi \sin\delta + \cos i \cos\delta$

$$\alpha = \tan\delta \cot i - \sin\phi/R$$

$$\beta = \cos\phi/R$$

$$\gamma = -\tan\delta\cos\phi/R$$

where $R^2 = (1 + \tan^2\delta \cot^2 i + \tan^2\delta\cos^2\phi - 2\sin\phi\tan\delta\cot i)^{\frac{1}{2}}$

The apparent angles of incidence, apparent azimuth and new apparent velocity of the rays can then be obtained from the direction cosines l, m, n as follows:

$$\cos i_o = n$$

$$\phi' = \tan^{-1}(m/l)$$

$$v' = v_1/\sin i_o$$

$$= v_1/(1-n^2)^{\frac{1}{2}}$$

The actual procedure was as follows. A dipping interface between the crust and mantle was taken as having a velocity ratio of 0.7. Taking a fixed dip direction of 10^{o} and a fixed dip angle of 0.5 , the azimuth Ø was varied at intervals of 20^{o} from 0^{o} to 360^{o}. It was assumed from the J-B tables that the expected values of $dT/d\Delta$ for the DF branch lay in the range of 2.022 sec/deg. at 113^{o} to 0.3 sec/deg. at 176 (where 113^{o} to 176^{o} was the distance range of the DF data), corresponding to expected apparent velocities of 55 km/sec to about 380 km/sec. Consequently, keeping the dip direction and angle fixed at the values chosen, four quantities were calculated at each value of azimuth from 0^{o} to 360^{o} at 20^{o} intervals. These four values were:

(1) The apparent azimuth Ø, and consequently the azimuth anomaly.

(2) The measured apparent velocity V', and consequently

(3) The measured $dT/d\Delta$ obtained from V'.

(4) The ratio of measured velocity/expected velocity

where the expected velocities used varied from 55 km/sec - 100 km/sec in 2 km/sec steps from 100 km/sec - 200 km in 10 km/sec steps and from 200 - 380 km/sec in 20 km/sec steps. Thus the entire range of expected apparent velocities corresponding to the entire range of expected $dT/d\Delta$ values for DF was covered. The dip direction was then varied from 10^{o} to 360^{o} at 10^{o} intervals, and keeping the dip angle fixed at 0.5, the entire procedure was repeated at each new dip direction. The dip angle was increased by 0.5^{o} from 0.5^{o} to 10.0^{o}, and at each new dip angle value, the calculations were again performed for dip directions from 10^{o} to 360^{o} as before. Thus, an entire set of tables was generated to enable corrections to be applied to the $dT/d\Delta$ and azimuth measurements for the DF bnanch.

The corrections were made as follows: The true azimuth Ø, and measured dT/dΔ and azimuth, and therefore the azimuth anomaly of the event were noted. The tables were checked for a point where at the same true azimuth Ø the corresponding dT/dΔ value and azimuth anomaly in the tables agreed as closely as possible with the measured dT/dΔ and azimuth anomaly. The dip direction and dip angle so specified were then assumed to be the parameters of the plane dipping interface responsible for this particular set of anomalies in dT/dΔ and azimuth measurement. In this manner, a dip direction and dip angle were worked out for each dT/dΔ and azimuth determination for the DF branch.

On the assumption that the same method of correcting for local structure could be applied to the other phases as well, the entire procedure was repeated for the measured values of the GH, IJ and AB traveltime branches. For the GH and IJ data, expected apparent velocities of 30 to 37 km/sec corresponding to dT/dΔ values of about 3.6 to 3.0 sec/deg were used, respectively, at approximately 2 km/sec intervals. The range of dT/dΔ values for IJ branch was taken onthe basis of the measured dT/dΔ values which seemed to have their majority of values in this range and the corresponding range of expected dT/dΔ values per the Adams and Randall (1964) model. The range of expected dT/dΔ values for the GH branch was estimated in the same manner as in the IJ case, but it was extended to a maximum value of about 2.9 sec/deg in order to cover the range of expected dT/dΔ values in the Bolt (1968) model as well. For the AB corrections expected apparent velocities of 25-31 km/sec corresponding to dT/dΔ values ofa bout 4.4 to 3.6 sec/deg were used, again at roughly 2 km/sec intervals. Thus, a dip direction and dip angle was worked out for each dT/dΔ and azimuth determination for the GH, IJ and

AB branches.

In effect, all that was done was to take a measured $dT/d\Delta$ and azimuth value that had been assigned to a particular branch, place limits on the expected true value of $dT/d\Delta$ for that branch, and search the tables for a combination of dip angle and dip direction, until the azimuth anomaly and $dT/d\Delta$ of the measured data agreed with that of the tables, for the particular $\emptyset$ (true azimuth) in question.

A certain amount of ambiguity is involved in this method of correction. For example, it is quite possible for a measured $dT/d\Delta$ and azimuth value, assigned to the DF branch, to be corrected to an expected $dT/d\Delta$ value, lying somewhere on the GH or the IJ branches, and for a measured IJ value to be corrected to an expected value lying somewhere on the DF branch. The two restraining factors used to remove this ambiguity were (1) As previously mentioned, a fixed range of expected $dT/d\Delta$ values, based on the distribution of the measured values and on expected values taken from existing models for the appropriate distance range, was assigned to correct a particular branch. These ranges did not overlap for the different branches. (2) Evidence has shown that the dip angle of the dipping interface responsible for the anomaly is close to 7^{o}, and consequently the dip angles obtained in the corrections should all be close to, or around this value. An important fact in connection with this is that the larger the anomaly in the measurement, the larger was the dip angle of the plane needed to correct this anomaly. Consequently, if a measured IJ value was desired to be corrected to some expected value lying, for example on the GH or AB branches, the dip angle needed to effect this correction would be much larger than that needed to correct the measured value to some point on the expected IJ branch. In particular, it was observed that the measured $dT/d\Delta$ and azimuth

values for the early part of the IJ branch could be corrected to be on the GH branch, thus resulting in a traveltime model similar to Bolt's (1964) model. On the basis of the larger dip angles, greater than 10^{o}, needed for this correction, and since the phase IJ was clearly observed on array seismograms in that distance range (Bolt did not observe this phase at all), the correction to Bolt's model was rejected.

The dip angles of the correcting planes were found to be centered around the value of 6^{o} - 7^{o}, although in some cases the dip angle reached as low as 0.5^{o}. In even fewer cases, it reached as high as 10^{o}. The dip directions were concentrated around 100^{o} and 200^{o} but a few dip directions as low as 10^{o} or as high as 350^{o} were obtained. Often the three measurements in any one event would have closely similar dip angles and dip directions, as would most events around the same azimuth Ø, but it was possible though unusual to have all three measurements in any one event with vastly differing dip angles and dip directions. This disparity was due to the changes in the magnitude of the anomalies for the three measurements. In turn these could be due to systematic changes in waveform from one seismometer to another as a result of random noise effects, extremely rapid variations in the local structure, irregularities in the source region or the deepest point of the ray path, or more than one phase arriving at nearly the same time.

The appropriate dip vectors were divided into groups so that each group contained dip vectors of approximately the same value, and the distance and azimuth ranges in each group were not too large. The

data for the DF branch was divided into 25 groups, the IJ into 15, the GH into 19, and the AB into 21. The distance range varied from 5° to 10° and the azimuth range from 3° to 10°. The purpose of the division into groups was to obtain an average dip vector for each group under the assumption that all the events in the particular group were affected by this 'average' structure determined, and that the fine structure variation in each group was merely a consequence of the empirical method of correction, and somewhat divergent from the degree of physical reality obtainable by this method.

The averaging of the dip vectors was approached as a problem of the statistics of a spherical distribution. This approach is commonly adopted in paleomagnetic studies and is described by Fisher (1953) and Watson (1956). The dip direction L and dip angle A of the mean dip vector are given by:

$$L = \mathrm{Tan}^{-1} (\Sigma w_i m_i / \Sigma w_i l_i)$$

$$A = \mathrm{Sin}^{-1} (\Sigma w_i n_i / R)$$

where m_i, n_i and l_i are the direction cosines of the dip vectors in the distribution, R is the length of their resultant vector and w_i is the weight of the individual vectors. The weights are normalized so that their sum is equal to the number of observations N in the group. A measure of the distribution of the individual vectors with respect to the mean vector is given by the quantity

$$K = N-1/N-R$$

The higher the value of K the more closely are the individual vectors grouped around their mean.

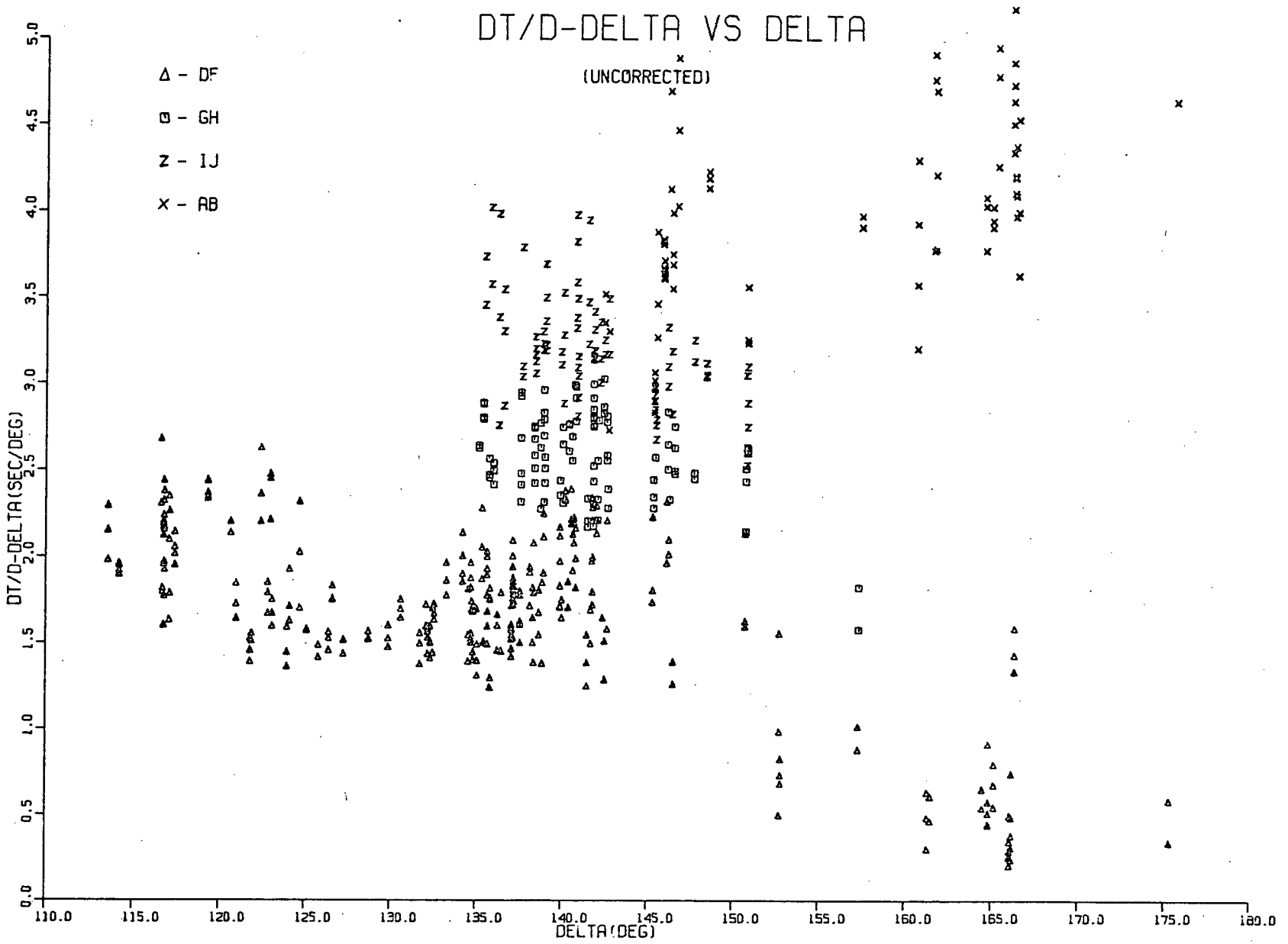

Figure 2.7. Measured DT/DΔ .

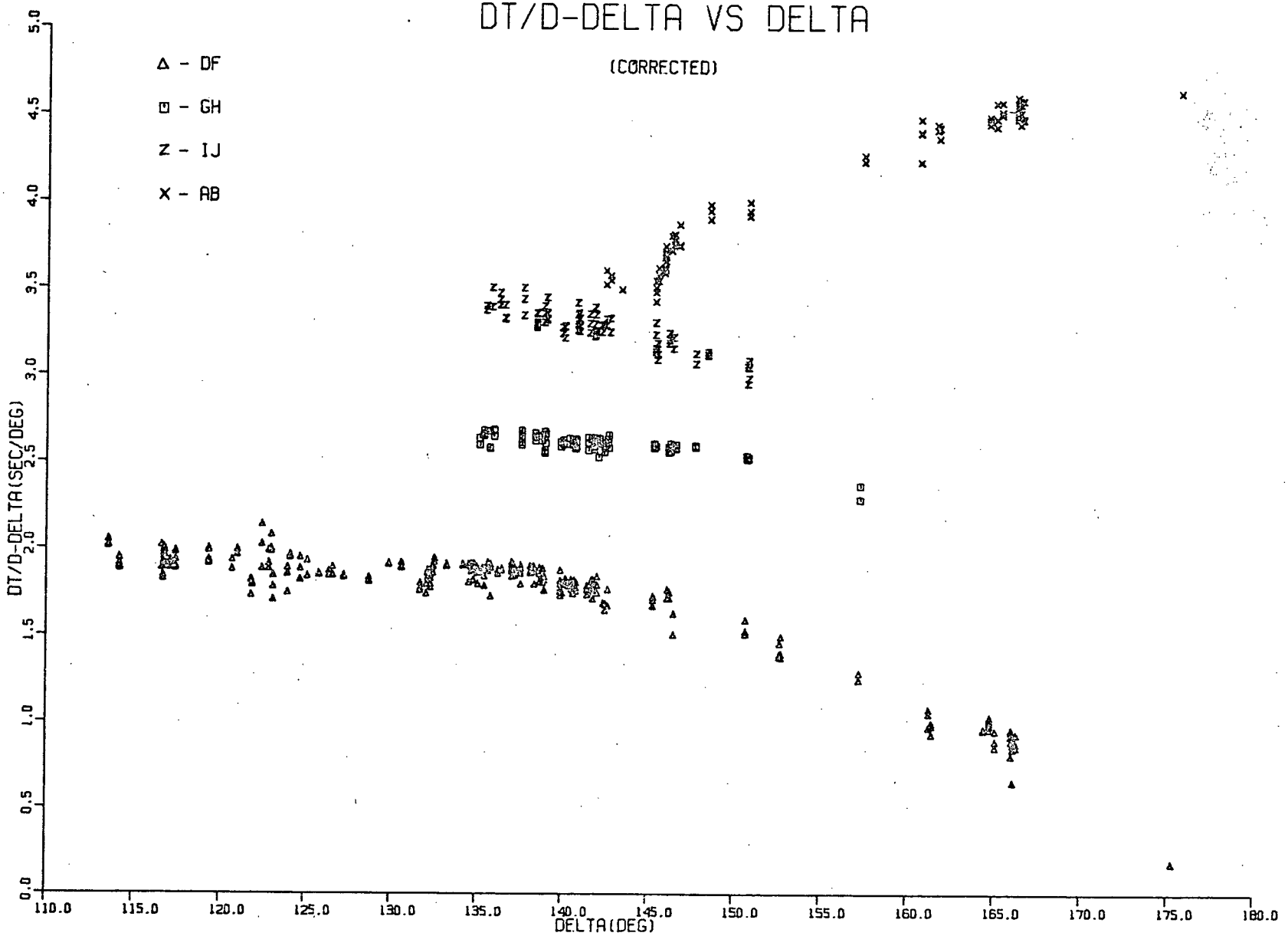

Figure 2.8. DT/DΔ corrected for local structure.

The measured azimuth, apparent velocity and dip vector for each observation in a particular group were used to calculate the angle of incidence i_o of the waves at the earth's surface as described in Niazi's theory. The direction cosines l_i, m_i, n_i were estimated for each vector from its' angle of incidence, and the quantities L, A and K were calculated for the entire group. The observations were rearranged if necessary to obtain satisfactory estimates of K. The weights W_i were taken as the square of the reciprocal of the root-mean square error on the corresponding $dT/d\Delta$ measurement.

The averaged dip vectors obtained in the manner were used to prepare tables as described previously and the final corrected $dT/d\Delta$ values were estimated from these tables.

It should be mentioned at this point that the statistical approach used for the problem of averaging the dip vectors is not strictly the correct one since the dip angle itself is known with greater precision than the dip direction, and the probability distribution is somewhat anisotropic. A correct statistical model would be one intermediate between a spherical and a circular distribution but the procedure then becomes somewhat too complex to be justified by the nature of the problem.

The $dT/d\Delta$ values as originally measured are shown in Figure 2.7. They exhibit considerable scatter and fitting a smooth curve through the values for each branch would be extremely difficult. The same $dT/d\Delta$ measurements corrected for structure in the manner just described are displayed in Figure 2.8. The improvement is self-evident and the scatter in the observations has been reduced sufficiently so that smoothing techniques could be applied meaningfully.

2.3 Smoothing of Corrected dT/dΔ Values

In the reduction of random errors by smoothing techniques, it is highly desirable that the errors be reduced as far as possible without losing valuable information, and that the magnitude of the reduction be estimated. Three possible techniques of smoothing in common use are: (1) To subtract a twelfth of the fourth difference from, or, add a quarter of the second difference to each observed value except the two end points. (Jeffreys, 1937). This method has two severe disadvantages. Firstly, the magnitude of the reduction cannot be properly estimated since the errors in neighbouring points tend to be correlated, and secondly, it does not remove as much of the error as the uncertainties would allow (Jeffreys, 1934) nor does it give any control over the amount of smoothing to be applied. (2) To fit a simple function such as a polynomial or a series of polynomials to the data by least squares. In this way, it is possible to get as much smoothing as desired or justified, but the standard errors in the coefficients of the function are not a convenient measure of the reduction of the error unless the coefficients themselves have some physical significance. A variation of this technique was used for comparison as discussed in Section 2.3.2. (3) The method of summary values devised by Jeffreys (1937, 1961) in which the amount of smoothing can be controlled, no valuable information is lost as ascertained by a significance test, and the magnitude of the reduction can be estimated. This method is superior to the other two and was adopted for smoothing purposes in this study. Appendix IV contains a description of this method.

2.3.1 Smoothing of dT/dΔ by the Method of Summary Values

The method of summary values involves fitting a linear and quadratic curve to each of several groups of the data. The curvature

in each group is estimated beforehand to be reasonably small. From an appropriate calculation (Appendix IV) the coordinates of intersection of the linear and quadratic forms can be determined and are known as the summary points. They best represent the data in the appropriate range. The summary points determined for the several groups are interpolated to give the complete smoothed curve.

A computer program based on the theory of Appendix IV was written by C. Wright and was used in this study. The corrected $dT/d\Delta$ values for any one branch were divided into groups in which the distance ranges were small, and the curvature also estimated to be small. The program was used to calculate the summary points and their corresponding uncertainties for each range of the branch. The summary points were then interpolated at 0.01° intervals by means of divided differences, the size of the interval being chosen so as to facilitate comparison of the calculated values with the measured values in which the distance coordinates were given to 0.01°. The residuals between the calculated and measured $dT/d\Delta$ values were determined and in order to determine whether adequate smoothing had taken place a chi-squared test was performed on these residuals. The χ^2 value for each residual was taken as the product of the weight for the corresponding $dT/d\Delta$ measurement and the square of the residual, the total χ^2 for each range being the sum of the individual χ^2 of the points in that range. An overall χ^2, the sum of the χ^2 for each of the ranges in the particular branch was calculated also. For adequate smoothing, and assuming the error to be wholly random, χ^2 must be in the range $\nu \pm \sqrt{2\nu}$ where ν is the

number of degrees of freedom. Thus ν is equal to the number of fixed parameters less the number of adjustable parameters. In this case ν is equal to the number of observations used, less the number of summary points for the case being considered (i.e. for one range with M points, the number of summary points is 2, and $\nu = M - 2$, so that the χ^2 for that range must be within $(M - 2) \pm \sqrt{2(M-2)}$. If there are N ranges in the entire branch, then the number of summary points is 2N, and if the entire number of observations in the branch is M_o, then the overall χ^2 must be in the range $(M_o - 2N \pm \sqrt{2(M_o - 2N)}$ If χ^2 is too large (i.e. if the residuals are too large) then the summary points do not represent the data in the range as accurately as they could, the curvature is being underestimated, and significant features are being lost. To correct this problem, the number of ranges should be increased so that the summary points fall closer to the data in any given range and the residuals are thereby reduced. If χ^2 is too small, insufficient smoothing is taking place and possibly meaningless detail is being retained in the curve. To correct this problem, the number of ranges should be increased, so that the residuals in any given range would increase also.

In practice, owing to the heavy concentration of data in some distanceranges, and relative lack in the other regions, some difficulty was encountered in attempting to obtain a satisfactory value of χ^2 for each of the ranges, and at the same time a satisfactory overall χ^2 for the entire branch. After somewhat exhaustive attempts to obtain a satisfactory solution with regard to the χ^2 for each range, the overall χ^2 for the branch and the retention of reasonably small distance ranges, the following procedure was adopted: that solution

for which the maximum number of ranges gave satisfactory values of χ^2 and the overall value of χ^2 for the entire branch remained satisfactory was allowed to stand. The result of this procedure is thatthe larger part of the branch is adequately smoothed but there were possibly one or two regions on it that were either undersmoothed or oversmoothed. Since at this stage the data was being smoothed to determine a correction term corresponding to constraining the data to an acceptable traveltime curve, this lack of adequate smoothing over the entire branch is not too important (Wright, 1970).

In order to constrain the smoothed data to an acceptable traveltime curve and consequently to reduce any remaining systematic errors even further, the area under each smooth curve (i.e. in each range) was evaluated by Simpson's rule of integration and subtracted from the traveltime difference between the end points of the range. If T_1 and T_2 are the traveltimes at the end points of the range of integration Δ_1 and Δ_2 respectively, and if σ_1 and σ_2 are the respective standard errors in T_1 and T_2 and if, also, the area under the smooth curve in that range is A with a standard error σ_3, then the correction C is given by:

$$C = ((T_2 \pm \sigma_2) - (T_1 \pm \sigma_1) - (A \pm \sigma_3))/\Delta_2 - \Delta_1$$
$$= (T_2 - T_1 - A)/\Delta_2 - \Delta_1 \pm (\sigma_1^2 + \sigma_2^2 + \sigma_3^2)^{\frac{1}{2}}/\Delta_2 - \Delta_1$$

where the second term on the right is the error in the correction term C. This correction C was calculated for each of the ranges in the different branches, and applied to each of the $dT/d\Delta$ values in these ranges, a procedure which merely involved changing the baseline of the $dT/d\Delta$ values in the individual ranges. The traveltime curves to which the smoothed $dT/d\Delta$ data were restrained are the J-B tables for the DF and AB branches (which branches for comparison were also restrained to the Bolt (1968) tables) and the Adams and Randall (1964)

TABLE 2.1(a) SUMMARY POINTS FOR DF BRANCH
314 DATA POINTS
RESTRAINED TO J.B. TRAVEL-TIME CURVE

INITIAL SUMMARY POINTS:

Δ (DEG)	dT/dΔ (SEC/DEG)	σ (SEC/DEG)	χ^2	ν	C (SEC/DEG)
115.45	1.956	0.018	49.32	45	+0.006
118.98	1.946	0.017			
122.10	1.858	0.030	21.02	18	+0.083
123.68	1.857	0.033			
125.55	1.890	0.016	38.06	35	+0.034
131.26	1.862	0.017			
134.06	1.886	0.010	48.41	78	-0.039
138.08	1.867	0.010			
143.06	1.748	0.012	148.11	128	+0.023
165.22	0.896	0.016			

Total χ^2 = 304.92 on 304 degrees of freedom

FINAL SUMMARY POINTS:

Δ (DEG)	dT/dΔ (SEC/DEG)	σ (SEC/DEG)	χ^2	ν
115.30	1.962	0.016	49.48	45
118.78	1.952	0.013		
122.56	1.940	0.016	29.64	32
125.38	1.924	0.016		
131.58	1.895	0.011	81.53	77
134.93	1.846	0.010		
138.04	1.828	0.010	106.27	108
147.81	1.706	0.015		
155.34	1.432	0.019	46.09	42
165.32	0.919	0.016		

Total χ^2 = 313.01 on 304 degrees of freedom.

σ = STD. ERROR ON dT/dΔ VALUE OF SUMMARY POINT

ν = NO. OF DEGREES OF FREEDOM

C = CORRECTION FOR RESTRAINING DATA TO TRAVELTIME CURVE

TABLE 2.1(b) SUMMARY POINTS FOR GH BRANCH

105 DATA POINTS
(a) RESTRAINED TO A-R TRAVELTIME CURVE

INITIAL SUMMARY POINTS:

Δ (DEG)	dT/dΔ (SEC/DEG)	σ (SEC/DEG)	χ^2	ν	C (SEC/DEG)
136.08	2.653	0.020	69.36	84	-0.008
141.77	2.624	0.021			
143.97	2.605	0.019	19.21	17	-0.008
151.83	2.501	0.037			

Total χ^2 = 88.57 on 101 degrees of freedom

FINAL SUMMARY POINTS:

Δ (DEG)	dT/dΔ (SEC/DEG)	σ (SEC/DEG)	χ^2	ν
136.20	2.645	0.018	79.42	84
141.93	2.613	0.017		
143.75	2.601	0.015	15.21	17
151.94	2.494	0.024		
(158.0	2.300			)*

Total χ^2 = 94.63 on 101 degrees of freedom.

*Taken from A-R curve in order to extend branch beyond 152°

(b) RESTRAINED TO BOLT TRAVELTIME CURVE

FINAL SUMMARY POINTS: C= 0.087 (SEC/DEG)

Δ (DEG)	dT/dΔ (SEC/DEG)	σ (SEC/DEG)	χ^2	ν
136.19	2.740	0.019	77.59	84
141.91	2.704	0.020		
143.75	2.692	0.020	16.15	17
151.91	2.588	0.021		
(156.00	2.100			)*

Total χ^2 = 93.74 on 101 degrees of freedom.

* Taken from Bolt's curve in order to extend branch beyond 152°

TABLE 2.1(c) SUMMARY POINTS FOR IJ BRANCH
81 DATA POINTS
RESTRAINED TO A+R TRAVEL-TIME CURVE

INITIAL SUMMARY POINTS:

Δ (DEG)	dT/dΔ (SEC/DEG)	σ (SEC/DEG)	χ^2	ν	C (SEC/DEG)
135.68	3.455	0.032	47.42	60	+0.024
140.46	3.317	0.015			
146.62	3.195	0.017	19.54	17	+0.003
150.82	3.054	0.030			

Total χ^2 = 66.96 on 77 degrees of freedom.

FINAL SUMMARY POINTS:

Δ (DEG)	dT/dΔ (SEC/DEG)	σ (SEC/DEG)	χ^2	ν	C
135.68	3.459	0.030	57.23	60	
140.46	3.320	0.013			
146.65	3.198	0.016	18.61	17	
150.87	3.056	0.021			

Total χ^2 = 75.84 on 77 degrees of freedom.

TABLE 2.1(d) SUMMARY POINTS FOR AB BRANCH
70 DATA POINTS
(a) RESTRAINED TO J.B.

INITIAL SUMMARY POINTS:

Δ (DEG)	dT/dΔ (SEC/DEG)	σ (SEC/DEG)	χ^2	ν	C (SEC/DEG)
146.01	3.670	0.017	33.01	37	+0.145
149.896	4.010	0.024			
*157.642	4.279	0.034	3.56	12	
161.599	4.416	0.032			
165.716	4.488	0.026	29.73	21	-0.093
173.441	4.495	0.008			

Total χ^2 = 66.30 on 70 degrees of freedom.

* Not used in interpolation because of unsatisfactory behaviour of curve in that region.

FINAL SUMMARY POINTS:

Δ (DEG)	dT/dΔ (SEC/DEG)	σ (SEC/DEG)	χ^2	ν
146.01	3.814	0.015	35.67	37
149.896	4.165	0.020		
161.599	4.319	0.030	27.94	26
165.716	4.395	0.028		
173.441	4.419	0.033		

Total χ^2 = 63.61 on 63 degrees of freedom.

(b) RESTRAINED TO BOLT

FINAL SUMMARY POINTS:

C = -0.055 sec/deg and -0.081 sec/deg respectively

Δ (DEG)	dT/dΔ (SEC/DEG)	σ (SEC/DEG)	χ^2	ν
146.01	3.625	0.013	36.75	37
149.89	3.968	0.020		
161.60	4.335	0.026	24.32	26
165.72	4.406	0.022		
173.44	4.409	0.032		

Total χ^2 = 61.07 on 63 degrees of freedom.

NOTE: (1) All values of unsmoothed $dT/d\Delta$ above 4.5 restrained to 4.5.

TABLE 2.2. DT/DΔ SMOOTHED BY THE METHOD OF SUMMARY VALUES

DISTANCE	DT/DΔ (SEC/DEG)					
(DEG)	DF	GH (A-R)	GH (BOLT)	IJ	AB (J-B)	AB (BOLT)
113.0	1.962					
114.0	1.962					
115.0	1.962					
116.0	1.962					
117.0	1.959					
118.0	1.956					
119.0	1.952					
120.0	1.944					
121.0	1.941					
122.0	1.941					
123.0	1.941					
124.0	1.939					
125.0	1.931					
126.0	1.921					
127.0	1.915					
128.0	1.910					
129.0	1.906					
130.0	1.902					
131.0	1.897					
132.0	1.882	2.651	2.747			
133.0	1.878	2.649	2.745			
134.0	1.865	2.649	2.744	3.484		
135.0	1.854	2.648	2.743	3.464		
136.0	1.852	2.646	2.741	3.444		
137.0	1.849	2.643	2.738	3.408		
138.0	1.829	2.639	2.734	3.378		
139.0	1.824	2.634	2.729	3.351		
140.0	1.818	2.629	2.724	3.328		
141.0	1.808	2.622	2.717	3.307		
142.0	1.794	2.615	2.710	3.288		
143.0	1.773	2.606	2.701	3.270		
144.0	1.756	2.597	2.692	3.252		
145.0	1.738	2.587	2.682	3.232	3.600	3.500
146.0	1.718	2.576	2.671	3.211	3.820	3.610
147.0	1.697	2.564	2.659	3.187	3.920	3.720
148.0	1.673	2.551	2.649	3.159	4.010	3.810
149.0	1.648	2.537	2.632	3.128	4.090	3.890
150.0	1.620	2.523	2.580	3.090	4.170	3.970
151.0	1.591	2.507	2.550	3.047	4.200	4.100
152.0	1.559	2.491	2.500	3.030	4.200	4.200
153.0	1.526	2.473	2.450		4.200	4.300
154.0	1.489	2.455	2.400		4.200	4.300
155.0	1.451	2.436	2.305		4.300	4.400
156.0	1.411	2.415	2.210		4.300	4.400
157.0	1.368	2.394			4.300	4.400
158.0	1.323	2.303			4.300	4.400
159.0	1.275				4.300	4.400
160.0	1.225				4.300	4.400
161.0	1.172				4.320	4.410
162.0	1.116				4.340	4.420
163.0	1.058				4.360	4.430
164.0	0.997				4.370	4.435
165.0	0.933				4.390	4.440
166.0	0.715				4.400	4.446
167.0	0.623				4.410	4.450
168.0	0.605				4.420	4.457
169.0	0.598				4.420	4.458
170.0	0.554				4.420	4.458
175.0	0.300				4.420	4.459
180.0	0.000				4.420	4.459

tables for the IJ and GH branches, this latter branch also being restrained to the Bolt (1968) tables for the sake of interest. Since none of these tables provided standard errors in their traveltimes, it was not possible to estimate the error on the correction C for any of the ranges.

With the appropriate correction C applied to each group in the particular branch, the corrected $dT/d\Delta$ values of the entire branch were once again smoothed by the method of summary values to obtain the new summary points. These were interpolated at 1^{o} intervals to give the final smoothed $dT/d\Delta$ values.

The initial and final summary points used in obtaining the final smoothed $dT/d\Delta$ values for the respective branches are listed in Tables 2.1(a) to 2.1(d) inclusive. Note that the GH branch has been restrained to the traveltime curves of both Adams and Randall and Bolt. The AB branch was restrained to both J-B and Bolt. Owing to lack of data in the range 150^{o} to 160^{o} for AB, it was not possible to obtain satisfactory summary points for this region, so the procedure adopted was to smooth the data in the ranges $145 - 150^{o}$ and $160 - 175^{o}$ separately, and to fill in the gap so created with the values of J-B and Bolt respectively. In addition, values of $dT/d\Delta$ for the AB branch that were greater than 4.5 sec/deg were restrained to this value, as it is the maximum given for P_cP phases in the 1968 tables.

The final smoothed $dT/d\Delta$ values are listed in Table 2.2 Figure 2.9 shows these values restrained to the different traveltime branches. From the figure, it is seen that the GH branch restrained

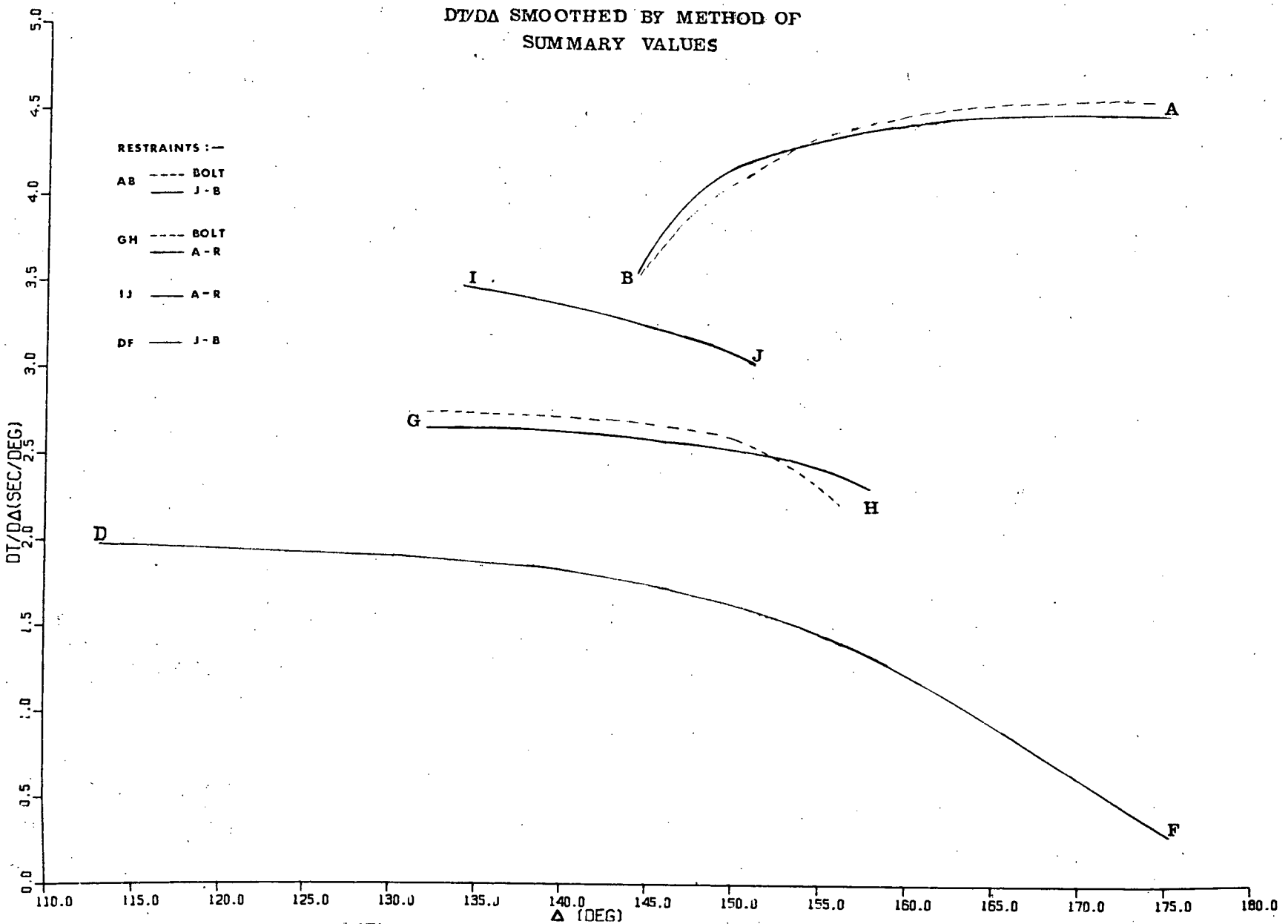

Figure 2.9 DT/DΔ smoothed by the method of Summary Values

to Bolt's data has greater curvature near 150^{o} than the one restrained to that of Adams and Randall. The AB branch restrained to the J-B traveltimes has greater curvature near its beginning than the one restrained to Bolt's times. Also, it is shifted to a lower level near the latter part of the range. On the basis of the best fit to the data, the $dT/d\Delta$ curve for the GH branch restrained to Adams and Randall's traveltimes and the $dT/d\Delta$ curve for the AB branch restrained to the J-B traveltimes were selected for the purpose of inversion. The curves as shown for branches IJ and DF were used in the inversion procedure.

2.3.2 Smoothing of $dT/d\Delta$ data by UBC Triangular Regression Package - TRIP

Mainly for the sake of comparison, the $dT/d\Delta$ values corrected for local structure were also smoothed by polynomial regression using the U.B.C. computer program U.B.C. TRIP (1972). The method is briefly described in Appendix V.a.

The regression equations determined as giving the best fit to the data are listed in Table 2.3. The independent variables for the DF, GH, IJ and AB branches were taken as $(\Delta - 113^{o})$, $(\Delta - 132^{o})$ $(\Delta - 134^{o})$ and $(\Delta - 145^{o})$ respectively where the numerical quantities are the turning points of the respective branches. The turning points were taken as that distance, truncated to a whole number, at which the individual phases were first observed. Smoothed curves at 1^{o} intervals for the different branches were generated from the appropriate regression equations. The calculated valves are listed in Appendix Vb, and are shown in Figure 2.10. For comparison, the smoothed curve obtained by the method of summary values is shown in dashed lines. The lesser

TABLE 2.3: REGRESSION EQUATIONS FOR SMOOTHED $dT/d\Delta$ DATA

DE BRANCH — 314 data points

$R^2 = 0.9643$

INDEPENDENT VARIABLE	COEFFICIENT	STD. ERROR	F-PROB	TOLERANCE
CONSTANT	1.9587	0.0180		
$(\Delta-113°)$	$-0.1384/10$	$0.2528/10^3$	0.0000	1.0000
$(\Delta-113°)^2$	$0.1095/10^2$	$0.1384/10^4$	0.0000	1.0000
$(\Delta-113°)^3$	$-0.3608/10^4$	$0.1146/10^5$	0.0000	1.0000
$(\Delta-113°)^4$	$0.2432/10^6$	$0.5876/10^7$	0.0001	1.0000

$$P = {}^{dT}/d\Delta = 1.9587 - 0.01384\ (\Delta-113) + 0.1095\left(\frac{\Delta-113}{10}\right)^2 - 0.0360\left(\frac{\Delta-113}{10}\right)^3 + 0.0024\left(\frac{\Delta-113}{10}\right)^4$$

GH BRANCH — 106 data points

$R^2 = 0.7573$

INDEPENDENT VARIABLE	COEFFICIENT	STD.ERROR	F-PROB	TOLERANCE
CONSTANT	2.6878	0.01990		
$(\Delta-132°)$	$-0.1694/10$	$0.5931/10^3$	0.0000	1.0000
$(\Delta-132°)^2$	$0.1326/10^2$	$0.8486/10^4$	0.0000	1.0000
$(\Delta-132°)^3$	$-0.4839/10^4$	$0.1301/10^4$	0.0004	1.0000

$$P = 2.6878 - 0.01694\ (\Delta-132) + 0.1326\left(\frac{\Delta-132}{10}\right)^2 - 0.0484\left(\frac{\Delta-132}{10}\right)^3$$

IJ BRANCH — 81 data points

$R^2 = 0.8156$

INDEPENDENT VARIABLE	COEFFICIENT	STD.ERROR	F-PROB.	TOLERANCE
CONSTANT	3.4556	0.0255		
$(\Delta-134°)$	$-0.1833/10$	$0.1376/10^2$	0.0000	1.0000
$(\Delta-134°)^2$	$-0.3761/10^3$	$0.3076/10^3$	0.0223	1.0000

$$P = 3.4556 - 0.0183\ (\Delta-134) - 0.03761\left(\frac{\Delta-134}{10}\right)^2$$

AB BRANCH — 70 data points

$R^2 = 0.9756$

INDEPENDENT VARIABLE	COEFFICIENT	STD.ERROR	F-PROB	TOLERANCE
CONSTANT	3.5480	0.0194		
$(\Delta-145°)$	0.1172	$0.8280/10^3$	0.0000	1.0000
$(\Delta-145°)^2$	$-0.5964/10^2$	$0.2310/10^3$	0.0000	1.0000
$(\Delta-145°)^3$	$0.1203/10^3$	$0.4134/10^4$	0.0650	1.0000

$$P = 3.5480 + 0.1172\ (\Delta-145) - 0.5964\left(\frac{\Delta-145}{10}\right)^2 + 0.1203\left(\frac{\Delta-145}{10}\right)^3$$

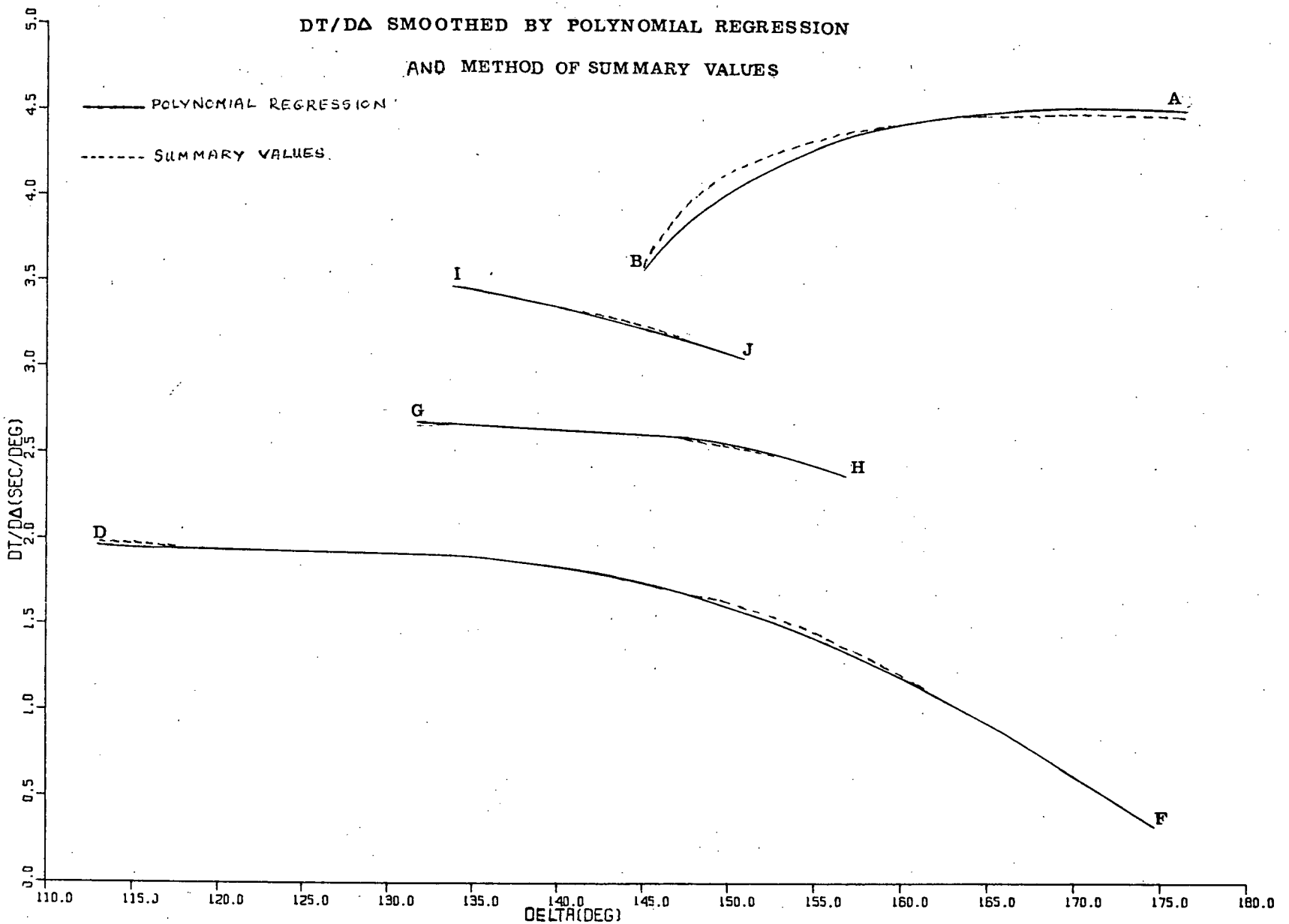

Figure 2.10 Comparison of DT/DΔ smoothed by Polynomial Regression and method of Summary Values.

curvature near the start of the AB branch fitted by polynomial regression can be attributed to the lack of data in the range 150^{o} to 160^{o}. Thus excellent agreement between the sets of curves was obtained. However, the smoothed $dT/d\Delta$ values interpolated from the summary points were used for the inversion process.

2.4 Inversion of Smoothed $dT/d\Delta$ values using the Herglotz-Wiechert Integral

2.4.1 Description of the Herglotz-Wiechert inversion technique

As was shown in Appendix I for a spherical and symmetrical earth model, the ray parameter p is given by

$$p = r \sin i / v = dT/d\Delta$$

Also, the integrals for the distance Δ_{12} and traveltime T_{12} for a ray of parameter p terminating at levels r_1 and r_2, where $r_1 > r_2$, were derived:

$$\tfrac{1}{2}\Delta_{12} = p \int_{r_2}^{r_1} r^{-1}(\eta^2 - p^2)^{-\frac{1}{2}}\, dr \qquad \ldots\ldots\ldots\ldots\ldots (1)$$

$$\tfrac{1}{2}T_{12} = \int_{r_2}^{r_1} \eta^2 r^{-1}(\eta^2 - p^2)^{-\frac{1}{2}}\, dr \qquad \ldots\ldots\ldots\ldots\ldots (2)$$

where $\eta = r/v$ for convenience. These integrals may be solved either by numerical approximation or by direct integration when the velocity function is suitably defined. Consider the latter case for a multi-layered earth where the velocity in each layer is described by a power law of the form $v = ar^{b}$, with a and b constants. Note that b is identical with β of Appendix I. Thus v(r) is continuous but dv/dr is in general discontinuous at each tabulated point. If $v = a_{12} r^{b_{12}}$ in the layer bounded by radii r_1 and r_2, substitution in equations (1) and (2) yields (Engdahl et al, 1968)

$$\tfrac{1}{2}\,\Delta_{12} = (1-b_{12})^{-1}\left(\cos^{-1}(p/\eta_1) - \cos^{-1}(p/\eta_2)\right) \quad \ldots\ldots\ldots (3)$$

$$\tfrac{1}{2}\,T_{12} = (1-b_{12})^{-1}\left((\eta_1^2-p^2)^{\frac{1}{2}} - (\eta_2^2-p^2)^{\frac{1}{2}}\right) \quad \ldots\ldots\ldots (4)$$

where η_1 and η_2 are the values of n at r1 and r2 respectively. For the ray which reaches it's deepest point within the layer, the value of P is equal to η_2, so that (3) and (4) become

$$\Delta_{12} = 2\,(1-b_{12})^{-1}\cos^{-1}(p/\eta_1) \quad \ldots\ldots\ldots\ldots (5)$$

$$T_{12} = 2\,(1-b_{12})^{-1}\,(\eta_1^2-p^2)^{\frac{1}{2}} \quad \ldots\ldots\ldots\ldots (6)$$

The radius of penetration r_p for this particular ray is determined from the velocity relationship and is easily seen to be given by

$$r_p = (a_{12}\,p)^{c_{12}} \quad ; \quad c_{12} = (1-b_{12})^{-1} \quad \ldots\ldots\ldots (7)$$

Using equations (3) to (6), the traveltime and distance of any ray or ray segment can be determined by building up the times and distances over the proper number of layers, each layer being represented by new values of a, b, and η. The values of a and b are calculated from a given velocity distribution for that layer bounded by radii r_1 and r_2 $(r_1 > r_2)$ where

$$b_{12} = \ln(v_1/v_2)\,/\ln(r_1/r_2) \quad \ldots\ldots\ldots\ldots (8)$$

$$a_{12} = v_1 r_1^{-b_{12}} \quad \ldots\ldots\ldots\ldots (9)$$

and v_1 and v_2 are the given values of v at r_1 and r_2 respectively.

The theory embodied in equations (3) to (9) has several important applications. It can be used in ray tracing to investigate complexity in traveltime curves caused by regions of high velocity gradients or low velocity layers or to correct epicentral distances for focal depth (see Section 2.2.1). Of importance to this study, however, is the fact that it can be used to derive T-Δ and P-Δ curves for a specified velocity distribution, thus enabling models to

be generated for comparison with the observational data. As well, the equations can be used to strip the earth to any required depth h by calculating the contribution Δ_{12} of the region down to h to the total distance Δ in question. The adjusted distance or the distance corresponding to the stripped earth is given by ($\Delta - \Delta_{12}$) and the adjusted traveltime by ($T-T_{12}$).

Equations (3) to (9) formed the basis of the computer program (Wright, 1970) written to invert the $dT/d\Delta$ values by the Herglotz-Wiechert method and so generate a corresponding velocity distribution. Provided that $\eta = r/v$ is a monotonic decreasing fuction of depth beneath the surface, equation (1) can be solved to yield (Bullen, 1963).

$$\ln r_0/r_1 = \pi^{-1} \int_0^{\Delta_1} \cosh^{-1}(p/p_1)\, d\Delta \qquad \text{.....(10)}$$

where r_0 is the mean radius of the earth, r_1 is that radius where the velocity of the wave is V_1, $P_1 = \eta_1$ is the parameter of a ray that penetrates to a depth $r_0 - r_1$ and reaches the surface at a distance Δ_1 from the source, and $V_1 = r_1/p_1$. For convenience (10) can be written

$$r_1 = r_0 \exp\left(-\pi^{-1} \int_0^{\Delta_1} \ln\left(p/p_1 + \left((p/p_1)^2 - 1\right)^{\frac{1}{2}}\right) d\Delta\right) \qquad \text{.....(11)}$$

To evaluate v_1, $dT/d\Delta$ as a function of distance from 0 to Δ_1 is required so that r_1 can be calculated from (11). $V = r_1/p_1$ can then be estimated. If a discontinuity exists, the earth must be stripped of the region down to the discontinuity before the calculations can proceed for the region beneath the discontinuity. If h is the depth to the discontinuity and $dT/d\Delta$ values are known from the observational data over the distance range Δ_2 to Δ_1 ($\Delta_1 > \Delta_2$),

some existing model is used to fill in the distance range from 0° to Δ_2. Then the contributions to the distances in the range Δ_2 to Δ_1 due to that region to depth h, for values of $dT/d\Delta$ between $p(\Delta_2)$ and $p(\Delta_1)$ are calculated by summation over the appropriate number of layers. The contributions are then subtracted fromthe appropriate distances between Δ_2 to Δ_1 so that a $dT/d\Delta$ curve characteristic of a stripped earth of radius r_o - h is obtained. The computations then proceed as before, using equation (11) with the difference that r_o is now replaced by r_o - h, and the distance range of integration is that of the stripped distances corresponding to Δ_2 to Δ_1. The first stripped distance, i.e. corresponding to Δ_2 should be equal to 0, meaning that the depth h to the discontinuity used in the stripping technique is the maximum depth attained by the ray path of parameter $p(\Delta_2)$. The stripped distances increase from Δ_2 to Δ_1.

The computer program mentioned previously enabled the earth to be stripped to any appropriate discontinuity by evaluating (3) from an assumed velocity-depth model above the discontinuity. The quantity p in equation (3) refers to the observational $dT/d\Delta$ values to be inverted, η_1 and η_2 represent the $dT/d\Delta$ values, calculated from the velocity model assumed above the discontinuity for the corresponding velocity values V_1 and V_2. Thus a table of $dT/d\Delta$ values versus stripped distance is obtained. It is interpolated to give values at 1° distance intervals, beginning at the first stripped distance of 0°. This is to facilitate evaluation of the radius of penetration r_1 in equation (11) by means of Simpson's rule of integration. r_1 is evaluated for every third point in the table (i.e. the range of integration is from 0° to 2°, then 0° to 4°, then 0° to 6° etc. to obtain values of r_1, at 2°, 4°, 6°, etc.) Since $v = r/p$, and both r and p are known, the velocity v for the appropriate depth could

be calculated. Consequently, a velocity versus depth table can be derived from the measured $dT/d\Delta$ values in conjunction with an assumed velocity model above the discontinuity.

Finally, equations (3) and (4) are used to calculate the true distances and traveltimes at $dT/d\Delta$ intervals of 0.02 sec/deg. for both the assumed and the calculated velocity distribution. These values together with the correspoinding $dT/d\Delta$ values, radius and depth of penetration as well as the velocity values at each $dT/d\Delta$ interval of 0.02 sec/deg. were the final output of the computer program. Close examination of this table enabled assessment of any adjustments in velocity and discontinuity-depth values which might be necessary to ensure a better fit to the data. The entire procedure can be repeated for additional discontinuities.

2.4.2 Application of the Herglotz-Wiechert method to $dT/d\Delta$ values for the earth's core.

The boundary between the earth's mantle and core is discontinuous with a sharp decrease in compressional wave velocity from about 13.6 km/sec to 8.1 km/sec. (J-B values). Consequently, if the smoothed $dT/d\Delta$ for the AB branch are to be inverted to obtain a velocity distribution for the outer core, the earth must be stripped to the mantle-core boundary. For this purpose, the velocity distribution corresponding to the J-B values was assumed to the mantle-core boundary at a depth of 2894 km. This distribution and the smoothed $dT/d\Delta$ values for the AB branch were used to determine the velocity-depth distribution for the outer core. Because of the large discontinuous decrease in velocity at the core-mantle boundary, some difficulty was encountered in obtaining a satisfactory velocity-depth distribution, and an alternative but by no means poorer, procedure was adopted. The outer core

was assigned an initial velocity-depth distribution corresponding to the J-B tables. From this initial model the corresponding $dT/d\Delta$ and traveltimes values were calculated. The model was adjusted until a satisfactory fit of the calculated and the measured value was obtained.

The smoothed $dT/d\Delta$ data for the IJ branch were used to determine the depth to the first discontinuity in the transition region. This was done by using the velocity-depth distribution determined for the AB branch, together with the J-B distribution abouve the mantle-core boundary, to strip the earth to the depth where it was assumed that the discontinuity producing the receding BI branch was situation. This depth was adjusted until the stripped distance for the first IJ data point was as near 0^{o} as possible. This ensured that the advancing IJ branch would start at the desired distance of about 134^{o}. If this first stripped distance was positive, it meant that the depth to the discontinuity chosen was too shallow, with the result that the advancing IJ branch would start earlier than desired, while the receding BI branch would be correspondingly too long. Likewise, a negative stripped distance meaning that the discontinuity was too deep would result in a receding branch too short, and a later turning point for the advancing branch. The depth to the discontinuity was adjusted to give satisfactory results regarding the turning point of the advancing branch and the length of the receding branch. The corresponding velocity-depth values and traveltimes for the IJ branch were calculated as previously described. They were used in conjunction with the calculated velocities above the discontinuity (i.e. the AB velocities and JB model) to determine a satisfactory turning point for the GH branch using the smoothed $dT/d\Delta$ data for GH. This was repeated for the DF branch, fine adjustments of calculated velocities were necessary to obtain the best possible fit with the calculated traveltimes while at the same time ensuring that the

turning points for the various branches remained satisfactory, and that the measured $dT/d\Delta$ values required no significant adjustment.

In this manner, the measured $dT/d\Delta$ values for all four observed traveltime branches were inverted to obtain a velocity model for the earth's core. This model is discussed further in Chapter 3, along with a general discussion on the results of the measurement and analysis procedures used in this study.

CHAPTER 3

DISCUSSION

3.1 General Observations

During the measurement and analysis procedures described in Chapter 2, a number of peculiar observations were made. Generally, there has been no documentation in the published literature of similar observations. Because such observations may be relevant to other workers in the field, this section is devoted to a discussion of them.

While analysing the DF branch in the range 113° to 120°, a phase with a slightly lower $dT/d\Delta$ value and higher amplitude than the phase identified as PKP_{DF} was consistently observed less than one second after the DF phase arrived. This second arrival with different apparent velocity may simply be a diffracted effect due to irregularity in structure at the source or at some point in the path of the array. Rapid lateral variation in elastic parameters near the array site may also be a possible explanation. The first arrival with higher $dT/d\Delta$ value and earlier traveltime may even suggest the presence of an additional discontinuity quite near to the inner core boundary, the second arrival in this case being the true DF phase. More data is needed before such a possiblility could be investigated. That this anamalous observation may be azimuthally dependent is suggested by the fact that the events in question arrived from azimuths near 300° and 60°, and at different distances.

In the range 120° to 130°, similar effects were noted somewhat sporadically, with great variation in the amplitude of the first arrival with respect to the second. Of particular interest in this range, however, is that at distances of 120.6°, 121.7° and 121.8°,

the second arrival, approximately 1.5 seconds after the DF arrival had higher $dT/d\Delta$ value and amplitude than the DF phase. These may well be observations of the receding branch HD, and their amplitudes with respect to the amplitudes of the DF phase agree with Buchbinder's (1971) predictions.

Four events in particular deserve special mention. Those are events numbers 25, 26, 29, and 30 in the distance range 125° to 130°, all arriving from azimuths near 150°. These were the first events over the entire range to show any sign of precursors, but analysis of the precursors yielded puzzling results. For the first three events, precursors were observed just 3 to 4 seconds before the arrival of the DF phase. Analysis of their $dT/d\Delta$ values yielded results varying from 1.0 to 1.5 sec/deg for the first two events and 1.7 to 2.0 sec/deg for the third. The fourth event showedaprecursor only 1 to 2 seconds before DF, and with similar values as the above mentioned precursors. The $dT/d\Delta$ value for PKP_{DF} was low for all four events - approximately 1.4 to 1.5 sec/deg - and this was a general observation for all events in the azimuth range 100° to 160°. All four events showed a second set of presursors some 5 to 7 seconds before PKP_{DF}. Their $dT/d\Delta$ values were, on the average, slightly higher than the DF values, and on the basis that the DF values were low, they could have been, in the extreme, taken as belonging to the GH traveltime branch. This was not done, however, because their traveltimes, according to any existing models were too slow to belong to this branch. The focal depths of the events ruled out the possibility of them being $pPKP_{GH}$ arrivals. A third set of precursors was noted on all four events approximately 8 to 9 seconds (and in one case 15 seconds) before DF, but their $dT/d\Delta$ values were too low to be meaningful. These observations could be an azimuthal

effect as the events all occur at azimuths near 150°, but at different distances. No satisfactory explanation for the precursors can be given.

At least ten events in the range 134° to 139° showed precursors which were unusual. Some of these arrived approximately 4 seconds before PKP_{DF} with $dT/d\Delta$ values of about 3 to 4 sec/deg while others arrived only 1 to 2 seconds before DF with $dT/d\Delta$ values of 2.6 sec/deg. Yet others had $dT/d\Delta$ values of about 3.3 to 3.7 sec/deg but arrived only one second before DF. (The above mentioned values are the $dT/d\Delta$ values uncorrected for local structure. Such a correction, on the basis of the PKP_{DF} $dT/d\Delta$ value, would result in about a 5% increase in their magnitude). The possibility of these phases being $pPKP_{IJ}$ and $pPKP_{GH}$ were ruled out on the basis of focal depth of the events in question. It may be possible that they are due to some source of multiple arrivals deep in the crust (as for example faulting near the base of the crust (Wright, 1970)). On the basis of travel-times and $dT/d\Delta$ values it is likely that some of them are observations of the receding branches BI and JG.

In the distance range 131.6° to 138.9°, some 20 events showed phases arriving 2 to 4 seconds after the DF phase. In the majority of cases, these 2nd arrivals had slightly higher $dT/d\Delta$ values and amplitudes than the DF phase. They could probably be observations of the receding brand HD, but if Buchbinder (1971) is correct, their amplitudes at the distances in question should be lower than that of the DF arrivals. This lower amplitude behaviour was observed in only four of the 20 events. The high-amplitude data of 9 of these events also showed precursors some 2 to 4 seconds before the DF arrival, with $dT/d\Delta$ values approximately equal to or only slightly lower than the $dT/d\Delta$ values for the DF phase. Wright (personal communication, 1972) has made similar observations of the precursors

over the same distance range from seismograms recorded at the Yellowknife seismic array. However, no satisfactory explanation for these phases can be made at the present time.

3.2 Specific Observations Concerning PKP Phases

3.2.1 Identification of Phases

Since ultimately the model generated in this study depends upon the identification of the individual phases, a few comments on this subject would seem to be appropriate. The DF phase was easily identified up to distances of about 140^{o} as being the most prominent arrival on the record. This is in addition to identification on the basis of $dT/d\Delta$ and traveltime measurements. At distances of about 140^{o} to about 146^{o}, identification became somewhat difficultdue to the near-simultaneous arrivals of all the phases. Beyond 146^{o}, it was easily identified on the basis of traveltime and apparent velocity. Identification of the AB phase likewise proved easy in the distance range 150^{o} to 176^{o} because of its $dT/d\Delta$ values and longer traveltime which effectively separated it from the other phases. Even in the early part of its range from about 145^{o} to 150^{o}, no problem was encountered in separating PKP_{AB} from PKP_{IJ}, both of which tend to have similar values of $dT/d\Delta$ near 145^{o}. The AB phase always arrived after the IJ phase and its uncorrected $dT/d\Delta$ value was always slightly higher than that of the IJ phase.

In the range 132^{o} to 138^{o}, separation of the IJ and GH phases proved easy on the basis of their $dT/d\Delta$ and traveltime measurements. However, in the range 138^{o} to 142^{o} where the time separation of the two phases narrowed greatly and the true $dT/d\Delta$ values were sometimes masked by local structural effects, identification became more difficult and was often made after close examination of the $dT/d\Delta$ values obtained using rejection levels of both 0.02 and 0.04

seconds on the seismometer residuals. The greatest weight was attached to the 0.02 sec. rejection measurement since this is the higher precision measurement. In one or two instances, the identification was made solely on a traveltime basis if it was not possible to discriminate from one $dT/d\Delta$ value to another. Near 145°, the GH branch was masked by the IJ branch. In the latter part of the range beyond 145°, the two phases could once more be easily separated on the basis of their $dT/d\Delta$ and traveltime measurements.

On the basis of the measured $dT/d\Delta$ values and traveltimes, limited amplitude information (which will be discussed in Section 3.2.3) and an overall detailed analysis of all seismograms, it is believed that the PKP phases used in this study have been correctly identified.

3.2.2 Turning Points and End Points for the Traveltime Branches

At this point, it should be noted that it was not possible to determine precisely the turning point of the branch DF due to lack of data in the immediate region before 113.6°. As previously mentioned, the turning point was taken as the truncated value of 113.6 for use in the inversion techniques. This is not unreasonable as Adams and Randall (1964) place it at 110°, Bolt (1964) at 111.3°, Shurbet (1967) near 110°, and Ergin (1968) near 114°. Buchbinder (1971) placed the turning point near 120° on the basis of amplitude data.

The GH phase was first identified at a distance of 132.2°. The $dT/d\Delta$ values (uncorrected) for this phase were lower than the expected value by approximately 23%, but it arrived at the expected time per the Adams and Randall model. Since the DF $dT/d\Delta$ values on the same event were also 23% lower than expected, the phase was accepted as belonging to the GH branch. The same applies to the second observation of GH at a distance of 134.8°. The first clear

and strong GH phase was observed at a distance of 134.8°. Thus, the turning point for the GH branch was selected as being 132.0°.

Possible IJ precursors occurring approximately 12 to 13 seconds before DF could be barely recognized at distances of 132.0°, 133.11°, 134.5°, and 134.7°, but were too small, even on high amplitude data, to be analysed. The first identification of PKP_{IJ} was also made on the record at a distance of 134.8°. Although its amplitude was similar to that of the background noise, $d\tau/d\Delta$ measurements could be made. Thus, it is likely that the IJ branch has its turning point in the range of 132° to 135°. For the purpose of inversion, it was selected as being 134°.

Failure to observe either the GH or IJ phases at shorter distances may be due, apart from the obvious explanation that the phases simply do not exist in this part of the range, to several other reasons. For example, after 1967, the array was triggered by an arrival at the cluster with a 13 second delay loop for recording. If GH or IJ were present for distances less than 132° their amplitudes were insufficient to trigger the array, but the DF phase would trigger it. Unfortunately at these distances, the 13 seconds would not necessarily be sufficient to enable recording of the earliest precursons. This could have an important bearing in determining the turning points of the branches for, according to Buchbinder (1971), the turning point is that distance at which the amplitudes increase at greater distances but decrease rapidly at smaller distances. Any phases observed before the turning point are attributed to those phases partially reflected from the discontinuity and partially transmitted through it. Consequently, if the GH and IJ phases existed in the early part of the range, their amplitudes are so small, that by Buchbinder's criterion they do not in any case belong to the totally

transmitted advancing branches which were determined in this study. Another possible reason for failure to observe these phases, but which essentially leads to the same conclusion as above, is that the high-amplitude data was at times far too noisy for any coherent signals to be picked out. In other cases, there was a lack of high-amplitude data all together. In Section 3.1, four events which showed precursors in the range 125^{o} to 130^{o} were discussed. None of these precursors appeared even remotely to belong to either of the IJ or GH branches. This fact suggests that these phases do not exist in the range.

Owing to the sparseness of data in the range 150^{o} to 160^{o} it was not possible to define absolutely the end points of the IJ and GH branches. The last clear observation of IJ occurred at a distance of 150.89^{o} . Events at distances 152.7^{o} and 157^{o}showed no evidence of the phase so that it seems likely that the end point of the branch is somewhere near 151^{o}. This cannot be said with any certainty because of lack of data in this region. The last clear observation of GH also occurred at 150.89^{o}. The event at 157.2^{o} yielded a phase at the expected time of GH, but with $dT/d\Delta$ values lower than the expected value by about 25%. Since the DF $dT/d\Delta$ value was also low by approximately the same amount, the phase observed at 157.2^{o} was accepted as belonging to the GH branch. Thus, the end point for the branch had to be greater than this distance and was chosen to be 158^{o}.

The turning point for the AB branch was assumed to be somewhere in the range 143^{o} to 145^{o}. Strong arrivals of a phase that looked like AB, were recorded at distances of 142.31^{o} and 142.59^{o} but inclusion of these values in the smoothing of the AB data resulted in an undesirable flattening out of the AB branch.

These arrivals possibly belong to the receding BI branch. Because of this ambiguity, they were not included in the $dT/d\Delta$ data for the AB branch. For purposes of inversion, the turning point for this branch was selected as being at 145°. The phase was observed out to 175°, the greatest distance for any event analysed in this study.

3.2.3 Amplitude Observations

Although absolute amplitudes from one event to another could not be compared because of lack of information as to the gain used on each seismogram, it was possible to compare the relative amplitudes of the different phases for any one particular event. This showed that at distances less than 142°, the largest phase on the seismogram is the DF phase, followed in magnitude by the GH, then the IJ phases. The GH amplitude varied from about $\frac{1}{4}$ to 1/3 that of DF near 135°, to about 4/5 that of DF near 140°. The IJ amplitude varied from about 1/10 to 1/4 that of DF near 135° to $\frac{1}{2}$ to 3/4 that of DF near 140°. Thus the variance in amplitude of the IJ phase was more pronounced than the GH phase in the distance range less than 142°, although it always remained smaller than the GH phase at these distances. At distances greater than 142° PKP_{IJ} became more prominent than PKP_{GH}, but both were still smaller than the DF phase. Then, at about 145°, IJ exceeded DF in amplitude while GH was approximately equal to or only slightly larger than DF in amplitude. IJ continued to be the most prominent phase for the rest of its distance range attaining a maximum amplitude 10 times that of DF. The GH amplitude usually lay just beneath the IJ amplitude. The AB phase, entering at about 145° did so with amplitude greater than the DF amplitude but by 160°, its amplitude had fallen to approximately the same or slightly less than the DF amplitude. Of particular interest is the fact that while Adams and Randall (1964)

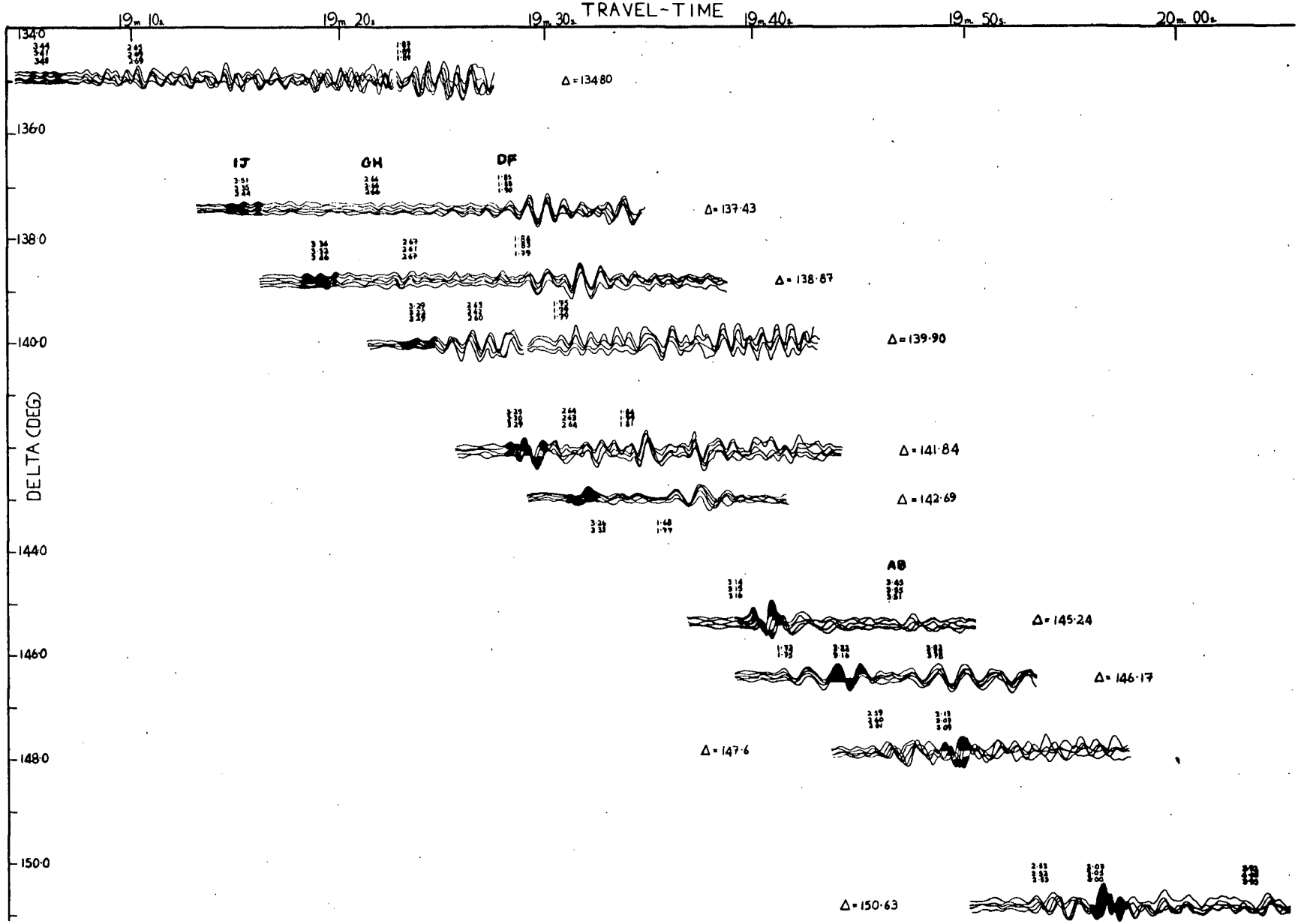

Figure 3.1 A Record Section for the Phases DF,GH,IJ,AB.The IJ Phase is shown darkened.

indicate that the GH phase is the most prominent on the record at distances between 145° and 153°, in this study the IJ phase is the most prominent at these distances. Close examination of the behaviour of the theoretical amplitudes determined by Buchbinder (1971) indicate good agreement with the observations just discussed.

3.2.4 A Record Section for Core Phases.

Figure 3.1 is a traveltime - distance section for seismograms in the range where the precursor branches GH and IJ were present. In compiling this record section, only 5 of the possible 20 traces have been reproduced for the sake of clarity.

The phases are identified by their $dT/d\Delta$ values on the record. In particular, the IJ phase is shown darkened throughout the record. This phase has not easily been observed in the past, and its clear observation is one of the significant results of this study.

Many of the observations discussed in the previous three sections are exemplified in this figure. The first seismogram at 134.80° is the one on which the IJ phase was first observed, and the GH phase was clear and prominent. The amplitude of the IJ branch with respect to the other branches can be seen to increase until at a distance of about 146° it exceeds the DF phase in amplitude. It becomes the most prominent phase, followed by GH, for the rest of its distance range. The decrease in time separation between the phases near 143° can be clearly observed. By 146.17°, the IJ (and possibly GH) phase becomes a later arrival to the DF phase. At 147.6° the IJ phase is seen arriving after the GH phase. The AB phase is first observed at 145.24°. The decrease in slope of the traveltime branches from IJ to DF can be clearly observed.

3.3 Discussion of the Analysed Data

3.3.1 Corrected $dT/d\Delta$ Measurements.

The corrected $dT/d\Delta$ measurements smoothed by the method of Summary values and by a polynomial regression technique were shown in Figures 2.9 and 2.10. The effect of restraining the AB curve to both the Bolt traveltime tables and the JB traveltimes indicated that the restraint to the J-B times gave a better fit to the corrected $dT/d\Delta$ data particularly in the early part of the AB range where the curvature is steep. Even so, the best fit to the data in this region would have been one with greater curvature than that given by the J-B restraint but this necessitated having summary points at almost the same distance but with widely differing $dT/d\Delta$ values. This could not be obtained with the distribution of available data for the region. The AB curve smoothed by polynomial regression lies between the two curves smoothed by summary values, but in the early part of the range it tends to lean heavily in favour of the J-B restrained curve. Owing to the lack of data in the range 150° to 160° the curve here has slightly less curvature than would be expected. For the same reason, the curves smoothed by summary values in this region behaved somewhat erratically and were simply replaced by the expected J-B values.

The IJ branch smoothed by both methods agree reasonably well, as does the DF branch. The GH branch restrained to the Adams and Randall traveltime curve and smoothed by the summary values method agrees almost exactly with that obtained by the polynomial regression method. Owing to the fact that the Bolt restraint for this branch was truncated at 156° instead of 158° (Bolt places his GH end point at 156°) and that his traveltimes all lie beneath the Adams and Randall traveltimes for the same distances, the curve restrained to his model was shifted to higher $dT/d\Delta$ values and at

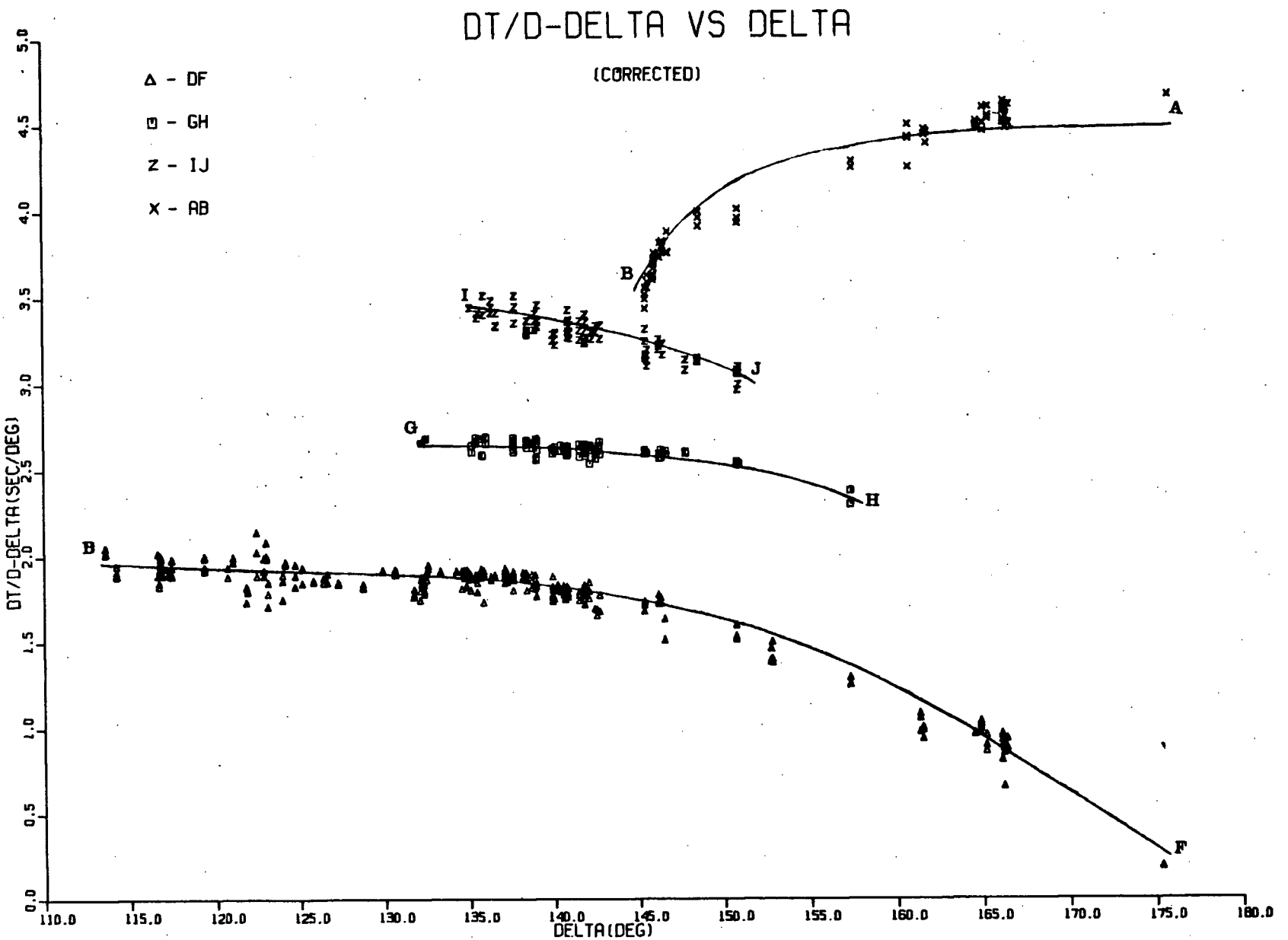

Figure 3.2 Fit of smoothed DT/DΔcurves on to corrected data.

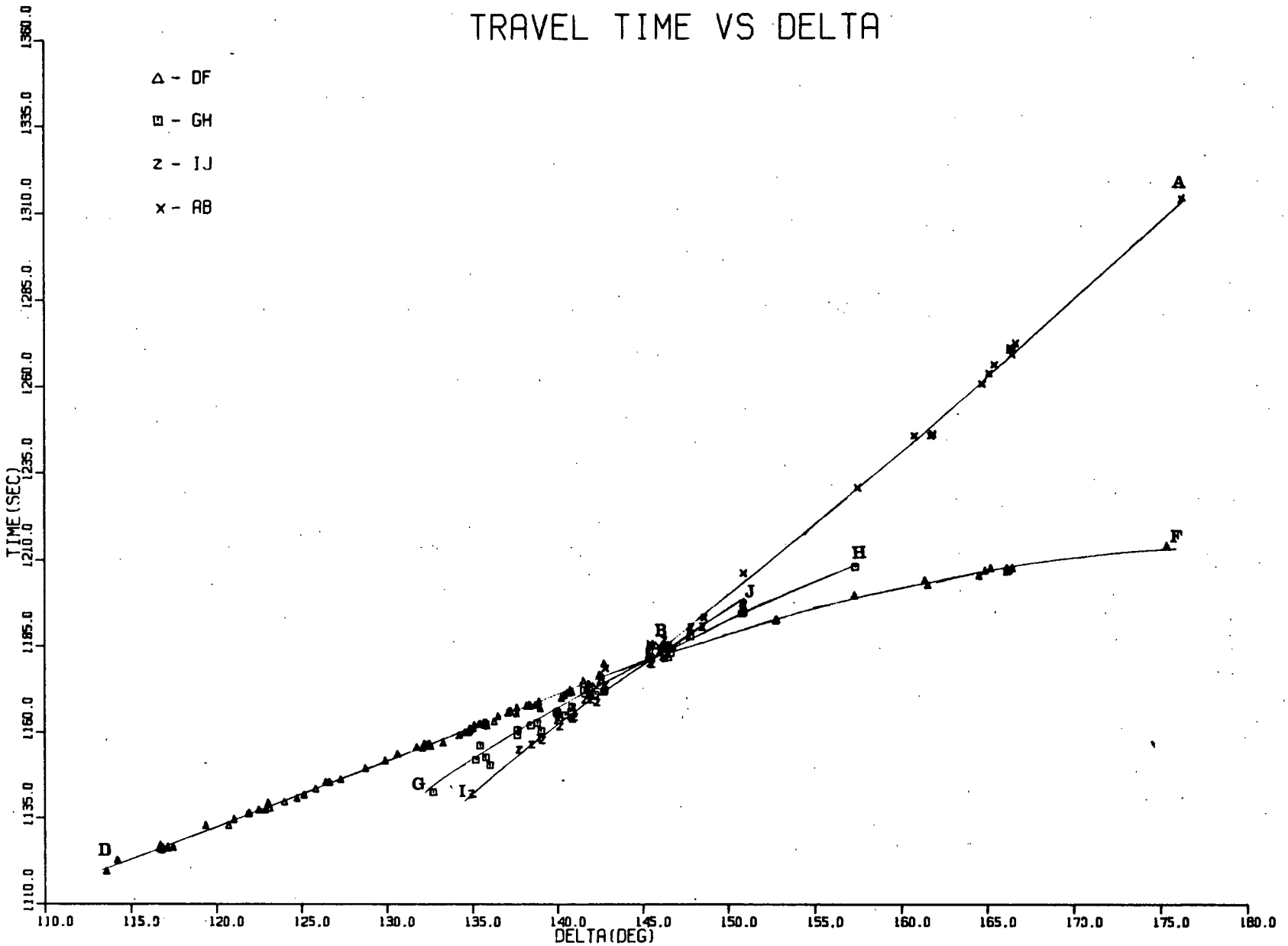

Figure 3.3 Fit of smoothed traveltime curves on to data.

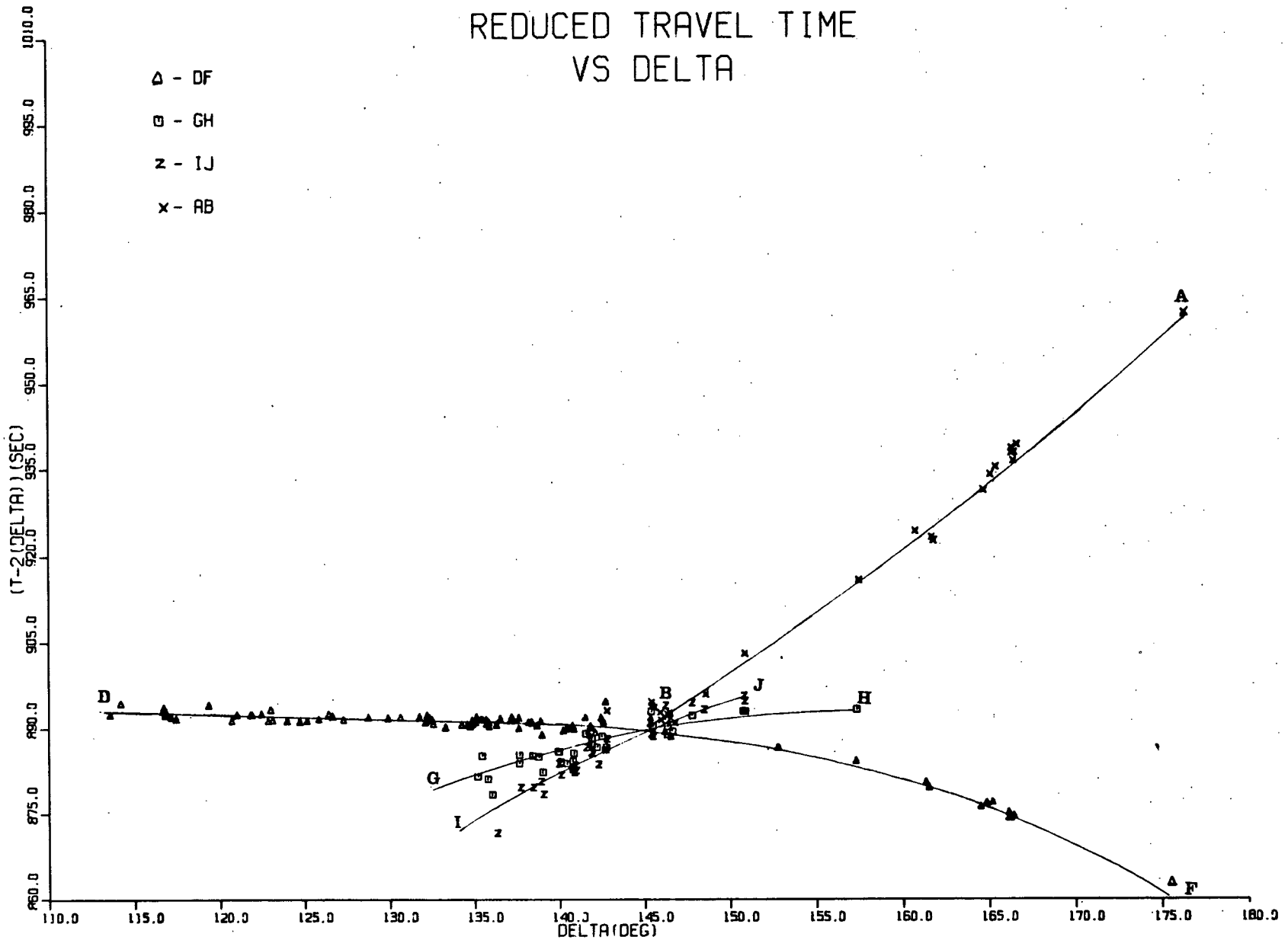

Figure 3.4 Fit of smoothed reduced traveltime curves on to data.

the same time fell off more sharply near 156°.

The smoothed $dT/d\Delta$ values used in the actual inversion procedure were the AB values restrained to J-B, the IJ and DF data, and the GH data restrained to the Adams and Randall model. The fit of these curves to the corrected $dT/d\Delta$ measurements is shown is Figure 3.2. As determined by the χ^2 tests (Section 2.3.1) for the final summary points used in deriving these curves, the fit is good for all the branches observed in this study.

3.3.2 Travel-time Measurements

The traveltime measurements, after corrections for ellipticity and focal depth had been applied, were smoothed using the U.B.C. TRIP program as described in Appendix Va. The independent variables were the same as those used in the smoothing of the data, and the resulting regression equations are listed in Table 3.1. These equations were used to calculate the traveltimes at 1° intervals. The corresponding traveltimes and reduced traveltime curves are superimposed on the data in Figures 3.3 and 3.4 respectively. That the fit is a good one is evident from the parameter R^2 (which is discussed in Appendix Va) for the different branches as shown in Table 3.1. Basically, the closer R^2 is to the value unity, the better is the fit of the regression equation to the data. R^2 has the lowest value of 0.986 for the GH branch.

It should be noted that no corrections for structure beneath the array were applied to the measured traveltimes on the assumption that at the large distances involved, such corrections would be negligible.

The residuals (O - C), between the smoothed and measured times are shown in Figure 3.5. A positive residual implies a late arrival with respect to the smoothed times and vice versa. The

TABLE 3.1 REGRESSION EQUATIONS FOR SMOOTHED TRAVELTIME DATA

DF BRANCH 105 data points

$R^2 = 0.9985$

INDEPENDENT VARIABLE	COEFFICIENT	STD.ERROR	F-PROB	TOLERANCE
CONSTANT	1119.4653	0.3729	0.0000	1.0000
(Δ-113)	1.7656	$0.6556/10^2$	0.0000	1.0000
$(\Delta-113)^2$	0.1222/10	$0.3536/10^3$	0.0000	1.0000
$(\Delta-113)^3$	$-0.2681/10^3$	$0.2779/10^4$	0.0000	1.0000

$$T = 1119.4653 + 1.7656(\Delta-113) + 1.222\left(\frac{\Delta-113.0}{10}\right)^2 - 0.2681\left(\frac{\Delta-113}{10}\right)^3$$

GH BRANCH 34 data points

$R^2 = 0.9863$

INDEPENDENT VARIABLE	COEFFICIENT	STD.ERROR	F-PROB	TOLERANCE
CONSTANT	1141.2908	1.1931		
(Δ-132°)	3.2137	0.0566	0.0000	1.0000
$(\Delta-132°)^2$	-0.2175/10	$0.7953/10^2$	0.0000	1.0000

$$T = 1141.2908 + 3.2137(\Delta-132) - 2.175\left(\frac{\Delta-132}{10}\right)^2$$

IJ BRANCH 26 data points

$R^2 = 0.9915$

INDEPENDENT VARIABLE	COEFFICIENT	STD.ERROR	F-PROB	TOLERANCE
CONSTANT	1140.2857	1.1746		
(Δ-134°)	3.7487	0.0655	0.0000	1.0000
$(\Delta-134°)^2$	-0.19410	0.0142	0.01808	1.0000

$$T = 1140.2857 + 3.7487(\Delta-134) - 1.9410\left(\frac{\Delta-134}{10}\right)^2$$

AB BRANCH 23 data points

$R^2 = 0.9979$

INDEPENDENT VARIABLE	COEFFICIENT	STD.ERROR	F-PROB	TOLERANCE
CONSTANT	1180.8818	0.7517		
(Δ-145°)	3.8276	0.0432	0.0000	1.0000
$(\Delta-145°)^2$	0.13923/10	$0.6171/10^2$	0.0338	1.0000

$$T = 1180.8818 + 3.8276(\Delta-145) + 1.3923\left(\frac{\Delta-145}{10}\right)^2$$

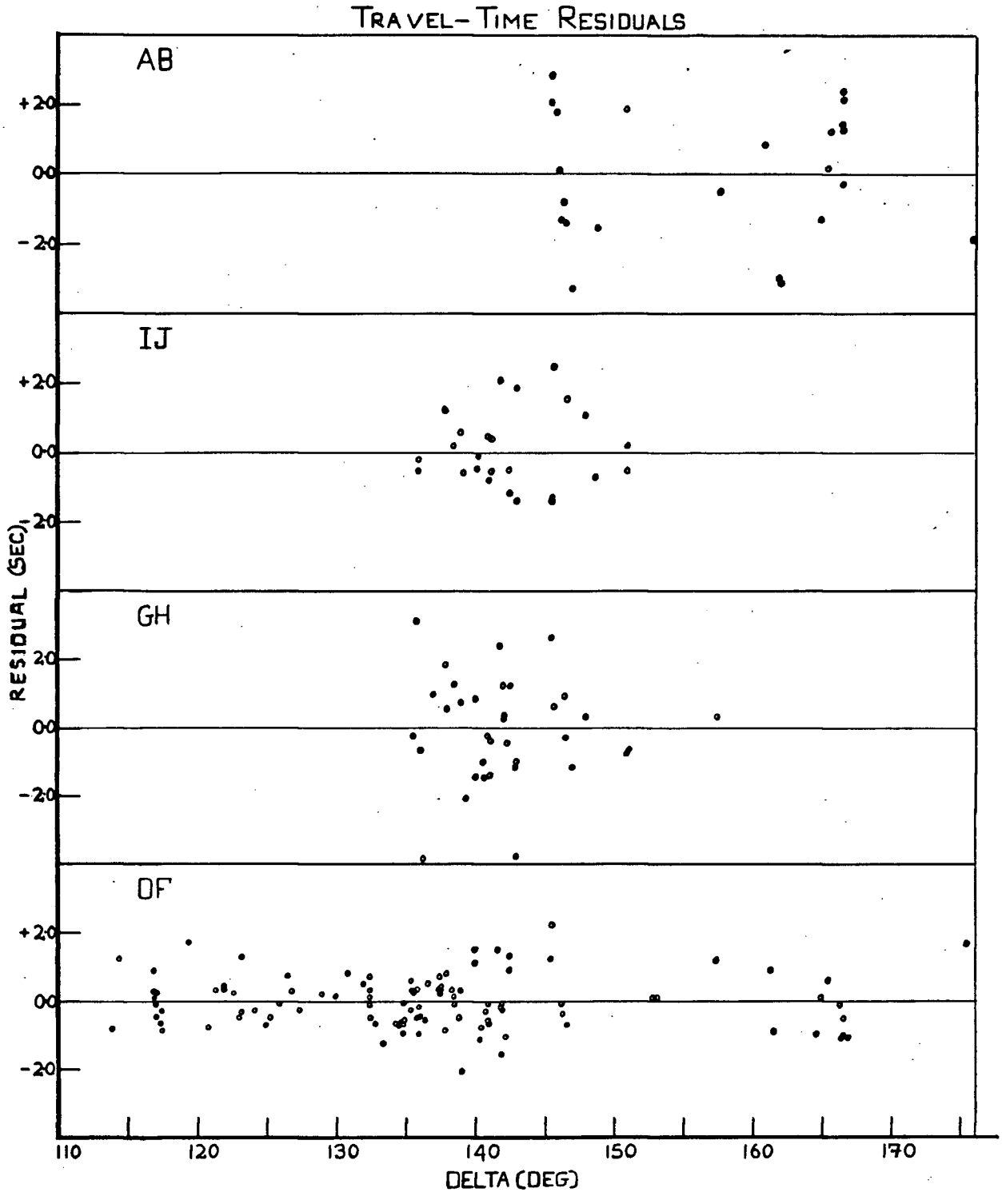

Figure 3.5 Traveltime Residuals (O-C).

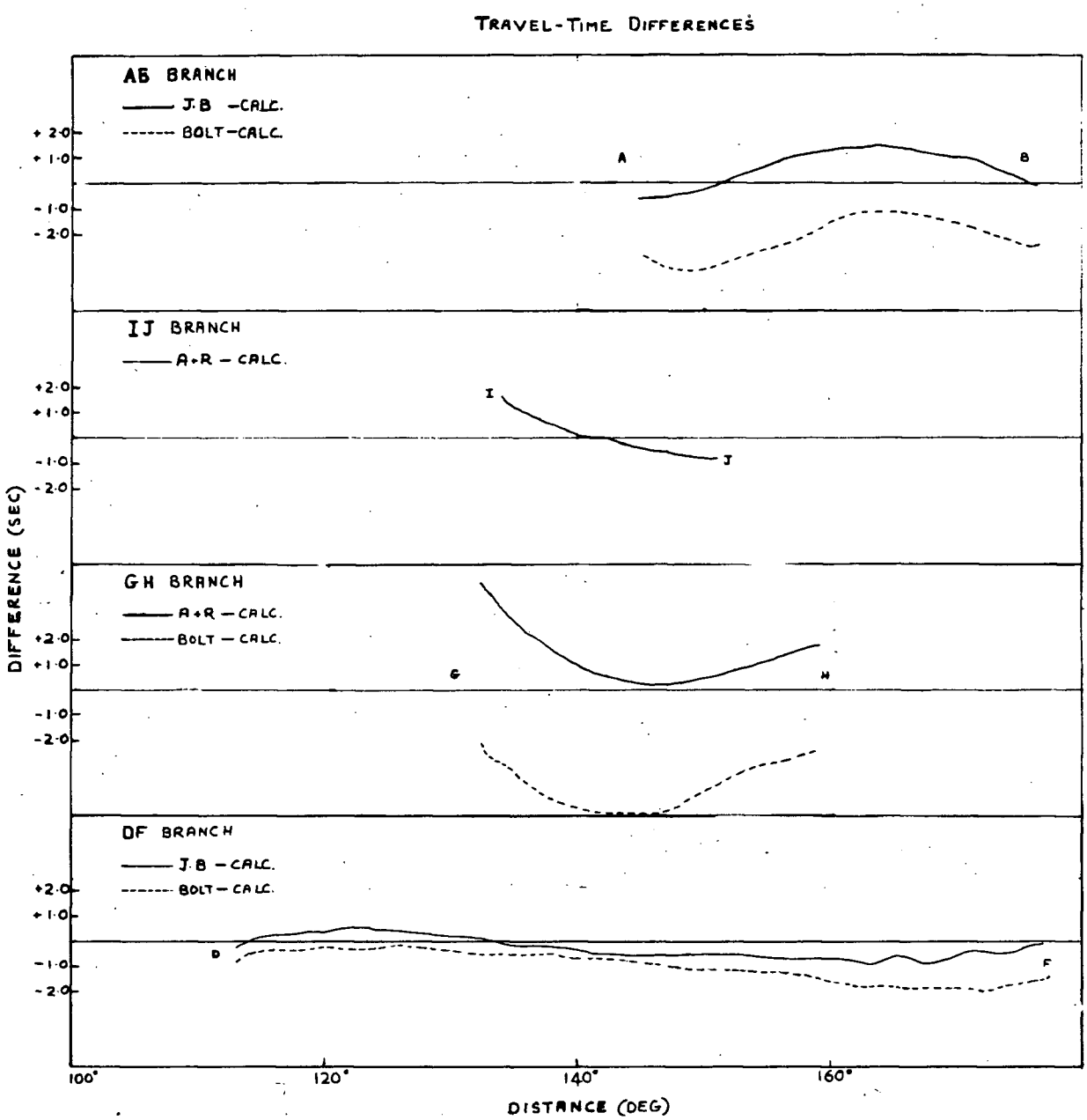

Figure 3.6 Traveltime Differences.

residuals show the least scatter for the DF branch. This is a natural consequence of the fact that the unsmoothed times for the branch closely defined the regression curve. The larger scatter in the unsmoothed IJ and GH times (Figure 3.3) are duplicated by their corresponding residuals. The scatter of the residuals for the AB branch may be more a consequence of the sparseness of the data points over the large distance range of the branch, so that the regression curve could not be precisely defined by the data. Also the onset of this phase is often difficult to pick.

The traveltime differences of the smoothed times with respect to various traveltime models already in existence are shown in Figure 3.6. The smoothed AB and DF times agree more closely with the corresponding J-B values, but the smoothed AB times may indicate that lesser curvature is required in the J-B curve near 155°, so that the new times are about 1 second later than the present J-B times. It should be remembered, however, that the smoothed AB traveltime curve may not be an adequate representation of the true situation owing to the lack of data over the range. The IJ branch requires greater curvature than the Adams and Randall model near its beginning and lesser curvature near its end point. The GH branch is shifted to lower traveltime than those defined by the Adams and Randall model, and to higher times with respect to the Bolt model. It requires greater overall curvature than that demanded by both models. Again, the behaviour of the smoothed traveltimes of the precursor branches near their end points may simply be a consequence of the least squares fit in which too large emphasis is placed on values near the end points of the branches. Obviously, any error in these end points would tend to bias the resulting smoothed times near these regions in a

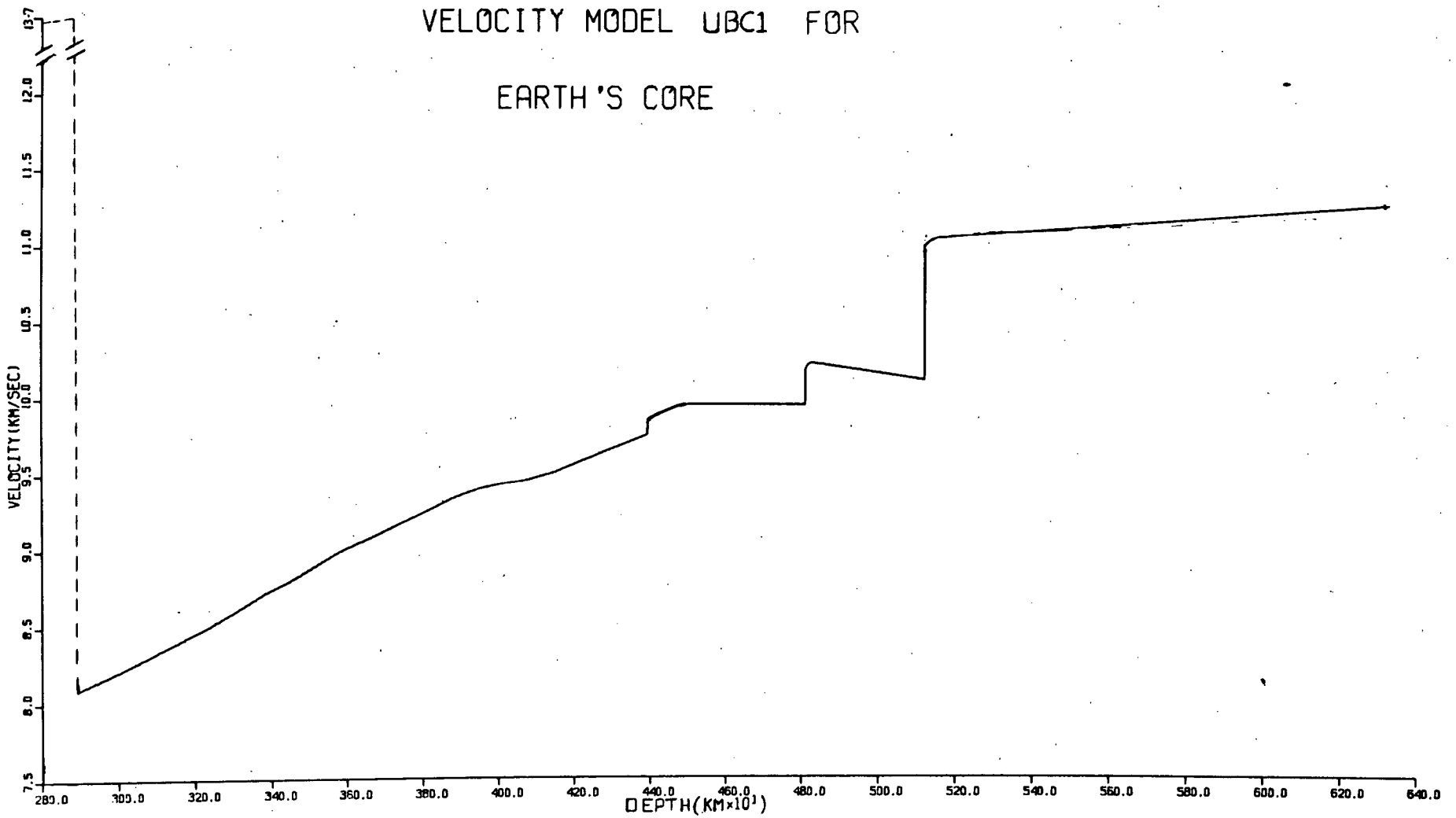

Figure 3.7 Velocity Model UBC1. for Earth's Core.

corresponding manner. This fact is important when it comes to adjusting the final velocity model in order to obtain agreement between the calculated and the smoothed times. On account of this biasing of times near the end points of the precursor branches, exact agreement of the model times and smoothed times in these regions is not to be exclusively demanded. It is of more importance, however, that the agreement be within the limits imposed by the scatter of the travel-time residuals themselves, for the respective branches.

3.4 Velocity Model UBC1

Figure 3.7 shows the velocity model, UBC1, which represents the best fit to all data analysed in this study. Of all the models described in Section 1.2, it most closely resembles that suggested by Adams and Randall (1964).

The basic difference in the two models lies in the location of the turning points for the different branches and in the magnitude of the change in $dT/d\Delta$ along the receding branches. From these two differences arise the other dissimilarities: depth to the corresponding discintinuities, magnitude of the velocity jumps at these dicontinuities, and traveltime gradients in the two shells defined by the discontinuities.

In the process of fitting the AB branch to the data, it was found that the J-B values of velocity for the outer core had to be reduced slightly from a depth of about 4000 km downwards, in order to get agreement between the calculated and measured traveltimes and $dT/d\Delta$ values. Too great a reduction at this depth however, resulted in an undesired feature, the formation of a caustic in the early part of the AB branch and traveltimes that were too slow. Thus, a good restraint was put on the magnitude of the velocity reduction.

The first velocity discontinuity in UBC1 giving rise to the receding branch BI of the traveltime curve is at a depth of 4393 km (0.569 Rc). The end point of the branch AB is at 144.4°. The turning point of the advancing branch IJ is located at 134.2° and the magnitude of the jump at this discontinuity is 0.108 km/sec. The value of $dT/d\Delta$ near B is 3.52 sec/deg and near I it is 3.48 sec/deg. The turning point I in UBC1 is 4.2° later than that in the A & R model and this results in the slightly deeper discontinuity for the UBC1 model. The change in $dT/d\Delta$ along the receding branch BI for UBC1 is slightly less than that in the A & R model, and this, together with the later turning point I for UBC1, results in a smaller velocity jump. The depth to the first discontinuity in model UBC1 is well above the level 0.54 Rc (depth 4497 km) to which rays would have to penetrate in order to form a caustic at a distance of about 143°. It should be noted that the large amplitude arrivals near this distance (see Figure 3.1) were associated with arrivals of the IJ phase, rather than as the result of a caustic at B.

The second discontinuity giving rise to the receding JG branch, occured at a depth of 4810 km. in UBC1. The magnitude of the velocity jump at the discontinuities 0.237 km/sec. The end point of the IJ branch occurs at 131.9° with $dT/d\Delta$ value of 2.66 sec/deg. The later starting point for G, and the smaller change in $dT/d\Delta$ along JG for model UBC1 results in a smaller velocity jump for this model than in the A & R model.

The effect of using the higher $dT/d\Delta$ values for the GH branch, due to restraining the smoothed data to the Bolt traveltime curve rather than the A & R curve, was to raise the discontinuity to about 4765 km and to cause a slightly higher velocity jump of 0.287 km/sec at

the discontinuity. The change in $dT/d\Delta$ along JG remained the same as before, but the turning points J and G were slightly earlier and later respectively. However, UBC1 was generated from the $dT/d\Delta$ measurements restrained to the A & R curve.

The velocity gradient in the first shell defined by the first two discontinuities of UBC1 is initially positive then slightly less than zero and the thickness of the shell is 417 kms. Adams and Randall required a more negative gradient in the region on account of their larger velocity jump at the discontinuity.

The third discontinuity at the inner core boundary, producing the receding branch HD, occurs at exactly the same depth as that obtained by Jeffreys (1939) - 5120 km. This implies an inner core of radius 1251 km. The magnitude of the velocity jump at the discontinuity is 0.92 km/sec while the end point H or branch GH is located at 158.6° with $dT/d\Delta$ value of 2.16 sec/deg. The turning point D is located at 113.2° with $dT/d\Delta$ value of 1.96 sec/deg.

The second and third velocity discontinuities define a second shell surrounding the inner core. This shell is 310 km. thick and has slightly negative gradient. This negative gradient can only be eliminated by placing the turning point D at a later distance and the end point H at at an earlier distance. The depth to the second discontinuity would increase and the velocity jump at the discontinuity would decrease, enabling the gradient in the second shell to be non-negative. Such requirements cannot be met by the data. The velocity distribution in the inner core closely follows that of Buchbinder (1971).

A direct consequence of the smaller negative velocity gradients and smaller velocity jumps in the transition region of

TABLE 3.2a POSITION OF CUSPS FOR MODEL UBC1.

CUSP	Δ	T		DT/DΔ
	(DEG)	MIN	SEC	(SEC/DEG)
B	144.4	19	38.7	3.52
I	134.2	19	2.2	3.48
J	152.6	20	2.3	2.74
G	131.9	19	4.1	2.66
H	158.6	20	12.1	2.16
D	113.2	18	39.4	1.96
RESULTS OBTAINED BY RESTRAINING GH DATA TO BOLT'S TRAVELTIME CURVE:				
J	151.6	19	58.9	2.82
G	132.3	19	4.8	2.74
H	158.9	20	11.9	2.16

TABLE 3.2b VELOCITY-DEPTH VALUES FOR UBC1.

DEPTH (KM)	VELOCITY (KM/SEC)	DEPTH (KM)	VELOCITY (KM/SEC)	DEPTH (KM)	VELOCITY (KM/SEC)
2894	13.6700	3659	9.1100	4810	10.0000
2894	8.1000	3728	9.2000	4810	10.2370
2964	8.1800	3798	9.2800	4829	10.2698
3033	8.2600	3868	9.3700	4900	10.2440
3103	8.3500	3937	9.4800	5000	10.2070
3172	8.4400	4076	9.5000	5120	10.1600
3242	8.5300	4146	9.5500	5120	11.0800
3311	8.6300	4215	9.6200	5400	11.1300
3381	8.7400	4393	9.8000	5600	11.2400
3450	8.8300	4393	9.9080	5800	11.2600
3520	8.9300	4488	10.0105	6200	11.2800
3589	9.0300	4500	10.0000	6371	11.2800

RESULTS OBTAINED BY RESTRAINING GH DATA TO BOLT'S TRAVELTIME CURVE

4500	10.0000
4765	10.0000
4765	10.2870
4829	10.2698

TABLE 3.3 TRAVELTIMES FOR MODEL UBC1.

(SURFACE FOCUS)

DISTANCE	DF		GH		IJ		AB	
(DEG)	MIN	SEC	MIN	SEC	MIN	SEC	MIN	SEC
130.0	19	12.0						
131.0		13.9						
132.0		15.8	19	4.4				
133.0		17.7		7.1				
134.0		19.5		9.7	19	1.6		
135.0		21.4		12.4		5.1		
136.0		23.2		15.1		8.5		
137.0		25.0		17.7		11.9		
138.0		26.9		20.3		15.3		
139.0		28.7		22.9		18.7		
140.0		30.5		25.5		22.0		
141.0		32.3		28.1		25.6		
142.0		34.0		30.7		28.9		
143.0		35.7		33.3		32.3		
144.0		37.4		35.9		35.6		
145.0		39.2		38.5		38.8	19	40.4
146.0		40.9		41.1		42.0		44.2
147.0		42.6		43.7		45.2		48.1
148.0		44.2		46.3		48.4		52.0
149.0		45.8		48.8		51.5		56.1
150.0		47.4		51.3		54.6	20	0.2
151.0		48.9		53.8		57.7		4.4
152.0		50.4		56.3	20	0.6		8.6
153.0		51.8		58.7				12.8
154.0		53.2	20	1.2				17.0
155.0		54.5		3.6				21.2
156.0		55.8		6.0				25.5
157.0		57.2		8.4				29.8
158.0		58.5		10.7				34.1

model UBC1 is that they would cause the central density of the earth's core to have a lower value than that necessitated by the Adams and Randall model (see Section 1.3.1) without greatly affecting the rigidities of the transition region and the inner core (Section 1.3.2.).

The position of the traveltime cusps and the velocity - depth relationship for UBC1 are shown in Tables 3.2a and 3.2b respectively. The uncertainties in the depths to the discontinuities are estimated at being of the order of 10 km on the basis of obtaining satisfactory turning points for the various branches.

The traveltimes of model UBC1 listed in Table 3.3 agree with the smoothed traveltimes determined in this study within the limits imposed by the scatter of the residuals. The greatest discrepancy was obtained for the early part of the GH branch. It appeared that the smoothed times were too early by about two seconds in this vicinity. This was undoubtedly the result of a biasing of the regression curve towards early times owing to the first measured arrival time being early, possibly as a result of epicentre mislocation. The model times for the GH branch tend to be shifted downwards by an average of about 1 second with respect to the Adams and Randall times, and upwards by about 3 to 5 seconds with respect to Bolt's traveltimes in the latter and earlier part of the branch respectively. The model times for the IJ branch agree almost exactly with the model times of Adams and Randall, the only difference being that the UBC1 times are about 0.2 seconds earlier up to about 146°, and 0.1 seconds later beyond this. The model times for the AB and DF branches agree with those of the J-B traveltime tables.

It must be emphasized that model UBC1 is that model which

gave the best fit to the $dT/d\Delta$ and traveltime measurements made in this particular study. A more efficient distribution of data than that used in the study could result in small modifications (such as changes in location of the turning points of the branches, with resulting effects) to this model.

CHAPTER 4

CONCLUSION

Measurements of traveltime and traveltime gradients $dT/d\Delta$, have been made at the Warramunga seismic array for PKP phases from 115 earthquakes over the distance range 113° to 176°. The data have been used to obtain a velocity-depth model for the earth's core.

The $dT/d\Delta$ measurements at WRA were strongly perturbed by local structure beneath the array and an empirical method of correcting for this effect was employed. The corrected $dT/d\Delta$ values were smoothed by the method of summary values and a polynomial regression technique. Both methods gave results which were in reasonably good agreement. The traveltime gradient measurements smoothed by the summary value method were the ones actually used in inverting the data to obtain a velocity model since they had been restrained to acceptable traveltime curves in order to remove any random error.

The smoothed $dT/d\Delta$ values were inverted by the Herglotz-Wiechert method to derive a velocity-depth model for the earth's core. This model, UBC1, was the one which gave the best fit to the measured $dT/d\Delta$ and traveltime data.

The significance of this study is that it revealed clearly the existence of two precursor branches - IJ and GH - to the main DF traveltime branch for the earth's core. Previously, only one of these branches, the GH one, had been widely accepted. This single precursor branch resulted in a transition region for the earth's core containing two velocity discontinuities and one "shell" surrounding the inner core. On the other hand, the existence of two precursor branches, GH as well as IJ, gives rise to three velocity discontinuities

and two shells surrounding the inner core. This additional branch, PKP_{IJ}, accounting for the earliest precursors to PKP_{DF} at distances less than 145°, has been consistently observed in this study. The consequences of its observation are manifested in the form of a triple-discontinuity, double-shell transition region for model UBC1.

The first velocity discontinuity of 0.11 km/sec occurs at a depth of 4393 km. The region between the core-mantle boundary at a depth of 2894 km. and this discontinuity generates the AB traveltime branch for the earth's core. This branch has its' turning point at 144.4° and initial slope of 3.52 sec/deg.

The second discontinuity with an associated velocity jump of 0.24 km/sec occurs at a depth of 4810 km. The region between the first and second discontinuities, a shell approximately 417 km. thick generates the earliest precursor branch IJ. This branch begins at 134.2° with an initial slope of 3.48 sec/deg and terminates at 152.6° with a slope of 2.74 sec/deg.

The third velocity discontinuity of magnitude 0.92 km/sec occurs at the inner core boundary at a depth of 5120 km. The region between the second and third discontinuities, a shell approximately 300 km thick, generates the second precursor branch GH. This branch has its turning point at 131.9° with an initial slope of 2.66 sec/deg at that point and extends to 158.6° with a slope of 2.16 sec/deg.

The region beneath the third discontinuity, i.e. the inner core of radius 1251 km., generates the main traveltime branch, DF, for the earth's core. The turning point of this branch is 113.2° and its' initial slope is 1.96 sec/deg. The branch terminates at 180.0° with zero slope.

The consequences of a double-shell transition region would

be manifested in other core phases as well. Thus, phases other than PKP (such as SKP,PKS,SKS) should be closely examined for corroborative evidence of a triple-discontinuity transition region. Such a region would have the same effect, producing two additional branches to the traveltime curve, on all core phases although the magnitude of the effect would vary. Some problems could arise in such a study. The phases SKS, PKS, and SKP never occur as first arrivals and the first two require horizontal component seismometers for optimum recording. Also, since the periods of these phases are considerably longer than that for PKP, identification and subsequent measurement of the precursors could be more difficult.

Amplitude measurements in addition to $dT/d\Delta$ and traveltime studies similar to those made in this project would be most useful in defining closely the turning points of the traveltime branches. This could have important consequences on the final core model derived.

While it is not expected that the proposed velocity model, UBC1, for the earth's core will be accepted as the ultimate one, major changes to this model are not presently envisaged. The methods used in this study have enabled a more definitive identification of the traveltime branches and it is upon such identification that any reliable velocity model depends.

BIBLIOGRAPHY

Adams, R.D. and M.J. Randall, 1963. Observed Triplication of PKP, vol. 200, NO. 4908, 744-745

Adams, R.D. and M.J. Randall, 1964. The fine structure of the Earth's core, B.S.S.A., vol. 54, NO. 5, 1299-1313

Adams, R. D. and M. J. Randall, 1969. Distance corrections for deep focus earthquakes. Geophys. J. R. astr. Soc., vol. 18 329-330.

Arnold, E.P., 1968. Smoothing traveltime tables. B.S.S.A., vol. 58, 1345-1351

Birtill, J.W. and F.E. Whiteway, 1965. The application of phased arrays to the analysis of seismic body waves. Phil. Trans. Roy. Soc. Lond. A, vol. 258, 421-493

Bolt, B.A., 1959. Traveltimes of PKP up to 145 . Geophys. J.R. astr. Soc., vol. 2, 190-198

Bolt, B.A., 1962 Gutenberg's early PKP observations. Nature vol. 196, 122-124

Bolt, B.A., 1964. The velocity of seismic waves near the Earth's centre. B.S.S.A., vol. 54, 191-208

Bolt, B.A., 1968. Estimation of PKP traveltimes. B.S.S.A., vol. 58, NO. 4, 1305-1324

Cleary, J. R., C. Wright and K. J. Muirhead, 1968. The effects of local structure upon DT/DΔmeasurements at the Warramunga seismic array. Geophys. J., vol. 16, 21-29

Buchbinder, G.R.R., 1971. A velocity structure of the Earth's core. B.S.S.A., vol. 61, NO.2, 429-456

Bullen, K.E., 1938. Ellipticity corrections to waves through the earth's central core. M.N.R.A.S., Geophys. Suppl., vol. 4, 317-331

Bullen, K.E., 1963. An introduction to the theory of Seismology, 3rd Edition, Camb. Univ. Press, Cambridge

Carder, O.S., D.W. Gordon and J.N. Jordan, 1966. Analysis of surface foci traveltimes. B.S.S.A., vol. 54, 815-840

Cleary, J.R. and A.L. Hales, 1966. An analysis of the traveltime of P waves to North American stations, in the distance range 32 to 100 . B.S.S.A., vol. 56, 467-489

Corbishley, D.J., 1970. Multiple array measurements of the P wave traveltime derivative. Geophys. J., vol. 19, 1-14

Engdahl, E. R., J. Taggart, J. L. Lobdell, E.P. Arnold and G. E. Clawson, 1968. Computational methods. B. S. S. A., vol. 58 1339-1344.

BIBLIOGRAPHY
(cont'd)

Ergin, K.,1967. Seismic evidence for a new layered structure of the Earth's core. J.G.R., vol. 72, NO.14, 3669-3687

Evernden, J.F., 1953. Direction of approach of Rayleigh waves and related problems - I. B.S.S.A., vol.43, 335-374

Fisher, R.A., 1953. Dispersion on a sphere. Proc. Roy. Soc. Lond, A, vol. 217, 295-305

Gogna, H.L., 1968. Traveltimes of PKP from Pacific earthquakes. Geophs. J., vol. 16, 489-514

Gutenberg, B., 1914 Ueber Erdbebenwellen, VIIA Nach. Ges. Wiss Goettingen. Math. Physik, KI., 166-218.

Gutenberg, G., 1957. The Boundary of the Earth's Inner Core. Trans. Amer. Geophys. Union., vol. 38, 750

Gutenberg, B., 1958. Caustics Produced by Waves Through the Earth's Core. Geophys. J., vol.3, 238

Gutenberg, B. and C.F. Richter, 1937. P' and the Earth's Core. M.N.R.A.S., Geophys. Suppl., vol. 4., 363

Hannon, W.J. and R.L. Kovach, 1966. Velocity filtering of seismic core phases. B.S.S.A., vol. 54, 441-454

Jeffreys, H., 1934. On smoothing and differentiation of tables. Proc. Camb. Phil. Soc., vol.30, 134-138

Jeffreys, H., 1937. On the smoothing of observed data. Proc. Camb. Phil. Soc., vol. 33, 444-450

Jeffreys,H., 1939. The times of core waves (second paper). M.N.R.A.S., Geophys. Suppl., vol. 4, 594-615

Jeffreys, H., 1961 Theory of probability. Third Edition, O.U. P. 214-216.

Jeffreys, H.,and K.E. Bullen, 1940, 1967. Seismological Tables British Association for the Advancement of Science, Gray Milne Trust, London

Julian, B.R., D.Davies and R.M. Sheppard, 1972. PKJKP. Nature, vol. 235, 317-318

Keen, C.G.,J. Montgomery, W.M.M. Mowat, J.E. Mullard and D.C. Platt, 1965. British seismometer array recording systems, The Radio and Electronic Engineer, Vol. 30, 297-306

Kelly, E.J., 1964. Limited network processing of seismic signals. Massachusetts Inst. Technol. Group Rept. 44

Knopoff, L. and J.G.F. Macdonald, 1958. Magnetic field and central core of the earth. Geophys. J., vol. 1, 216

BIBLIOGRAPHY
(cont'd)

Kuhn, W. and S. Vielhauer, 1953. Boziehungen zwischen der Ausbreitungvon Longitudinal und Transversalwellen in relaxierden medien 2. Phyzik. Chem., vol. 202,214.

Lehmann, I., 1936. P'. Publ. Bur. Central Seism. Intern., Ser A, Trav. Sci., vol. 14, 87-115

Muirhead, K.J., 1968. Eliminating false alarms when detecting seismic events automatically. Nature, vol. 217, 533-534

Nguyen-Hai, 1961. Propagation des ondes dans le noyeau terrestre d'apres les seismes profonds de Fidji. Ann. Geophys., vol. 17, 60-66

Niazi, M., 1966. Corrections to apparent azimuths and traveltime gradients for a dipping Mohorovicic discontinuity, B.S.S.A., vol. 56, 491-509

Niazi, M., and D.L. Anderson, 1965. Upper mantle structure of western North America from apparent velocities of P waves. J.G.R., vol. 70, 4633-4640

Otsuka, M., 1966. Azimuth and slowness anomalies of seismic waves measured on the central California Seismic Array., B.S.S.A., vol. 56, 223-239 and 655-675

Shima, E., K. McCamy and R.P. Meyer, 1964. A Fourier transform method of apparent velocity measurement. B.S.S.A., vol. 54, 1843-1854

Shurbet, D.M., 1967. The earthquake P phases which penetrate the earth's core. B.S.S.A., vol. 57, 875-890

Stacey, F.D., 1969. Physics of the earth's interior. Wiley, New York

Truscott, J.R., 1964. The Eskdalemuir sesmic array. Geophys. J., vol. 9, 59-67

Underwood, R., 1967. The seismic network and its applications. Ph.D. Thesis, Australian National University, Canberra

Watson, G.S., 1956. Analysis of sispersion on a sphere. M.N.R.A.S., Geophys. Suppl., vol. 7, 153-159

Whiteway, F.E., 1965. The recording and analysis of seismic body waves using linear cross arrays, The Radio and Electronic Engineer, vol. 29, 33-46

Wright, C., 1968. Evidence for a low velocity layer for P waves at a depth close to 800 km. Earth Planet. Sci. Letters, vol. 5, 35-40

BIBLIOGRAPHY
(cont'd)

Wright, C., 1970. P wave investigations of the Earth's Structure using the Warramunga Seismic Array. Ph.D. Thesis, Australian National University, Canberra

APPENDIX I

A Short Review of Seismic Ray Theory

If the velocities of elastic waves were uniform within the earth, then seismic rays would be straight lines following chords as in Figure A.1a, and the traveltime from a surface focus to an observatory at an angular distance Δ from the focus would be

$$T = 2R/V \ \text{Sin} \ \Delta/2 \qquad (1)$$

However, observations of traveltimes indicate that they increase less strongly with distance than is indicated by (1), and the T-Δ curves are more curved than this equation would suggest. The velocity at depth is thus greater than at the surface and seismic rays are refracted as in Figure A.1b.

Bullen (1963) has developed the theory applicable to an earth in which the velocity increases with depth. Figure A.1b shows the geometry of a ray in a multi-layered earth in which the velocity v increases with depth from the surface. It is assumed that the Earth is spherical and completely symmetrical about its centre in all its properties, and diffraction effects are ignored. Applying Snell's law to each of the boundaries A, B in Figure A-1b then

$$\text{Sin} \ i_1/v_1 = \text{Sin} \ f_1/v_2 \ ; \ \text{Sin} \ i_2/v_2 = \text{Sin} f_2/v_3 \qquad (1.a)$$

But from the two triangles,

$$q = r_1 \text{Sin} f_1 = r_2 \text{Sin} \ i_2$$

From equation (1.a)

$$\text{Sin} \ i_1/v_1 = r_1 \text{Sin} f_1/v_2 = r_2 \text{Sin} \ i_2/v_2 = r_2 \text{Sin} f_2/v_3$$

or more generally,

$$r \text{Sin} \ i/v = \text{constant} = p \qquad (2)$$

where i is the acute angle between the ray and the radius at any point. p is called the parameter of the ray, and is constant for all points along the ray. The value of p differs from member to member of a given family of rays, and at the deepest point of penetration of any ray, where

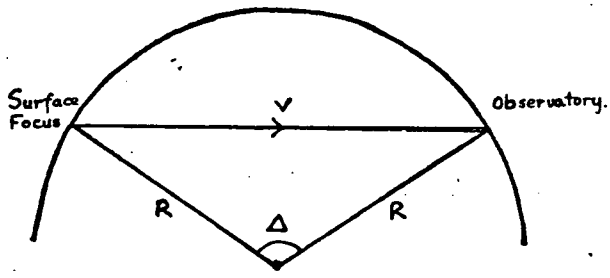

A-I(a). Path of a seismic ray through a hypothetical uniform earth.

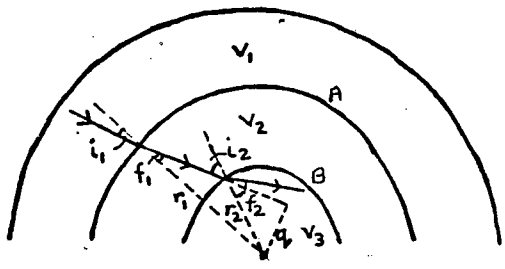

A-I(b). Seismic ray in three-layer earth.

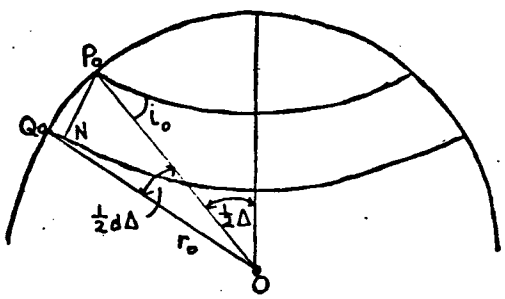

A-I(c).

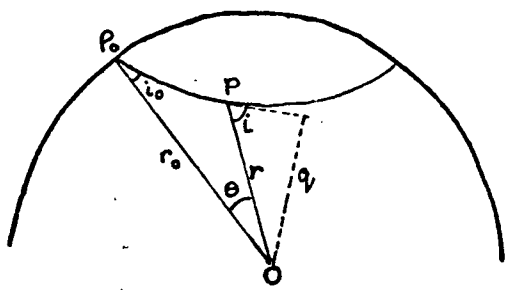

A-I(d).

Figure A-1 Seismic Ray Theory.

Sin i = 1, is equal to the value of r/v at that point

Consider two rays of a family of rays with parameters p, and p + dp, traveltimes T and T + dT subtending angles of Δ and $\Delta + d\Delta$ at 0 as shown in Figure A.1c, respectively. Let P_0N be the normal to the ray through Q_0. Then

$$\text{Sin } i_0 = NQ_0/P_0Q_0 = v_0 \cdot \tfrac{1}{2}dT/r_0 \cdot \tfrac{1}{2}d\Delta$$

and hence from equation (2),

$$p = r\text{Sin}i/v = dT/d\Delta \qquad (3)$$

Let P be any point of a ray whose parameter is p, with polar coordinates (r,e) as shown in Figure A.1d and let the arc length P_0P be s. Then, from (2)

$$r/v \; d\theta/ds = p \qquad (4)$$

and substituting for ds from the polar relation

$$(ds)^2 = (dr)^2 + (rd\theta)^2$$

equation (4) yields the relationship

$$d\theta = \pm \; pr^{-1} \; (\eta^2 - p^2)^{-\frac{1}{2}} \; dr \qquad (5)$$

where for convenience, the parameter $\eta = r/v$ (= p at the deepest point of the ray). Integrating (5) between P_0 and the deepest point of the ray, we obtain the expression for Δ,

$$\tfrac{1}{2}\Delta = p\int_{r_p}^{r_0} r^{-1}(\eta^2-p^2)^{-\frac{1}{2}}\, dr \qquad (6)$$

and the corresponding expression for T where

$$\tfrac{1}{2}T = \int_{r_p}^{r_0} \eta^2 r^{-1}(\eta^2-p^2)^{-\frac{1}{2}}\, dr \qquad (7)$$

At this point, it is convenient to introduce the important functions ζ and ξ where $\zeta = d\ln v/d\ln r = r/v\, dv/dr$, and $\xi = 2/1-\zeta = 2d\ln r/d\ln\eta$. It can be shown that the downward curvature of a ray with its lowest point at some level r in the earth is given by $1/v\; dv/dr$, and this curvature must be less than the curvature $1/r$ of the level surface at r, if the ray is to exist This condition implies that $\zeta < 1$, or $\xi > 0$, or $d\eta/dr > 0$.

Introducing the functions ζ and ξ into equations (6) and (7), and then differentiating the resulting equations lead to the expressions (Bullen, 1963)

$$d\Delta/d\rho = \xi_0(\eta_0^2-\rho^2)^{-\frac{1}{2}} + \int_{\xi_\rho}^{\xi_0}(\eta^2-\rho^2)^{-\frac{1}{2}}\,d\xi \qquad (8)$$

$$dT/d\rho = -\rho\xi_0(\eta_0^2-\rho^2)^{-\frac{1}{2}} + \int_{\xi_\rho}^{\xi_0}\rho(\eta^2-\rho^2)^{-\frac{1}{2}}\,d\xi \qquad (9)$$

where the subscripts 0 refer to the values of the parameters at the earth's surface.

These equations are further simplified by introducing the dimensionless variables $\mu = \eta/\eta_0$, $\lambda = \rho/\eta$, $T = t/\eta_0$, to become

$$d\Delta/d\lambda = -\xi_0(1-\lambda^2)^{-\frac{1}{2}} + \int_{\xi_\rho}^{\xi_0}(\mu^2-\lambda^2)^{-\frac{1}{2}}\,d\xi = -X + Y \qquad (10)$$

$$dT/d\lambda = -\xi_0\lambda(1-\lambda^2)^{-\frac{1}{2}} + \int_{\xi_\rho}^{\xi_0}\lambda(\mu^2-\lambda^2)^{-\frac{1}{2}}\,d\xi \qquad (11)$$

Consider the relationship between Δ and T corresponding to different types of variation of v with r. Normal or 'ordinary' behaviour of v with r entails that v increases slowly as r decreases, and that the rate of change of v is changing slowly. This implies that ξ is negative and moderate in value, $d\xi/dr$ and $d\xi/dr$ are small, also $d\eta/dr$ is positive and ξ_0 is negative. From the relation $p = \eta_0 \sin i_0$ p decreases steadily between η_0 and zero as i_0 goes from 90° (i.e. $\Delta = T = 0$) to 0°. Since ξ_0 is negative and $p = \eta_0$ when Δ is zero, it follows that for small values of Δ, X in equation (10) is large and positive. Owing to the smallness of $d\xi/dr$ and the range of integration for small Δ, Y is also small, so that for small Δ, $d\Delta/d\lambda$ is large and negative, and consequently $d^2T/d\Delta^2$ is negative tending to 0 for small Δ. For small Δ, then, equations (10) and (11) can be written

$$d\Delta/d\lambda = \xi_0(1-\lambda^2)^{-\frac{1}{2}} \qquad (12)$$

$$dT/d\lambda = -\xi_0\lambda(1-\lambda^2)^{-\frac{1}{2}} \qquad (13)$$

$$\Delta = \xi_0 \cos^{-1}\lambda \qquad (14)$$

$$T = \xi_0(1-\lambda^2)^{\frac{1}{2}} = \xi_0 \sin(\Delta/\xi_0) \qquad (15)$$

The above equations hold for small Δ for normal behaviour of v, and for rays terminating at the surface of the earth $r=r_0$. For that segment of a ray, taken as lying wholly on one side of the ray's lowest point and terminating at the levels r, and r_2 say, the values of Δ and T are from (14) and (15).

$$\Delta_{12} = \tfrac{1}{2}\xi_0\left(\cos^{-1}(\lambda/\mu_1) - \cos^{-1}(\lambda/\mu_2)\right) \quad (16)$$

$$T_{12} = \tfrac{1}{2}\xi_0\left((\mu_1^2-\lambda^2)^{\frac{1}{2}} - (\mu_2^2-\lambda^2)^{\frac{1}{2}}\right) \quad (17)$$

and the contributions to Δ, T and $d\Delta/d\lambda$ for the pair of segments of a whole ray which lie between levels r_0, and r_1 are given respectively by

$$\xi_0\left(\cos^{-1}\lambda - \cos^{-1}(\lambda/\mu_1)\right) \quad (18)$$

$$\xi_0\left((1-\lambda^2)^{\frac{1}{2}} - (\mu_1^2-\lambda^2)^{\frac{1}{2}}\right) \quad (19)$$

$$\xi_0\left(-(1-\lambda^2)^{-\frac{1}{2}} + (\mu_1^2-\lambda^2)^{-\frac{1}{2}}\right) \quad (20)$$

Consider a region L in which the behavior of v is normal being represented by $\xi = \xi_0 + \xi_0 r$ or $v = v_0 \exp(r\xi_0)$ extending down to a level r_1, to be underlain by a layer N extending for some distance beneath r_1. Suppose the velocity increases discontinuously at the level r_1, so that the velocity immediately above r_1, va, is less than vb, the velocity just beneath r_1. Thus μb is less than μa. Let ξ have the constant value $k\xi_0$ in layer N where $k < 1$, so that $\xi_b < \xi_a$. Rays for which $\mu a \leq \lambda \leq 1$ lie entirely in L and equations (12) - (15) apply for this region. From equation (12), it is seen that $d\Delta/d\lambda$ is initially negative and finite as previously described, becomes less and less negative as λ decreases. The behavior is shown in section AB of the curve in Figure A.2a. Rays for which $\mu b \leq \lambda \leq \mu a$ also lie entirely in L but consist of rays internally reflected off the boundary at r_1 and for these rays, from equations (18) - (20), we have

$$\Delta = \xi_0\left(\cos^{-1}\lambda - \cos^{-1}(\lambda/\mu a)\right) \quad (21)$$

$$T = \xi_0\left((1-\lambda^2)^{\frac{1}{2}} - (\mu a - \lambda^2)^{\frac{1}{2}}\right) \quad (22)$$

$$d\Delta/d\lambda = \xi_0\left(-(1-\lambda^2)^{-\frac{1}{2}} + (\mu a - \lambda^2)^{-\frac{1}{2}}\right) \quad (23)$$

From equation (23) at $\lambda = \mu a$, $d\Delta/d\lambda$ jumps discontinuously to $+\infty$ thereby decreasing through finite positive values as λ decreases, becoming zero at some point given by $(1-\lambda^2) = (\mu a^2 - \lambda^2)$

For rays whose lowest points are in N, $\lambda < \mu b$ and the appropriate

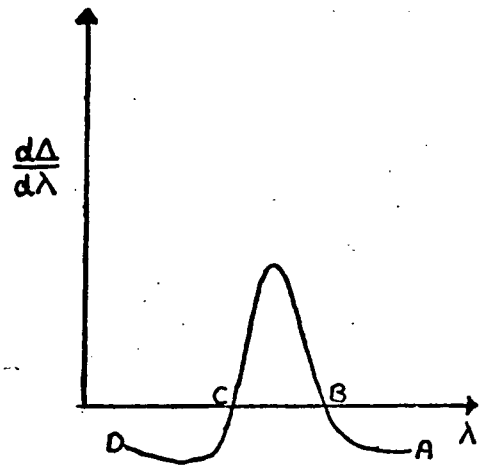

A-2(a).

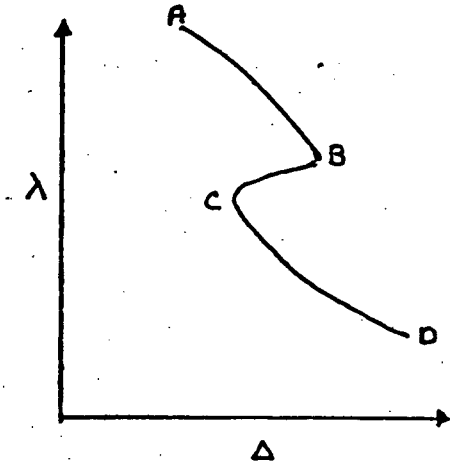

A-2(b).

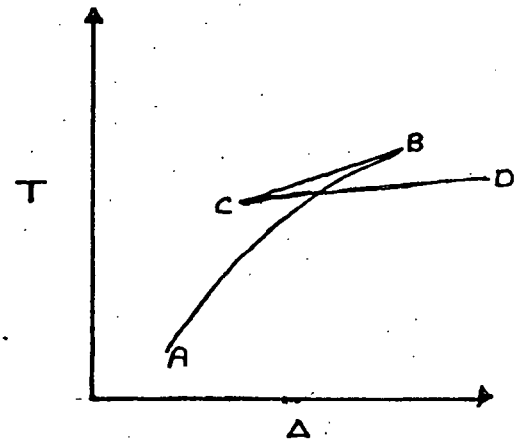

A-2(c).

Figure A-2. Behaviour of $d\Delta/d\lambda - \lambda$, $\lambda - \Delta$, and $T - \Delta$, curves for discontinous increase in velocity at a boundary.

equations are:

$$\Delta = \xi_0 \left(\left(\cos^{-1}\lambda - \cos^{-1}(\lambda/\mu_a) + k\cos^{-1}(\lambda/\mu_b) \right) \right) \quad (24)$$

$$T = \xi_0 \left(\left((1-\lambda^2)^{\frac{1}{2}} - (\mu_a^2-\lambda^2)^{\frac{1}{2}} + k(\mu_b^2-\lambda^2)^{\frac{1}{2}} \right) \right) \quad (25)$$

$$d\Delta/d\lambda = \xi_0 \left(-(1-\lambda^2)^{-\frac{1}{2}} + (\mu_a^2-\lambda^2)^{-\frac{1}{2}} - k(\mu_b^2-\lambda^2)^{-\frac{1}{2}} \right) \quad (26)$$

As λ decreases to the value μ_b in layer N, $d\Delta/d\lambda$ from (26) jumps discontinuously to $-\infty$, and as λ decreases beneath the value μ_b, $d\Delta/d\lambda$ increases through finite negative values resulting in the section CD of the $d\Delta/d\lambda$ curve. Equations (14), (15), (21), (22) and (24), (25) show that Δ and T are continuous functions of λ for rays in L and N. The $d\Delta/d\lambda$ (or $d\Delta/dp$) curve is illustrated in Figure A.2a, and the corresponding p-Δ and T-Δ curves in Figures A.2b and A.2c respectively. Of importance is the fact that neither of the cusps B and C are associated with large amplitudes since $d\Delta/d\lambda$, and therefore $d\Delta/de_o$ (where e_o, the angle of emergence is given by $p = \eta \cos e_o$) at these points are not equal to zero. Branch BC corresponds to rays reflected off the discontinuity (receding branch) whilst AB and CD correspond to rays refracted through layers L and N respectively. On the branch BC, $d\Delta/d\lambda$ and therefore $d^2T/d\Delta^2$ is zero at both B and C (where $\lambda = \mu_b$ and μ_a respectively) and consequently BC was virtually straight for some distance from B, any marked curvature being near C, and branch CD likewise runs virtually staight for some distance from C, any marked curvature being near D. It can be seen that the above discussion applies to the velocity discontinuities in the transition region, and imposes the constraints on the traveltime curve mentioned in section 1.2.

For the case of a discontinuous decrease in velocity, as at the mantle-core boundary, the situation is somewhat different. In this case, $V_b < V_a$ and $\mu_b > \mu_a$, and we assume that layer N extends downward far enough for μ to return through the value μ_a before the bottom of N is reached. For rays with lowest points in L, equations (12) - (15) still apply. For rays which penetrate N, (24) - (26)

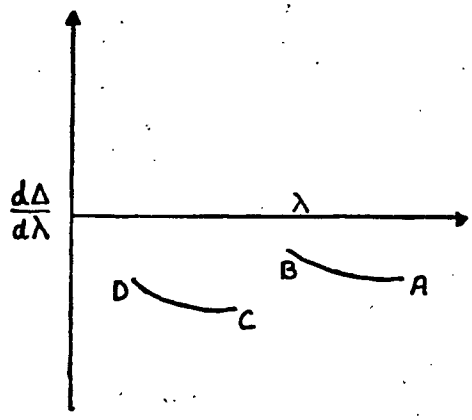

A-3(a).

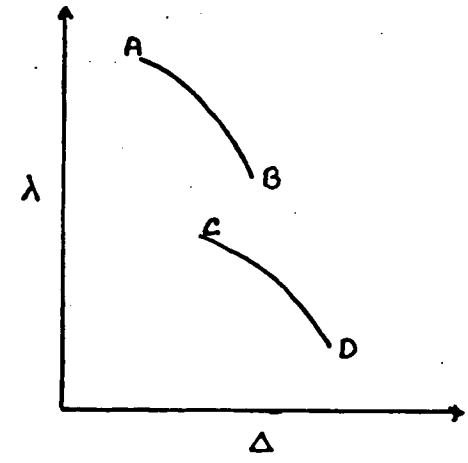

A-3(b).

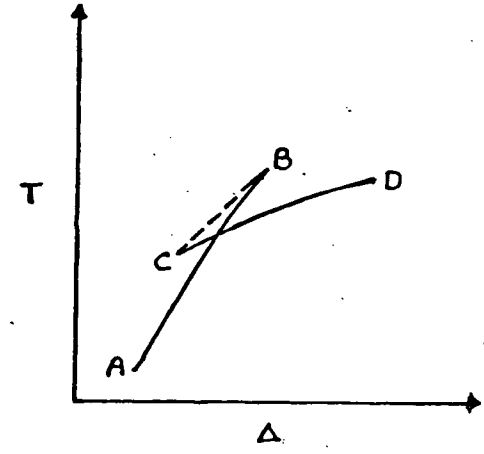

A-3(c).

Figure A-3. Behaviour of $d\Delta/d\lambda - \lambda$, $\lambda - \Delta$, and $T - \Delta$ curves for discontinous decrease in velocity at a boundary.

apply, but since $\lambda < \mu a$ for these rays, there are no rays with lowest points in the upper part of N for which $\mu a < \lambda < \mu b$. Consequently at $\lambda = \mu a$ there are discontinuities $\delta\Delta$ and δT in Δ and T given by subtracting (14) from (24) and (15) from (25) respectively:

$$\delta\Delta = k\xi_0 \cos^{-1}(\mu a/\mu b) \tag{27}$$

$$\delta T = k\xi_0 (\mu b^2 - \mu a^2)^{-\frac{1}{2}} \tag{28}$$

For rays penetrating N, $d\Delta/d\lambda$ from equation (26) has the value +00 at $\lambda = \mu a$ and decrease as λ decreases from μa. Thus Δ and T decrease rapidly as λ decreases from μa, and provided N is deep enough reach minima given by the value of λ satisfying the equation.

$$(1-\lambda^2)^{-\frac{1}{2}} + k(\mu b^2 - \lambda^2) = (\mu a^2 - \lambda^2)^{-\frac{1}{2}}$$

This minimum is the cusp D shown in Figure A.3c and since $d\Delta/d\lambda$ is zero at this point, D corresponds to a caustic. As before, at point C $d^2T/d\Delta^2$ is zero, and consequently the branch is virtually straight some distance from C, any marked curvature being near the caustic D. The corresponding $d\Delta/d\lambda - \Delta$ and $\lambda - \Delta$ curves are shown in Figures A.3a and A.3b.

The above discussions cover the variation in velocity obtained in the earth from the base of the mantle to the center of the earth's core. It is intended that they provide insight into the nature of the traveltime curves generated by velocity discontinuities in this region and the constraints imposed upon these curves by ray theory.

APPENDIX 2 LIST OF EARTHQUAKES USED IN STUDY

Event No.	Date	Origin Time Hr.	Min.	Sec	Latitude (Degrees)	Longitude (Degrees)	Distance (Degrees)	Focal Depth (Km.)	Magnitude	Azimuth (Degrees)
1	Jan.14/69	23	2	7.9	13.175N	29.203W	113.47	33.0N	5.5	301.6
2	Oct.24/69	8	29	12.1	33.292N	119.193W	114.11	10.0	5.1	61.6
3	Oct.1867	1	11	44.8	79.8 N	2.4 E	116.50	33.0	5.7	351.5
4	June 12/69	15	13	31.1	34.405N	25.061E	116.60	25.0D	5.8	299.2
5	Nov.23/67	13	42	1.6	80.2 N	1.0 W	116.70	10.0	5.8	352.3
6	Dec.19/68	16	30	0.0	37.232N	116.477W	116.80	0.0	6.3	57.6
7	Sept.16/69	14	30	0.0	37.314N	116.460W	116.82	0.0	6.2	57.5
8	Oct.8/69	14	30	0.0	35.257N	116.450W	116.83	0.0	5.5	57.6
9	Oct.29/69	22	1	51.4	37.143N	116.064W	117.12	0.0	5.7	57.8
10	Sept.6/68	14	0	0.1	37.135N	116.047W	117.13	0.0G	5.6	57.8
11	Dec.25/68	12	17	20.8	35.130N	24.330E	117.27	40.0	5.0	299.9
12	Nov.21/67	17	2	25.0	72.70 N	8.5 E	119.20	51.0	5.5	343.9
13	Nov.30/67	7	23	51.5	41.50 N	20.5 E	120.6	29.0	6.0	307.0
14	April 18/69	17	43	53.7	24.288N	107.738W	120.92	33.0	5.0	73.1
15	Sept.26/67	11	11	23.7	33.60 S	70.5 W	121.70	84.0	5.8	155.6
16	Jan.21/70	17	51	38.5	7.017N	104.298W	121.80	33.0N	6.2	94.1
17	Nov.1/69	11	8	20.9	23.148N	107.934W	122.36	33.0N	5.6	74.7
18	Dec.13/69	21	33	21.9	32.708S	69.972W	122.71	105.0D	5.6	155.6
19	Oct.27/69	8	10	58.3	44.923N	17.232E	122.91	33.0N	5.3	311.1
20	Sept.20/69	15	26	41.5	1.785N	101.031W	123.0	33.0N	5.5	101.2
21	Apr.26/69	6	2	49.0	30.645S	71.542W	123.87	33.0N	5.9	153.0
22	Nov.27/67	5	13	12.6	30.8 S	71.00 W	124.0	62.0	5.4	153.6
23	June 23/69	7	8	27.7	18.373N	104.546W	124.59	36.0	5.3	81.0
24	Oct.7/67	1	14	4.1	29.6 S	71.1 W	125.0	42.0	5.3	152.8
25	Nov.15/67	21	31	51.5	28.7 S	71.2 W	125.70	15.0	6.2	152.2
26	Nov.13/69	7	51	29.5	27.8 S	71.65 W	126.29	33.0N	5.8	151.2
27	Jan.6/68	23	27	21.3	27.8 S	71.1 W	126.50	33.0	5.8	151.7
28	Apr.17/69	17	37	22.4	28.26 S	67.786W	127.11	82.0	5.0	154.2
29	Sept.2/69	3	47	9.1	27.745S	66.491W	128.47	174.0D	5.5	156.2
30	Aug.20/67	15	3	36.2	25.2 S	69.0 W	129.70	109.0	5.6	152.2
31	Sept.8/67	8	59	59.3	23.4 S	70.7 W	130.50	33.0	5.5	149.2
32	Sept.21/69	2	0	54.3	23.552S	68.080W	131.55	120.0D	5.5	152.1
33	Dec.29/68	16	29	31.1	23.975S	66.673W	131.77	205.0G	5.5	153.9
34	Sept.13/69	10	52	58.0	22.883S	63.367W	132.00	106.0D	5.4	151.4
35	May 16/68	22	45	19.2	22.883S	68.6 W	132.00	104.0	5.0	151.1
36	Dec.25/67	10	41	31.6	21.50 S	70.4 W	132.20	53.0	5.8	148.2
37	June 6/69	22	25	37.3	22.511S	68.418W	132.27	125.0D	5.0	151.1

APPENDIX 2 LIST OF EARTHQUAKES USED IN STUDY

Event No.	Date	Origin Time			Latitude	Longitude	Distance	Focal Depth	Magnitude	Azimuth
		Hr.	Min	Sec.	(Degrees)	(Degrees)	(Degrees)	(km)		(Degrees)
38	July 25/69	6	6	42.4	25.552S	63.310W	131.63	579.0D	5 5	158.5
39	Oct 20/69	15	20	36.5	17.300N	95.188W	133.11	87.0	5.4	84 7
40	Sept 17/67	7	56	22.7	17.2 N	94.1 W	134.10	45.0	5.2	85.1
41	Oct 22/69	10	21	52.1	18.086S	71.542W	134 46	23 0	5 4	144 1
42	June15/68	5	11	17.2	14 4 N	92 9 W	134.60	25.0	5 4	89.2
43	July19/69	4	54	54.1	17.254S	72 519W	134.58	54.0D	5.9	142.7
44	June 22/69	14	30	10 7	16.929N	93 608W	134 52	151.0	5.1	85 6
45	Aug 23/68	22	36	51 3	21.986S	63.547W	134.70	38.0	6.5	129 1
46	Sept.3/67	21.	7	30 8	10.6 S	79.8 W	134.72	50.0	5 0	140 9
47	Nov 7/68	10	13	39 8	16.388S	73.460W	134.70		5 8	156 3
48	Oct 31/68	9	15	46.9	16.289S	73.298W	134.89	67.0D	5 7	141 0
49	Jan 8/68	18	44	24.5	18.6 S	69.9 W	134.90	116.0	5.4	146 6
50	Sept.25/68	10	38	38.4	15.571N	92.638W	135.15	137.8	5.7	87 7
51	Sept.28/68	13	53	35.3	13 160S	76 382W	135.31	70.0G	6.0	134 9
52	Sept.15/69	7	14	25.8	18.552S	69.021W	135.40	177.0D	5.2	147 6
53	Oct.5/67	9	41	31.4	14.5 S	75 4 W	135 50	100.0	5 6	137.2
54	Sept.27/67	6	2	39 5	7.3 S	81.3 W	135 70	37.0	5 1	124.1
55	Aug 23/68	23	14	52.7	21.819S	63.530W	134.96	541 0D	5.2	156 2
56	June 11/69	21	15	32.6	8 590S	79 688W	136.10	81.0	5 0	127.0
57	April 21/69	2	19	7 1	14.098N	91.015W	136.33	82.0	5 5	90 3
58	Jan 12/69	14	12	53.0	14 142S	72 747W	136.89	113.0	5.2	139.7
59	July24/69	2	59	21.0	11.851S	75.130W	137.10	1.0	5 9	135.0
60	Oct.20/69	18	0	28.7	11.859S	75.164W	137 07	12.0	5.1	134 9
61	Oct.6/69	0	37	59.6	11.737S	75.100W	137.20	3.0	5.1	134.9
62	Oct.6/69	6	36	45.2	11.782S	74.999W	137.23	4.0	5.3	134.0
63	Nov.16/69	10	30	1.7	13.351N	89.650N	137.43	79.0	4 9	91.8
64	Sept.6/68	7	49	42.0	5.767S	80.261W	137.44	66.0D	5.3	123.3
65	Nov.18/67	12	15	55.4	13.37N	89.07W	138.00	78.0	5.1	92.0
66	Dec.27/66	21	22	14.8	13.20N	88.81W	138.20	66.0	5.5	92.4
67	July18/69	23	17	10.6	18.241S	63.314W	138.28	19.0D	5.6	154.3
68	June11/68	5	52	33.5	13.90N	88.81W	138.40	199.0	5.3	91.4
69	June6/69	16	16	1.7	12.467N	88.000W	138.75	48.0	5.0	93.7
70	Nov.9/68	17	1	41.1	37.961N	88.464W	138.87	19.0	5.3	54.8
71	June 20/68	15	51	56.5	5.6 S	77.3 W	139.80	33.0	5.8	125.9
72	June21/68	0	26	7.8	5.7S	77 3W	139.80	22.0	5.6	126.1
73	June19/68	8	13	35.0	5 6S	77 2W	139.90	28.0	6.4	126.0
74	Oct.4/67	6	2	16.4	10.7N	86.0W	140 10	33.0	5.3	97.2

APPENDIX 2 LIST OF EARTHQUAKES USED IN STUDY

Event No.	Date	Origin Time Hr.	Min.	Sec.	Latitude (Degrees)	Longitude (Degrees)	Distance (Degrees)	Focal Depth (km.)	Magnitude	Azimuth (Degrees)
75	Oct.3/67	18	16	3.2	10.9N	85.9W	140.30	21.0	5.8	97.0
76	Sept.20/69	5	8	57.6	58.297N	32.189W	140.46	33.0N	5.6	348.9
77	Aug.27/67	13	8	55.9	12.3N	86.2W	140.40	183.0	5.2	94.7
78	Oct.15/67	8	0	50.3	11.9N	86.0W	140.50	162.0	6.2	94.5
79	June24/69	0	35	5.5	11.661N	85.717W	140.66	100.0G	5.3	95.9
80	June15/68	7	8	48.1	5.6N	82.6W	140.80	16.0	6.0	106.6
81	Oct.11/67	20	28	10.2	10.3S	71.2W	141.40	585.0	5.0	137.8
82	May 16/68	8	25	9.2	3.7S	76.6W	141.60	113.0	5.4	124.3
83	Jan.1/70	1	43	46.7	8.598N	83.525W	141.69	48.0	5.2	101.6
84	Nov.8/67	3	10	53.3	16.8N	85.9W	141.70	28.0	5.4	87.9
85	May 31/69	11	7	17.1	1.753S	77.744W	141.84	172.0	5.1	120.7
86	Dec.16/68	3	7	24.1	7.123N	82.243W	142.31	16.0	5.3	104.6
87	May28/69	13	30	8.9	2.086S	76.927W	142.30	177.0D	5.5	122.0
88	April25/69	3	34	17.7	7.450N	82.075W	142.59	25.0G	5.4	104.2
89	May 5/69	5	34	23.5	36.023N	10.390W	145.21	29.0	5.5	304.9
90	Sept.24/69	3	58	56.5	52.559N	31.841W	145.72	33.0	5.2	345.0
91	Dec.24/69	5	4	44.5	35.953N	10.396W	145.24	33.0N	5.1	304.8
92	Feb.28/69	2	40	32.5	36.008N	10.573W	145.36	22.0	7.3	304.9
93	Sept.24/69	4	20	52.9	52.499W	31.849W	145.78	33.0N	5.0	345.0
94	Sept.6/69	14	30	39.5	36.941N	11.887W	146.05	33.0N	5.7	307.1
95	Nov.14/69	6	52	5.3	4.934N	76.846W	146.17	53.0	4.7	112.0
96	Aug.31/68	21	47	38.5	4.505N	76.359W	146.39	97.5	4.6	113.1
97	Sept.22/67	8	8	4.3	0.7S	20.1W	147.60	33.0	5.3	233.6
98	Nov.21/67	21	50	24.3	48.2N	27.8W	148.30	33.0	5.0	237.0
99	Sept.1/68	4	48	52.2	0.995S	24.512W	150.63	33.0N	5.2	227.3
100	Sept.1/68	8	19	57.2	0.889S	24.519W	150.70	33.0N	5.0	227.4
101	Oct.20/69	13	11	37.0	10.796N	72.480W	152.61	40.0G	5.7	105.4
102	Oct.20/69	13	11	33.5	10.796N	72.480W	152.68	55.0	5.1	105.4
103	Oct.16/68	1	55	32.7	19.152N	69.838W	157.19	36.0	5.2	87.9
104	Sept.20/68	6	0	3.5	10.735N	62.669W	161.22	107.0D	6.2	116.7
105	Oct.22/69	12	52	22.2	10.921N	62.552W	161.41	79.0	5.4	116.4
106	Sept.22/69	13	47	52.2	4.977N	32.625W	160.45	33.0	5.7	222.1
107	Sept.3/68	15	37	0.2	20.631N	62.238W	164.42	33.0	5.5	84.6
108	May 15/69	20	43	33.4	16.573N	61.341W	164.77	50.0	5.7	99.5
109	Dec.24/67	20	3	10.9	17.4N	61.1W	165.10	24.0	6.4	97.3
110	Dec.25/69	22	31	2.3	16.083N	59.771W	166.03	8.0	6.0	103.7
111	Dec.25/69	21	32	27.3	15.772N	59.650W	166.04	7.0	6.4	105.1

APPENDIX 2

LIST OF EARTHQUAKES USED IN STUDY

Event No.	Date	Origin Time			Latitude	Longitude	Distance	Focal Depth	Magnitude	Azimuth
		Hr.	Min.	Sec.	(Degrees)	(Degrees)	(Degrees)	(km.)		(Degrees)
112	Dec.26/69	8	46	15.2	15.839N	59.57W	166.13	22.0	5.2	105.1
113	Dec.26/69	20	3	28.8	15.791N	59.555W	166.13	33.0N	5.4	104.9
114	Jan.8/68	20	22	15.6	8.2 N	38.2 W	166.30	33.0	5.4	212.7
115	Sept.24/69	18	3	19.0	15.237N	45.776W	175.31	33.0N	5.8	178.5

APPENDIX III

ELLIPTICITY AND FOCAL DEPTH CORRECTIONS TO MEASURED TRAVELTIMES

Bullen (1939, 1938, 1963) has shown that the ellipticity correction δT to the traveltime for geocentric latitudes is given approximately by the formula -

$$\delta T = f(\Delta)(h_0 + h_1) \qquad \ldots\ldots\ldots\ldots\ldots (1)$$

where h_0 and h_1 are the differences between the actual and mean radii of the earth at the epicentre and observing stations respectively, and are listed by Bullen, (1937). Also $f(\Delta)$ is given by Bullen (1938). The value of h_1 for WRA is +5.0 km while $f(\Delta)$ ranges from 0.10 to 0.095 for PKP_{DF} and 0.100 to 0.074 for PKP_{AB}.

Time corrections for focal depth were determined for earthquakes with focal depth less than 200 km. from the tables given by Bolt (1968), and the corresponding distance corrections resulting in a surface focus for the event were estimated from near-earthquake P tables. For focal depths greater than 200 km, the equation developed by Adams and Randall (1969) for deep-focus earthquakes, and derived especially for use with PKP phases was used:

$$\delta = (0.05 + 0.025\,h + 0.0028h^2)p \qquad \ldots\ldots (2)$$

where δ is the correction in degrees, h is the focal depth in units of hundredths of the earth's radius, and P is the ray parameter $dT/d\Delta$. δ is determined from the above formula and the corresponding time correction found from tables of near-earthquake traveltimes using the appropriate values of δ and h.

APPENDIX III

ELLIPTICITY AND FOCAL DEPTH CORRECTIONS TO MEASURED TRAVELTIMES

(cont.)

Thus all the events were adjusted to have surface foci. A check was made on the distance and time corrections obtained for all the earthquakes in the above manner by using a computer program designed to calculate these corrections for ray paths of specified parameter travelling through the earth. The method used in this program was to calculate the quantities Δ_{12} and T_{12} as described in Appendix I for radii down to the focal depth given, using an assumed velocity model for the crust and mantle. It was found that good agreement was obtained at most focal depths except for those in the vicinity of about 500 kilometres. In these cases the corrections given by the program were smaller by a maximum of about 0.12 deg. than the value obtained using the Adams and Randall equation. The latter values were assumed to be the correct ones. In either case, at the large distances in question, an error of 0.12 deg. is small, compared to the error in epicentre determiniation which can be as large as 0.5^{o}

All the epicentre coordinates listed in Appendix II are the preliminary determinations complied by N.O.A.A. on the basis of the J-B traveltime tables. Recent traveltime studies, for example Cleary and Hales (1966), have revealed systematically shorter traveltimes at teleseismic distances than those of Jeffreys and Bullen. Con-

APPENDIX III

ELLIPTICITY AND FOCAL DEPTH CORRECTIONS TO MEASURED TRAVELTIMES

(con't)

sequently, significant systematic errors in epicentre and focal depth determination may exist but until the traveltime controversy is satisfactorily resolved, very little can be done about this.

The effect of errors in epicentre location on $dT/d\Delta$ measurements is to increase the scatter of the data especially in those regions of the curve where $d^2T/d\Delta^2$ is large as in the neighbourhood of a caustic. Errors in focal depth determinations, particularly for deep focus earthquakes, may well produce as much scatter in the $dT/d\Delta$ values as epicentre mislocations. The view is commonly held that focal depth determinations of greater than 60 km are somewhat unreliable. In this study, more than 1/3 of the events had focal depths greater than 60 km, and many of these were restrained in some manner to a particular level. However, as discussed in Section 2.2.3, systematic errors in the $dT/d\Delta$ measurements are more significant than any others.

APPENDIX IV

METHOD OF SUMMARY VALUES

Jeffreys (1937, 1961) devised the method of summary values as a smoothing technique. The following description follows more closely that of Arnold (1968).

Consider a number of observed values of the function $p = f(\Delta)$ for a certain range of the argument in which there is very little curvature. If a straight line is fitted to the points in this range by the method of least squares, any two points (P_1, D_1) and (P_2, D_2) on this straight line can be taken to represent the data, but in general, the errors in P_1 and P_2 will not be independent thus making estimation of the magnitude of the reduction of error difficult. Moreover, if in this range the curvature is appreciable, the errors have been overestimated and valuable information may be lost. If curvature is accounted for by passing a quadratic through the data and choosing the points (P_1, D_1) and (P_2, D_2) to be the intersections of the linear and quadratic forms, then curvature may be safely neglected and at the same time the uncertainties in P_1 and P_2 are rendered independent. Arnold (loc cit) has shown that the ith equation of condition for a quadratic form is

$$\frac{\Delta_i - D_2}{D_1 - D_2} P_1 - \frac{\Delta_i - D_1}{D_1 - D_2} P_2 + a(\Delta_i - D_1)(\Delta_i - D_2) = p_i \quad \cdots\cdots (1)$$

If the weight of one observation is $w = 1/\sigma_i^2$ where σ_i is the standard error in p_i, the three normal equations for P_1, P_2 can be formed by multiplying equation (1) by the respective coefficients.

APPENDIX IV

METHOD OF SUMMARY VALUES

(con't)

The conditions that the errors in P_1, P_2 and a be independent, are that the coefficients of the off-diagonal elements of the left-hand side of the equation be zero, i.e.

$$\Sigma \omega_i (\Delta_i - D_1)(\Delta_i - D_2) = 0 \quad \ldots\ldots\ldots\ldots\ldots\ldots (2)$$

$$\Sigma \omega_i (\Delta_i - D_1)(\Delta_i - D_2)^2 = 0 \quad \ldots\ldots\ldots\ldots\ldots\ldots (3)$$

$$\Sigma \omega_i (\Delta_i - D_1)^2(\Delta_i - D_2) = 0 \quad \ldots\ldots\ldots\ldots\ldots\ldots (4)$$

Under these conditions, a cannot contribute to P_1 and P_2 and it may assume any value, but there are three equations and only two unknowns. However, if (4) is subtracted from (3), it reduces to (2) so that either (3) or (4) is superfluous, and a unique solution for D_1 and D_2 is possible. To find D_1 and D_2, the moments are formed:

$$\eta = \Sigma \omega_i \quad ; \quad \eta \mu_1 = \Sigma \omega_i \Delta_i \quad ; \quad \delta_i = \Delta_i - \mu_i$$

$$\eta \mu_2 = \Sigma \omega_i \delta_i^2 \; ; \quad \eta \mu_3 = \Sigma \omega_i \delta_i^3$$

Equation (2) then becomes, putting $d_1 = D_1 - \mu_1$ and $d_2 = D_2 - \mu_2$

$$\mu_2 + d_1 d_2 = 0 \quad \ldots\ldots\ldots\ldots\ldots\ldots (5)$$

and equation (3) reduces to

$$\mu_3 - \mu_2 (d_1 + d_2) = 0 \quad \ldots\ldots\ldots\ldots\ldots\ldots (6)$$

Substituting for either d_1 or d_2 from (5) into (6), we have

$$d^2 - (\mu_3/\mu_2) d - \mu_2 = 0 \quad \ldots\ldots\ldots\ldots\ldots\ldots (7)$$

Solution of equation (7) yields the values of D_1 and D_2, and Arnold

APPENDIX IV.

METHOD OF SUMMARY VALUES

(con't)

has shown how by substitution of equations (2) and (3) into the normal equations, the values of P_1 and P_2 are

$$P_1 = (D_1 - D_2)\frac{\Sigma w_i (\Delta_i - D_2)p_i}{\Sigma w_i (\Delta_i - D_2)^2} \pm \frac{|D_1 - D_2|}{\sqrt{(\Sigma w_i (\Delta_i - D_2)^2)}} \quad (8)$$

$$P_2 = (D_2 - D_1)\frac{\Sigma w_i (\Delta_i - D_1)p_i}{\Sigma w_i (\Delta_i - D_1)^2} \pm \frac{|D_1 - D_2|}{\sqrt{(\Sigma w_i (\Delta_i - D_1)^2)}} \quad (9)$$

where the uncertainties are independent, and reduce to the square roots of the inverse of the coefficients of P_1 and P_2.

P_1 and P_2 are called the summary values and represent $p(\Delta)$ in the range of argument used.

The summary values method of smoothing can also be used to fit a quadratic (Jeffreys, 1937) so that the errors at three points are independent of each other and of a possible cubic term. This method appears to be somewhat of an improvement on the first method of summary values, but it breaks down if the data are unevenly distributed or are not capable of precisely defining a curvature.

APPENDIX Va.

U.B.C. TRIP

TRIANGULAR REGRESSION PACKAGE

One method of smoothing data is to fit a polynomial to the data by the method of least squares. The computer programme, U.B.C. Trip, was designed with this (among other things) in mind.

A polynomial of degree, say m, is requested, being thought by visual examination to give the best fit to the data. The Trip program uses the data to calculate the coefficients of m regression equations, the first equation being a simple linear equation of the form $y=b_o + b_1x$, where y is the dependent and x the independent variable.

Successive equations are this linear equation augmented by a term in the next higher power of the independent variable, up to the power m. Thus, the second regression equation would be $y = b_o + b_1x + b_2x^2$ and the final regression equation would be $y = b_o + b_1x + b_2x^2 \ldots\ldots\ldots + b_mx^m$ After the coefficients of each of the equations have been calculated by obtaining the best possible fit of the equation to the data by the usual least squares technique (i.e. by calculating the equation to minimise the sum of the squares of the distances of the predicted values of y from the observed values) the program calculates several significant quantities that give an indication of the quality of the fit.

One of these quantities is the parameter R^2, thesquare of the multiple correlation coefficient, where $R^2 = \sum_{i=1}^{N} w_i(\hat{y}_i - \bar{y})^2 / \Sigma w_i (y_i - \bar{y})^2$ and $\hat{y}_i$ is the ith predicted value of y, $(\hat{y}_i = b_o + b_1x_i)$. y_i is the ith observed value of y, w_i is the weight of the ith observation, and $\bar{y}$ is the mean of the observed values of y. R^2 always takes a valueof between zero and unity, and its significance liesin the fact that the closer it is to the value unity, the better does the corresponding regression equation fit the data,

since the physical meaning of R^2 is that it represents that proportion of the total observed variance of the dependent variable y which is accounted for by the regression line. In addition, the program calculates quantities known as the F-ratio and F-probability for each of the coefficients b_i, already in the equation where the F ratio is given by

$$F_i = (b_i / \text{Std. Error in } b_i)^2$$

and the F-probabilty is the probability of obtaining a value of Fi greater than or equal to the one calculated, given that $b_i = o$. If this probability is less than 0.05, it is concluded that the coefficient b_i is significantly different from 0, and therefore meaningful.

The tolerance of each potential independent variable not yet in the regression equation (provided the present equation has not yet attained the degree m) is also calculated. This quantity is the proportion of the variance of the independent variable x which cannot be explained by the independent variables already in the equation, and if this tolerance falls beneath 0.001, the next higher power of x is not allowed in the equation. In addition, the F-probability of each potential independent variable x, not yet in the equation (again provided the equation has not yet attained the maximum degree m) is calculated, and this is simply the F-probability that the coefficient of the next higher power of x would have if it were admitted to the present regression equation. Unless requested otherwise, the critical value of F-prob. is assumed to be 0.05, and if the calculated value of F-prob. is less than 0.05, the next higher power of x would be added to the equation and the entire process repeated using the new equation. If F-prob. is greater than 0.05 however, the next higher power of x is not added to the equation and the

calculations stop. In practice, it was requested that the critical value of F-prob. be 1.0, so that all the powers of X up to the degree requested, were used to calculate a final regression equation, irregardless of whether the coefficients of the powers were significant or not as indicated by their F-prob. values. The residuals $y_i - \hat{y}_i$ were calculated, and a printer plot of the data together with points predicted by the final regression equation obtained. The values of R^2 and F-prob. for each of the coefficients in the final regression equation were then examined, along with the residuals and the printer plot. If the F-prob. of the last coefficient in the equation was found to be greater than 0.05, a new polynomial fit of degree m-1 was requested. If it was found to be less than 0.05, a polynomial fit of degree m + 1 was requested. The final regression equation chosen as best representing the data, was that one in which R^2 was the nearest to the value unit, the F-prob. of more of the coefficients were greater than 0.05, the residuals appeared to be evenly distributed about a mean value, and from visual examination of the printer plot, the fit of the regression equation to the data seemed satisfactory.

APPENDIX Vb. DT/DΔ SMOOTHED BY POLYNOMIAL REGRESSION

DISTANCE	DT/DΔ (SEC/DEG)			
(DEG)	DF	GH	IJ	AB
113.0	1.959			
114.0	1.950			
115.0	1.945			
116.0	1.936			
117.0	1.929			
118.0	1.922			
119.0	1.918			
120.0	1.914			
121.0	1.911			
122.0	1.908			
123.0	1.906			
124.0	1.904			
125.0	1.903			
126.0	1.901			
127.0	1.900			
128.0	1.898			
129.0	1.896			
130.0	1.893			
131.0	1.889			
132.0	1.885	2.688		
133.0	1.880	2.678		
134.0	1.874	2.668	3.456	
135.0	1.867	2.658	3.437	
136.0	1.859	2.648	3.417	
137.0	1.849	2.640	3.397	
138.0	1.838	2.628	3.355	
140.0	1.812	2.622	3.332	
141.0	1.797	2.617	3.309	
142.0	1.780	2.613	3.285	
143.0	1.762	2.607	3.260	
144.0	1.742	2.602	3.235	
145.0	1.720	2.595	3.208	3.548
146.0	1.696	2.588	3.181	3.659
147.0	1.671	2.579	3.154	3.760
148.0	1.644	2.568	3.125	3.849
149.0	1.615	2.555	3.096	3.929
150.0	1.584	2.540	3.066	4.000
151.0	1.550	2.523	3.035	4.063
152.0	1.517	2.502		4.118
153.0	1.481	2.479		4.166
154.0	1.443	2.451		4.208
155.0	1.403	2.421		4.244
156.0	1.361	2.386		4.276
157.0	1.318	2.347		4.304
158.0	1.273	2.300		4.329
159.0	1.226			4.351
160.0	1.178			4.371
161.0	1.129			4.390
162.0	1.077			4.409
164.0	0.971			4.448
165.0	0.916			4.470
166.0	0.859			4.494
167.0	0.802			4.501
168.0	0.743			4.501
169.0	0.684			4.503
170.0	0.624			4.506
175.0	0.316			4.509